Doctoral Dissertation

Electrochemical Characterization of Passive Films Formed on Ni Based Alloys

Whee-Sung Kim

January 2015

Division of Materials and Manufacturing Science
Graduate School of Engineering
Osaka University

Contents

Chapter 1 General Introduction

1.1 Passivity of metals and alloys

Recently, structural materials have been requested to be used in the more severe corrosive environments. Stainless steels and Ni-based alloys have attracted much attention due to their high corrosion resistance in such environments. The high corrosion resistance of the materials is attributed to passive films formed on the surfaces. Therefore, the characterization of the passive film is very important to understand corrosion resistance of the materials.

Characteristics of passive film have been studied intensively since the time of Faraday (1830s) and many theories and models have been proposed to explain the passivity of metals and alloys[1)-5)]. The structure and composition of passive films have been examined by surface analytical techniques.

1.2 Analytical methods of the passive film

As compositions, structure and electronic properties of passive film formed on metals and alloys are related to corrosion resistance of metallic materials, passive films have been extensively examined using various surface analytical techniques. The present section describes briefly typical surface analytical techniques that have been used for passivity research.

1.2.1 Ex-situ analytical techniques – XPS and AES

As information regarding the structure and chemical composition of passive films is very important to understand corrosion behaviors of metallic materials, passive films have been subjected to various surface analytical techniques. In particular X-ray Photoelectron

Spectroscopy (XPS) and Auger Electron Spectroscopy (AES) have been often used to analyze passive film.

X-ray Photoelectron Spectroscopy (XPS), commonly known as Electron Spectroscopy for Chemical Analysis (ESCA), is the most widely used surface analysis technique to examine the chemical composition of surfaces. XPS was developed in the mid-1960's by Kai Siegbahn[6]. The fundamental principle of XPS is based on the theory of photoelectric effect[7, 8] in which an electron is released from a material surface as X-rays with monochromatic wavelength are irradiated to the surface. Therefore, in XPS, kinetic energy of an electron, which is released as the material surface is subjected to X-rays irradiation, is measured. Through the measurement, it is possible to identify the coupling status of an electron within an atom. Since the core electrons of all elements have each unique energy level, the measurement can be used to identify the elements of material. XPS analysis is performed to observe the energy level of the core electrons which merely reflects the chemical status of material. In addition, the chemical shift is also observed according to the chemical status. It is easy to simply interpret the coupling status of an element. In other words, the core level of an electron causes the change of eV (chemical shift) according to the chemical coupling status of the material. XPS analysis technique has been recognized as a valuable method for the study of passive films analysis because of its high surface sensitivity. In the 1970s, XPS was for the first time applied for characterization of passive films on metals and alloys by Okamoto et al.[9], Asami et al.[10, 11] and Castle et al.[12]. Since then, many researchers have applied XPS to examine passive films formed on Ni-based alloys. For examples, Tjong[13] reported passive films formed on Ni in a borated buffer solution at various anodic potentials. Passive films formed on Ni consisted of $Ni(OH)_2$ and NiO at low anodic potentials whereas passive films at high anodic potentials were composed mainly of Ni_2O_3. Jeng et al.[14] studied the room

temperature oxidation of Ni-23Cr alloy and reported that oxide film formed on Ni-Cr alloy has a double layer structure, consisting of Ni hydroxide and Cr oxide at an outer part, and Cr oxide, NiO and some metallic Ni at an inner part. Furthermore, it was revealed that Cr depleted metallic layer were present beneath the oxide layer. Lim et al.[15] examined passive films formed on Ni-Cr alloys in 0.1M NaCl solution. They reported that passive films formed on Ni-Cr alloys included only Cr oxide due to the elective oxidation of Cr and the thickness of passive films varied from 0.4 nm to 1.4 nm.

Auger Electron Spectroscopy (AES)[16] is also a widespread method for analysis of surfaces, similar to XPS. AES uses a primary electron beam to probe the surface of a solid material, which leads to the emission of Auger electrons. In AES the kinetic energy of Auger electrons is measured. Elements that are included in the material are identified and quantified from the kinetic energy and the intensity of the Auger peaks. Since the kinetic energy of Auger electron has a unique value according to an element of material, the chemical composition of substance surface can be identified. AES is very sensitive to surface layer because of the low energy of Auger electron. Therefore, AES has been also utilized to examine chemical composition of passive film. In the 1970s, many researchers started to investigate for passive films on metals and alloys using AES. Lumsden et al.[17] analyzed passive films formed on the type 316 stainless steel. Bouyssoux et al.[18] reported anodic passive films on Cr. Analysis of anodic oxide films on Fe was carried out by Seo et al.[19]. Since then the passive films formed on Ni-based alloys were also studied by the AES analytical technique. For Ni-Cr alloys, Boudin et al.[20] examined passive films formed on Ni-Cr alloys in a borate buffer solution. Very thin films (less than 2.5 nm) were formed in the borate buffer solution showing a layered structure where a minor outer Ni oxy-hydroxide layer was grown, covering an inner protective barrier mainly composed of Cr oxide. Ries et al.[21] studied passive films formed on Alloy 600 in an acidic solution. It

was reported that passive films were extremely thin and composed of an inner Cr oxide layer and an outer iron-nickel mixed oxide layer. The film thickness of the passive films was found to be independent of the passivation potential.

These demonstrate that XPS and AES are powerful analytical techniques to examine passive films formed on metal and alloy surfaces. When the passive films are analyzed using the ex-situ analytical techniques, however specimen must be taken out of solution. This can denature the structure and composition of passive films. In addition, although interactions between a metal and a solution are essentially electrochemical reaction, the ex-situ techniques are not able to provide information concerning the transfer of electrons and ions. Therefore, passive films have been studied also with in-situ techniques. The following sections give description on in-situ techniques that have been applied for a passivity research.

1.2.2 In-situ analytical techniques - the photoelectrochemical response and the electrochemical impedance spectroscopy

The photoelectrochemical response is originated from the Becquerel effect where the light effect on electrochemistry was reported for the first time[22]. In the field of corrosion science the effect of light irradiation was reported by Kruger for Cu in a neutral solution[23]. In the 1950s and 1960s, the photoelectrochemical response, that is, photoelectrochemistry, was applied for compound semiconductors and oxide semiconductors in aqueous solutions[24)-29)]. The application of photo effect to characterize passive films formed on metals and alloys has been also reported since the early 1960s. The photoelectrochemical response was firstly applied for passivity research by Oshe et al.[30]. Since the first report by Oshe et al., many researchers have applied the photoelectrochemical response to passivity studies[31)-33)]. For examples, passive films on Fe and Ni were analyzed using the

photoelectrochemical response in detail by Hackerman et al. Stimming et al. also discussed correlation between the photoelectrochemical response and the electrochemical impedance spectroscopy obtained from passive films on Fe[34]. Transient behavior observed in photocurrent was investigated by Peter et al. for passive films on Fe[35]. In literatures the photoelectrochemical response for passive films formed on Ti[36)-41)], Nb[38)], Zr[40)-44)], Al[45)-49)], W[50)], Ta[51)], Zn[40), 41), 52)], Sn[40), 41), 53)-56)], Cu[40), 41), 57)], Fe[31), 58)-63)], Cr[62), 64)-67)] and Ni have been reported so far.

The photoelectrochemical response reveals semiconductive nature of passive films[68-71)]. For examples, information on the band gap energy of passive films and band bending can be obtained by measuring current changes induced by photo irradiation. When a passive film is irradiated with light with energy larger than its band gap energy, electron-hole pairs are generated. Then, electron-hole pairs are separated along potential gradient in space charge layer. When a band bending is created as shown in Fig. 1-1, holes delivered to electrolyte cause the oxidation while electrons migrate to the bulk material. Thus anodic photocurrent is generated. On the other hand, when a band bending is created as shown in Fig. 1-2, electrons and holes move towards electrolyte and bulk material, respectively. Thus a cathodic photocurrent can be obtained. When applied potential is varied, band bending is also changed. As a result, potential dependence of photocurrent is different depending on type of semiconductor, that is, for n-type semiconductor, photocurrent increases in the anodic direction with increasing applied potential whereas for p-type semiconductor, photocurrent increases in the cathodic direction with decreasing applied potential. Therefore, the photoelectrochemical response can reveal the band gap energy of passive films and their type of conduction.

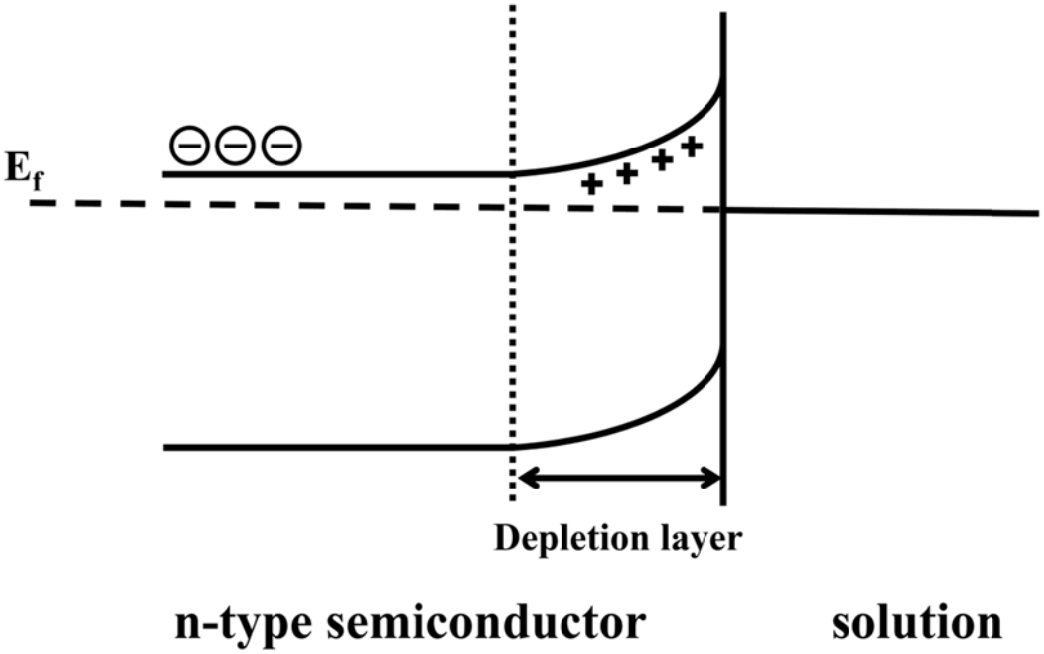

Fig. 1-1 Schematic illustration of the formation of a junction between n-type semiconductor and solution.

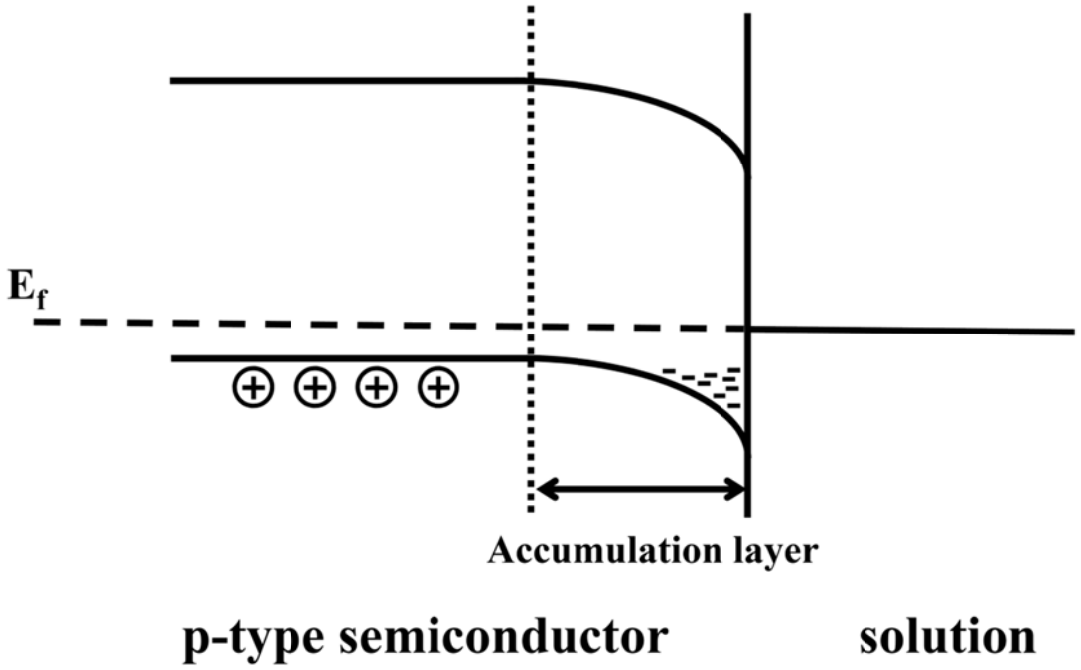

Fig. 1-2 Schematic illustration of the formation of a junction between p-type semiconductor and solution.

The electrochemical impedance spectroscopy (EIS) is also useful method for investigating electrochemical reactions and passive surfaces, in particular, very important information on electronic properties of passive film can be obtained. The first attempt to define the term "impedance" was achieved by Oliver Heaviside in the late 19th century[72]. E. Warburg[73] extended the concept of impedance to electrochemical system. He proposed that the interface could be represented by a polarization resistance in series with a polarization capacitor. After Warburg applied the impedance to electrochemical system, impedance analysis has been widely used to investigate kinetics or mechanism of passive state for the reaction on the surface of metals. When a semiconductor electrode is exposed to an electrolyte, the space charge layer is generated inside the semiconductor electrode at the interface between the electrolyte and the semiconductor electrode. The change of the applied potential leads to the variation of the space charge layer thickness. This results in the change of capacitance. From the value of impedance, therefore, the capacitance of passive film can be obtained. The obtained capacitance of passive film is analyzed by the theoretical Mott-Schottky approach, which establishes the following relationship between the capacitance and the applied potential,

$$\frac{1}{C^2} = \frac{2}{\varepsilon\varepsilon_0 qN}\left(E - E_{fb} - \frac{kT}{q}\right), \tag{1.1}$$

where N represents the carrier density, ε is the dielectric constant of the passive film, ε_0 is the vacuum permittivity, q is the elementary charge, k is the Boltzman constant, T is the absolute temperature and E_{fb} is the flat band potential. From Mott-schottky approach, the flat band potential of passive film and carrier concentration (donor or acceptor) can be estimated.

1.3 Characteristics of passive films formed on Ni-based alloys at room temperature

As described above, passive films have been extensively studied for various metals and alloys. The present section gives brief review on characteristics of passive films formed on pure Ni and Ni-base alloys at room temperature reported previously in literatures.

Wilhelm et al.[58] reported that the passive film formed on pure Ni in a pH 8.4 borate buffer solution behaved as p-type semiconductor with the band gap energy of 3.1 eV. Ohtsuka et al.[74] estimated the band gap energy of the passive films formed on pure Ni in a pH 0.9 sulfuric acid solution and a borate buffer solution as of 2.95 ~ 3.10 eV. Sunseri et al.[75] investigated the photoelectrochemical response for the passive films on pure Ni in pH 8.4 and pH 8.9 buffer solutions and proposed a duplex structure consisting of inner anhydrous layer with band gap energy of approximately 3.45 eV and the outer hydrated oxide layer with approximately 3.0 eV. Kwon et al.[76] also suggested a p/p heterojunction duplex structure consisting of inner NiO layer with the band gap energy of about 4.8 eV and outer $Ni(OH)_2$ layer with 3.05 eV as an electronic band structure model of the passive films formed on pure Ni in a pH 8.5 borate buffer solution as shown Fig. 1-3.

Passive films formed on Ni-Cr alloys have been also examined. For examples, T. Jabs et al.[77] reported that the passive films formed on Ni-20Cr and Ni-24Cr alloys in 1M NaOH solution have a duplex structure consisting of outer hydroxide and inner oxide part as shown Fig. 1-4. Bojinov et al.[78] studied the passive film formed on Ni-10Cr, Ni-15Cr and Ni-20Cr alloys in 0.1M $Na_2B_4O_7$ solution and reported that when Cr content was lower than 15 wt%, the passive films are similar to that of Ni. On the other band, they resembled that of Cr when Cr content is higher than 15 wt%. Boudin et al.[20] investigated the passive films formed on Ni-(0-30)Cr alloys in pH 9.2 borate buffer solution. The passive films were suggested to be a duplex structure which consisted of mainly inner Cr_2O_3 and minor

outer $Ni(OH)_2$ or Ni oxy-hydroxide. However the inner layer was composed of Ni oxide and Cr oxide when Cr content in the alloy was below 15 wt%. Lim et al.[15] reported that the passive films formed on Ni-10Cr, Ni-20Cr and Ni-40Cr alloys in 0.5M NaCl solution was composed of single layer with Cr_2O_3.

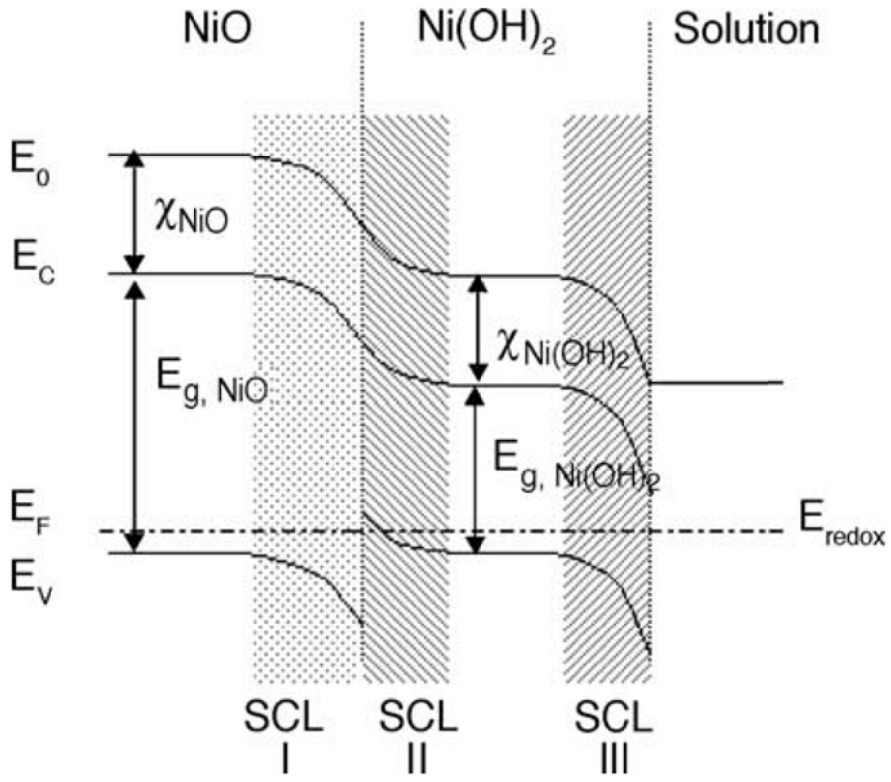

Fig. 1-3 A schematic presentation for the electronic energy band model of passive film formed on pure Ni at equilibrium. *E*c and *E*v are the electronic energy level of the conduction band and valance band, respectively. E_0 is vacuum level, E_F is Fermi level of each compound, and E_{redox} is redox potential of the electrolyte, χ_{NiO} and $\chi_{Ni(OH)_2}$ are electron affinities of NiO and $Ni(OH)_2$, respectively[76].

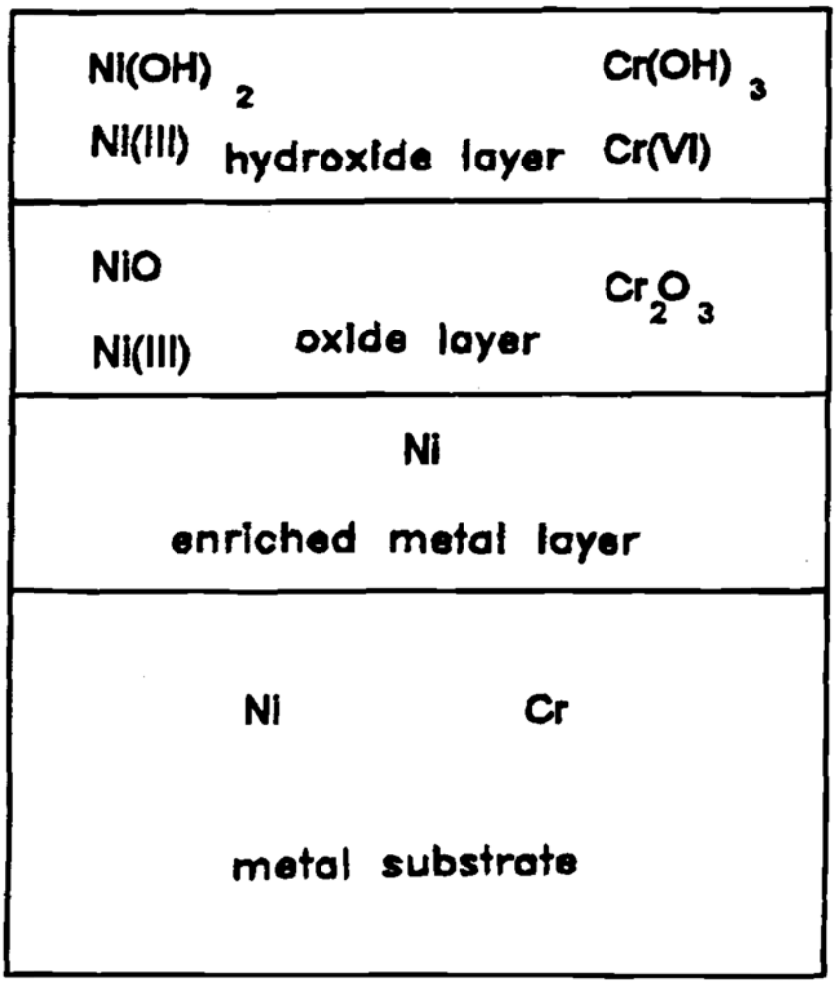

Fig. 1-4 A schematic presentation for the layer model of passive films formed on Ni-Cr alloys[77].

1.4 Characteristics of passive films formed on Ni-based alloys at high pressure and high temperature water

As described in the previous section passive films formed on Ni-based alloys have been extensively studied. As Ni-based alloys are often used in high temperature environment due to their high corrosion resistance, furthermore, passive films formed on Ni-based alloys at high temperature and pressure water were have been also investigated.

Bojinov et al.[79] measured the electrochemical behavior of oxide films formed on Ni-10Cr alloy, Ni-15Cr alloy and Ni-20Cr alloy at elevated temperatures such as 200°C and 300°C in 0.1M $Na_2B_4O_7$ solution and indicated that the electrochemical behavior changed from Ni-like to Cr-like when Cr content in Ni alloy was over 15 wt%.

Marchetti et al.[80] estimated semiconductive properties of the passive films formed on Ni-30Cr alloy, Alloy 600 and Alloy 690 at high temperature and high pressure water (pressurized water reactor, PWR). From the photoelectrochemical response, three different band gap energies, 2.2, 3.5 and 4.1 ~ 4.5 eV were obtained, attributed to the presence of Ni hydroxide and/or Ni ferrite, Cr_2O_3 and the spinel phase of $Ni_{1-x}Fe_xCr_2O_4$ with band gap in the range of 4.1 ~ 4.5 eV.

Belo et al.[81] studied that the oxide films formed on Alloy 600 and Alloy 690 in high temperature aqueous environments. In the Alloy 690, the semiconductive properties of chromium oxide and Fe, Ni oxide appeared at the inner and outer layers of the passive film, respectively at pH 8 and 10. In the Alloy 600, on the other hand, semiconductive properties of the passive film formed at pH 10 were originated from Ni oxide whereas for those of the passive film formed at pH 8 arose from Fe, Ni oxide. Passive films formed on Alloy 600 and Alloy 690 at pH 8 exhibited same band gap energy of 2.4 eV. In the case of pH 10, however, the band gap energy (2.9 eV) of the passive film formed on Alloy 600 was different from that (2.4 eV) of the passive film formed on Alloy 690.

Montemor et al.[82] reported the electronic band structure of oxide films formed on Alloy 600 and Alloy 690 in high temperature aqueous environments. The oxide films formed on Alloy 600 at pH 8 consisted of Fe, Ni oxides with n-type semiconductive property. In the case of pH 10, oxide films on Alloy 600 were composed of Ni oxide with p-type semiconductive property. On the other hand, oxide films formed on Alloy 690 at pH 5 and 8 consisted of inner Cr oxide with p type and outer Fe oxide with n-type semiconductive property.

Huang et al.[83] studied that electrochemical properties of the passive films formed on Alloy 690 in high temperature aqueous environments depended strongly on pH of solutions. In case of acidic solutions (low pH), the passive films on the alloy were mainly composed of p-type Cr_2O_3 and n-type Fe_2O_3 or hydroxides. Ni oxide was not formed due to the selective dissolution of Ni. On the other hand, in alkaline solutions (high pH), the passive films consisted of Cr_2O_3 and $FeCr_2O_4$ below the flat band potential and Ni oxide and $NiFe_2O_4$ above the flat band potential on the other hand. The semiconductive behavior of the passive films was discussed using an n-p-n heterojunction model.

Han et al.[84] investigated passive films on Alloy 690 in alkaline solutions at the temperature range from 25 to 300 °C. It was reported that the passive current density and donor density of passive films increased with increasing temperature. However, solution temperature did not affect the chemical composition and electronic structure of the passive films.

1.5 The purpose and structure of this thesis

As mentioned in the previous sections, semiconducting properties of passive films formed Ni-Cr alloys have been extensively studied using the photoelectrochemical response and the electrochemical impedance spectroscopy. Due to difficult of the in-situ measurements and the analysis of results, however, semiconductive nature of passive films on Ni-Cr alloys has not been fully understood. Furthermore how the chemical composition of substrate and the environments affect the semiconductive nature of passive film has not been clarified. Therefore the present thesis examines semiconductive properties of passive films formed on Ni-based alloys in various environments. This thesis consists of 6 chapters.

Chapter 1 gives background and purpose of this work.

In Chapter 2, semiconductive properties of passive films formed on pure Ni and various Ni-Cr alloys in sulfuric acid and borate buffer solutions are studied using the photoelectrochemical response.

Chapter 3 shows how chemical composition of the passive film formed on Ni-based alloys varies depending on pH of solution and affects resulting semiconducting properties.

Chapter 4 provides information on semiconductive properties of passive films formed on Ni-based alloys in high pressure and high temperature water environment.

In Chapter 5, oxide films on Alloy600 and Alloy690 formed in the simulated pressurized water reactor primary water environment are characterized using hard X-ray photo electron spectroscopy (HAX-PES).

In Chapter 6, the findings of the thesis are summarized and some further perspectives are outlined.

References:

1. D. D. Macdonald, J. Electrochem. Soc., **139** (1992) 3434.

2. N. Sato, Corros. Sci., **42** (2000) 1957.

3. P. Schmuki and H. Böhni, J. Electrochem. Soc., **139** (1992) 1908.

4. D. H. Hur, Corrosion, **59** (2003) 203.

5. F. Di Quarto and M. Santamaria, Corros. Eng. Sci. Technol., **39** (2004) 71.

6. K. Siegbahn, Nova Acta Regiae Soc. Sci., Ser IV, Vol. **20** (1967).

7. A. Einstein, Ann. Physik, **17** (1905) 132.

8. H. Hertz, Ann. Physik **31** (1887) 983.

9. G. Okamoto, Corros. Sci., **13** (1973) 471.

10. K. Asami, K. Hashimoto and S. Shimodaira, Corros. Sci., **18** (1978) 151.

11. K. Asami and K. Hashimoto, Corros. Sci., **19** (1979) 1007.

12. J. E. Castle and D. C. Epler, Suf. Sci., **53** (1975) 286.

13. S. C. Tjong, Mat. Res. Bull., **17** (1982) 1297.

14. S. P. Jeng, P. H. Holloway and C. D. Batich, Suf. Sci., **227** (1990) 278.

15. A. S. Lim and A. Atrens, Appl. Phys. A., **54** (1992) 343.

16. C. C. Chang, Surf. Sci., **25** (1971) 53.

17. J. B. Lumsden and R. W. Staehle, Scr. Metall., **6** (1972) 1205.

18. G. Bouyssoux, M. Romand, H. D. Polaschegg and J. T. Calow, J. Electron spectrosc. Relat. Phenom., **11** (1977) 185.

19. M. Seo, M. Sato, J. B. Lumsden and R. W. Staehle, Corros. Sci., **17** (1977) 209.

20. S. Boudin, J-L. Vignes, G. Lorang, M. Da Cunha Belo, G. Blondianux, S. M. Mikhailov, J. P. Jacobs and H. H. Brongersma, Surf. Interface Anal., **22** (1994) 462.

21. L. A. S. Ries, M. Da Cunha Belo, M. G. S. Ferreira and I. L. Muller, Corros. Sci., **50** (2008) 676.

22. A. E. Becquerel and C. R. Hebd. Sèan. Acad. Sci., 9, 58, **561** (1839) 711.

23. J. Kruger, J. Electrochem. Soc., **106** (1959) 847.

24. W. H. Brattain and C. G. B. Garrett, Bell System Tech. J., **34** (1955) 129.

25. W. W. Gärtner, Physical Rev., **116** (1959) 84.

26. H. U. Harten, J. Phys. Chem. Solids, **14** (1960) 220.

27. H. R. Schöppel, H. Gerischer and Ber. Bunsenges. Phys. Chem., **69** (1965) 578.

28. H. Gerischer, J. Electrochem. Sci., **113** (1966) 1174.

29. W. C. Tennant, J. Phys. Chem., **72** (1968) 1078.

30. K. E. Oshe and I. L. Rosenfeld, Electrokhim., **4** (1968) 1200.

31. S. M. Wilhelm, K. S. Yun, L. W. Ballenger and N. Harkerman, J. Electrochem. Soc., **126** (1979) 419.

32. E. Angelini, M. Maja and P. Spinelli, J. Physique, **38**, (1977) C5-261.

33. W. paatsch, Proc. 7th Int. Cong. Met. Corr., Rio de Haneiro, **1** (1978) 213.

34. U. Stimming, Proc. Of Int. Conf. On Passivity of Metals and Semiconductors, Ed. by M. Froment **477** (1983).

35. L. M. Peter, J. Li and R. Peat, J. Electroanal. Chem., **165** (1984) 29.

36. K. Leitner, J. W. Schultze and U. Stimming, J. Electrochem. Soc., **133** (1986) 1561.

37. J. R. Birch and T. D. Burleigh, Corrosion, **56** (2000) 1233.

38. S. Cattarin and M. Musiani, J. Electroanal. Chem., **571** (2001) 101.

39. A. W. E. Hodgson, Y. Mueller, D. Forster and S. Virtanen, Electrochim. Acta, **47** (2002) 1913.

40. T. D. Burleigh, Corrosion, **45** (1989) 464.

41. T. D. Burleigh, Corros. Sci., **31** (1990) 745.

42. A. Goossens, M. Vazquez and D. D. Macdonald, Electrochim. Acta, **41** (1996) 47.

43. F. Di Quarto, S. Piazza, C. Sunseri, M. Yang and S.-M. Cai, Electrochim. Acta, **41** (1996) 2511.

44. M. Okui, T. Nishizaki, M. Uno, K. Kurosaki, S. Yamanaka, K. Takeda and H. Anada, J. Allys Comp., **330-332** (2002) 645.

45. S. Menezes, R. Haak, G. Hagen and M. Kendig, J. Electrochem. Soc., **136** (1989) 1884.

46. F. Di Quarto, C. Gentile, S. Piazza and C. Sunseri, J. Electrochem. Soc., **138** (1991) 1856.

47. T. D. Burleigh, Materials Science Forum, **185-188** (1995) 447.

48. S. Lopez, J.-P. Petit, H. M. Dunlop, J.-R. Butruille and G. Tourillon, J. Eletrochem. Soc., **145** (1998) 823.

49. S. Piazza, G. L. Biundo, M. C. Romano, C. Sunseri and F. Di Quarto, Corros. Sci., **40** (1998) 1087

50. F. Di Quarto, A. Di Paola and C. Sunseri, Electrochim. Acta, **26** (1981) 1177.

51. F. Di Quarto, C. Gentile, S. Piazza and C. Sunseri, Corros. Sci., **35** (1993) 801.

52. P. Scholl, X. Shan, D. Bonham and G. A. Prentice, J. Electrochem. Soc., **138** (1991) 895.

53. T. D. Burleigh and H. Gerischer, J. Electrochem. Soc., **135** (1988) 2938.

54. C. A. Moina, F. E. Varela, L. F. Hernández, G. O. Ybarra and J. R. Vilche, J. Electroanal. Chem., **427** (1997) 189.

55. S. Kapusta and N. Hackerman, Electrochim. Acta, **25** (1980) 1001.

56. C. A. Monia and G. O. Ybarra, J. Electroanal. Chem., **504** (2001) 175.

57. T. D. Burleigh and R. M. Latanision, Corrosion, **43** (1987) 471.

58. S. M. Wilhelm and N. Hackerman, J. Electrochem. Soc., **128** (1981) 1668.

59. K. Azumi, T. Ohtsuka and N. Sato, Corros. Sci., **31** (1990) 715.

60. J. S. Kim, E. A. Cho and H. S. Kwon, Corros. Sci., **43** (1997) 1403.

61. C. Sunseri, S. Piazza and F. Di Quarto, J. Electrochem. Soc., **137** (1990) 2411.

62. S. Virtanen, P. Schmuki, H. Böhni, P. Vouristo and T. Mäntylä, J. Electrochem. Soc., **142** (1995) 3067.

63. M. Büchler, P. Schmuki, H. Böhni, T. Stenberg and T. Mäntylä, J. Electrochem. Soc., **145** (1998) 378.

64. F. Di Quarto, S. Piazza, C. Sunseri and Corros. Sci., **31** (1990) 721.

65. P. C. Searson and R. M. Latanision, Electrochim. Acta, **35** (1990) 445.

66. J. S. Kim, E. A. Cho and H. S. Kwon, Electrochim. Acta, **47** (2001) 415.

67. M. M. Huković and M. C. Cerić, J. Electrochem. Soc., **137** (1987) 2193.

68. H. Gerischer, Corros. Sci., **29** (1989) 191.

69. H. Gerischer, Corros. Sci., **29** (1989) 257.

70. H. Gerischer, Corros. Sci., **31** (1990) 81.

71. H. Gerischer, Electrochim. Acta, **35** (1990) 1677.

72. D. D. Macdonald, Electrochimica Acta, **51** (2006) 1376.

73. E. Warburg, Ann. Phys. Chem., **67** (1899) 493.

74. Y. Mito, M. Ueda and T. Ohtsuka, Corros. Sci., **51** (2009) 1540.

75. C. Sunseri, S. Piazza and F. Di Quarto, Mater. Sci. Forum, **185-188** (1995) 435.

76. H. J. Jang, C. J. Park and H. S. Kwon, Electrochim. Acta, **50** (2005) 3503.

77. T. Jabs, P. Borthen and H. H. Strehblow, J. Electrochem. Soc., **144** (1997) 1231.

78. M. Bojinov, G. Fabricius, P. Kinnunen, T. Laitinen, K. Mäkelä, T. Saario and G. Sundholm, J. Electroanal. Chem., **504** (2001) 29.

79. M. Bojinov, P. Kinnunen and G. Sundholm, Corrosion, **59** (2003) 91.

80. L. Marchetti, S. Perrin, Y. Wouters, F. Martin and M. Pijolac, Electrochim. Acta, **55** (2010) 5384.

81. M. F. Montemor, M. G. S. Ferreira, N. E. Hakiki and M. Da Cunha Belo, Corros. Sci.,

42 (2000) 1635.

82. M. F. Montemor, M. G. S. Ferreira, M. Walls, B. Rondot and M. Da Cunha Belo, Corrosion, **59** (2003) 11.

83. J. B. Huang, X. Q. Wu and E. H. Han, Corros. Sci., **51** (2009) 2976.

84. J. B. Huang, X. Q. Wu and E. H. Han, Corros. Sci., **52** (2010) 3444.

Chapter 2 Photoelectrochemical Characterization of Passive Films Formed on Ni-Cr Alloys

2.1 Introduction

Ni-Cr alloys exhibit the excellent corrosion resistance in various environments. The corrosion resistance of Ni based alloy is attributed to passive films on the surfaces. Therefore, knowledge on the chemical composition, structure and growth kinetics of passive films is important to understand corrosion behavior of the alloys. The composition and structure have been examined by using surface analytical techniques such as Auger electron spectroscopy (AES) and X-ray photoelectron spectroscopy (XPS)[1-4]. However, measurements using the ex-situ techniques may change the composition and structure of passive films because specimen should be taken out from solution and transferred into an UHV for the analysis. Therefore, it is difficult to obtain the real properties of passive films formed in aqueous solution by using the ex-situ analytical techniques. Moreover, although interactions between a metal and a solution are essentially electrochemical reaction, information concerning the transfer of electrons and ions cannot be obtained by the ex-situ techniques. It has been reported that passive films formed on various metals and alloys behave as semiconductor. The photoelectrochemical response is well known as one of in-situ techniques to study semiconductive properties of passive films[5)-9)]. As semiconductive properties of passive films have been considered to be related with corrosion resistance[10,11)], semconductive properties have been examined using the photoelectrochemical response[10,12-17)]. Although semiconductive properties of passive films on pure Ni have been extensively investigated, they have not been fully understood. Furthermore, semiconductive properties of passive films formed on Ni-Cr alloys have not been studied so much.

In the chapter 2, semiconductive properties of passive films formed on pure Ni and Ni-Cr alloys in a sulfuric acid solution and a pH 8.4 borate buffer solution were examined by the photoelectrochemical response. Some results obtained by the electrochemical impedance spectroscopy were also included.

2.2 Experimental

Materials examined were pure Ni (99.9%), Ni-8Cr and Ni-18Cr alloys. The sheets of materials were cut into specimens of 10×10×1 mm^3, connected with a wire and then embedded in an epoxy resin. The surface of specimen was polished mechanically with 2000 grit SiC paper and mirror finished with sub micron alumina pastes, followed by sonicating in ethanol, methanol and distilled water, successively. Electrochemical experiments were carried out in a three-electrode cell with a platinum counter electrode and a Ag/AgCl/ 3.3M KCl reference electrode. Electrolytes used in the present work were 0.1M H_2SO_4 and pH 8.4 borate buffer solution. Prior to electrochemical experiments, the electrolytes were deaerated for more than 12 hours with N_2 gas.

Polarization curves of specimens were measured with a scan rate of 1 mV/s. The photoelectrochemical response measurements were performed using a 150 W Xenon arc lamp with a grating monochromator. The monochromated light was irradiated on a specimen through a quarts window in the electrochemical cell. The specimen was polarized at a desired film formation potential, E_f, around the passive region of the specimens for 24 hours before the photoelectrochemical response measurements commenced. The photoelectrochemical response measurements were carried out using a potentiostat (Hokuto Denko, type-2090LN) connected to a low-pass filter (NF Electronic Instrument, E-3201B) with a threshold frequency of 4 Hz and a differential amplifier (NF Electronic Instrument, type5307). Figure 2-1 shows schematic drawing of apparatus for measurement of photocurrent. Photocurrent spectrum was measured at the film formation potential. Then the potential was changed from the film formation potential in the less noble direction stepwisely with the interval of 100 mV. Photocurrent spectra were measured also at each measuring potential, E_m. Photocurrent is defined as current change induced by light irradiation and shows some transient during irradiation. Therefore, in the present work, the

value of photocurrent was determined as current changes before irradiation and after 15s light irradiation. The wavelength of the incident light was varied from 250 to 500 nm. The electrochemical impedance was measured using a potentiostat and a frequency response analyzer with modulation amplitude of 10 mV in the frequency range of 20 kHz ~ 0.01 Hz. The impedance was measured in the similar manner to the photoelectrochemical response, that is, measured at a film formation potential and at various measuring potentials. The capacitance of space charge layer (C) was estimated from $C = -1/\omega Z''$, where ω is the angular frequency and Z'' is the imaginary part of the impedance[10].

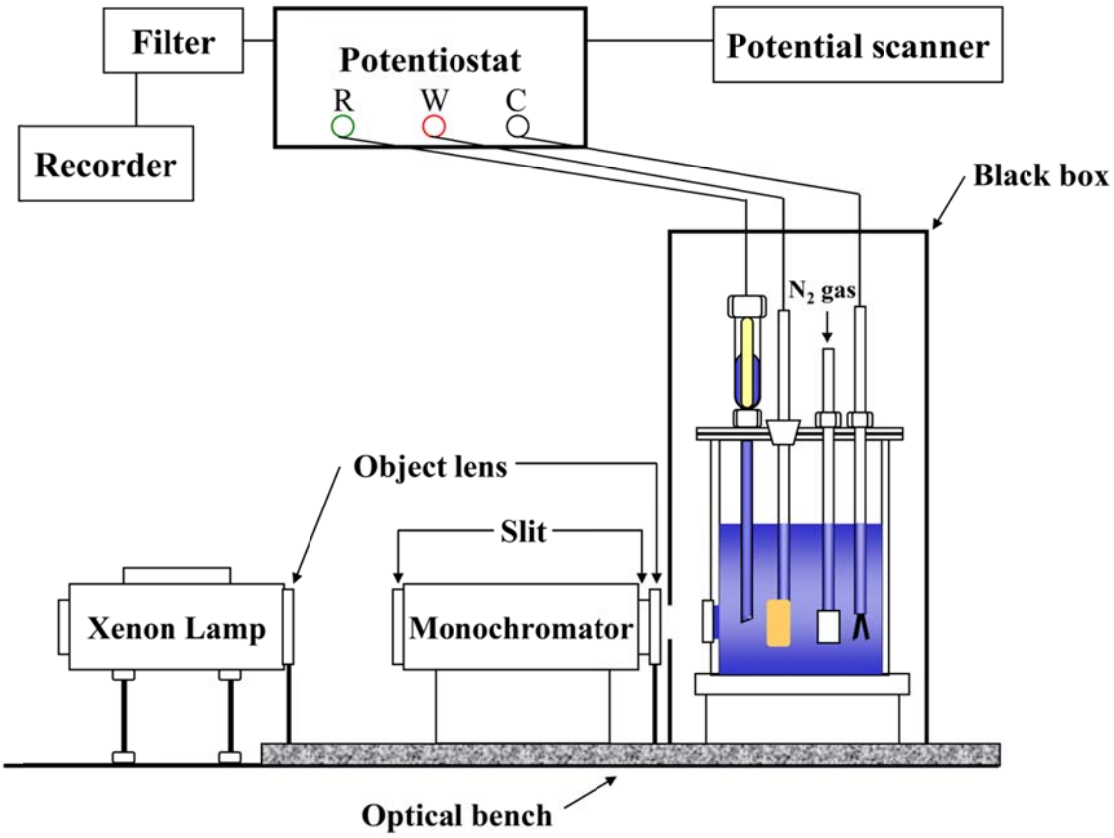

Fig. 2-1 Schematic drawing of apparatus for measurement of photocurrent.

2.3 Results

2.3.1 Polarization curves

Figures 2-2 and 2-3 show the polarization curves of pure Ni and Ni-Cr alloys measured in the sulfuric acid solution and the pH 8.4 borate buffer solution, respectively. The current density in the active and the passive regions decreases with increasing Cr content, indicating that the increase of Cr content leads to the improvement of corrosion resistance of Ni-based specimens. The increase of current density observed in the borate buffer solution in the range from approximately 500 to 900 mV is attributed to the transpassive dissolution of chromium. The current density increases again around 1000 mV by the oxygen evolution. Therefore, the passive region is located between -300 and 900 mV for pure Ni and between -400 and 400 mV for Ni-Cr alloys in the pH 8.4 borate buffer solution. In case of sulfuric acid solution, the passive regions of pure Ni located between 300 and 1100 mV and that for Ni-Cr alloys between 100 and 800 mV. Therefore, the photoelectrochemical response measurements and the electrochemical impedance measurements for passive films on pure Ni and Ni-Cr alloys were carried out around the passive regions.

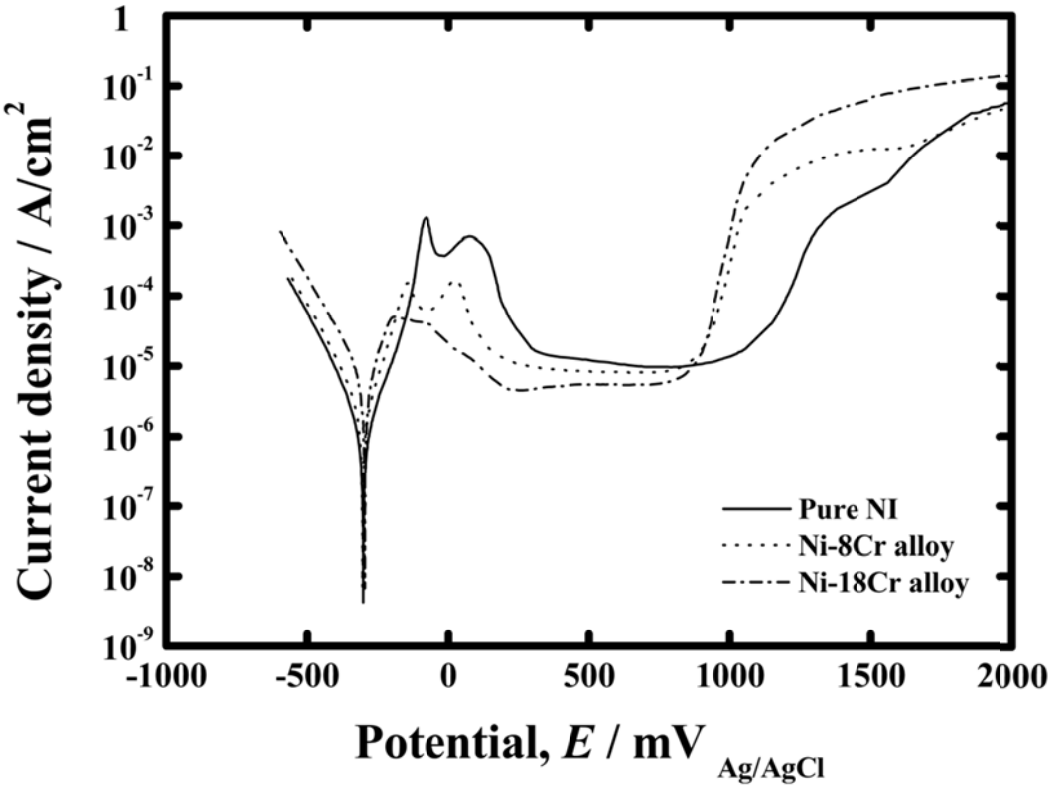

Fig. 2-2 Polarization curves of pure Ni and Ni-Cr alloys in the sulfuric acid solution.

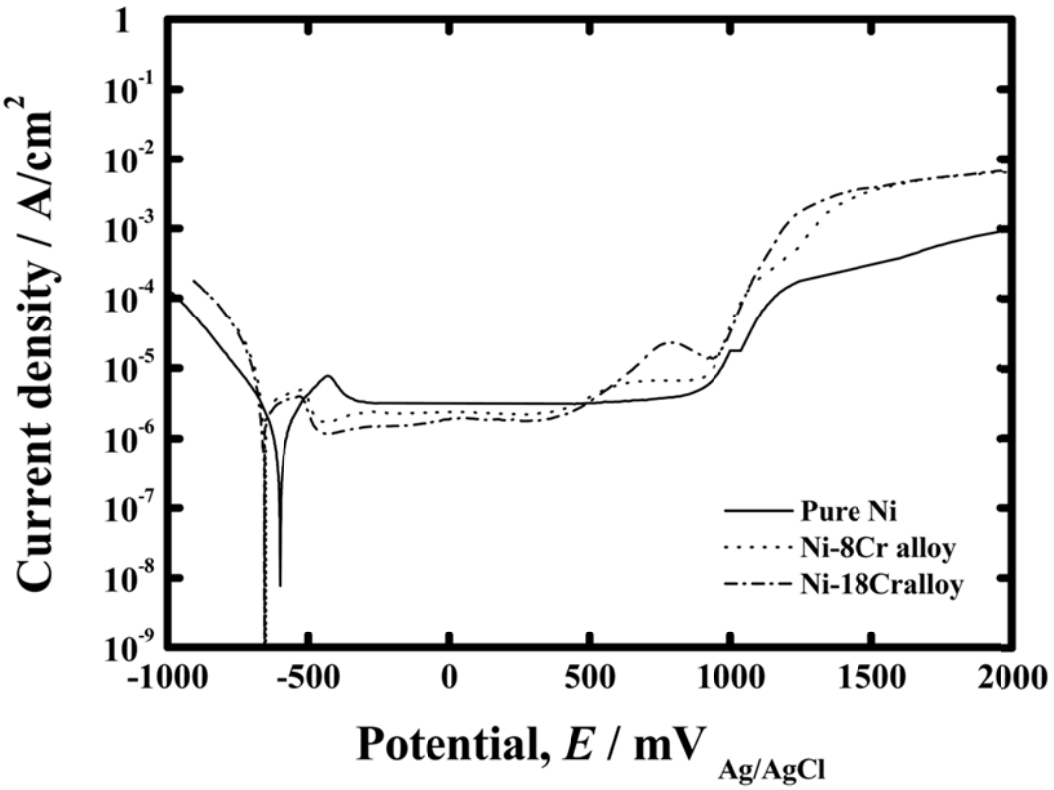

Fig. 2-3 Polarization curves of pure Ni and Ni-Cr alloys in pH 8.4 borate buffer solution.

2.3.2 Photoelectrochemical response in pH 8.4 borate buffer solution

Figure 2-4 illustrates typical photocurrent transients obtained in the present work. At lower potentials, as shown in Fig. 2-4(a), current rapidly changes in the cathodic direction just after photo irradiation commences and then during photo irradiation the current gradually increases in the cathodic direction to a steady state value. After photo irradiation is terminated the current returns back to the original level. This current behavior is observed independent of photon energy when polarized at lower potentials. At higher potentials, on the other hand, opposite photocurrent transients are obtained, that is, rapid increase of current in the anodic direction just after photo irradiation commences and subsequent gradual increase of the current during irradiation are observed as shown in Fig. 2-4(b). Photocurrent transients shown in Fig. 2-4(c) are observed only for Ni-Cr alloys at relatively higher potentials that may cause the transpassive dissolution of chromium. The shape of the transient is essentially similar to that shown in Fig. 2-4(b) except for current peaks observed just after photo irradiation commence or is terminated.

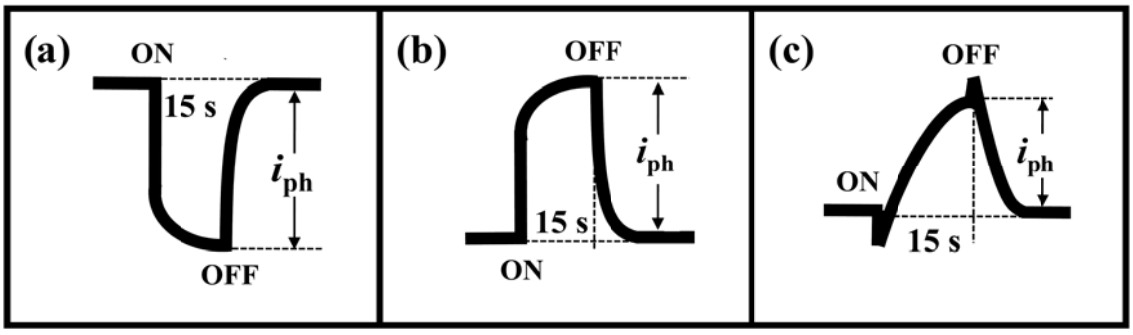

Fig. 2-4 Schematic illustration of photocurrent transients observed in the present work.

Figure 2-5 shows photocurrent spectra obtained for the passive film formed on Ni-18Cr alloy at 0 mV as a function of wavelength of incident light. As previously described, photocurrent value was determined in the present work as current change before

irradiation and after 15s light irradiation. Assuming that the photo excitation takes place as an indirect transition, which has been often reported for passive films[10),12),15),16)], photocurrent spectrum can be plotted according to Eq. (2.1) as photoelectrochemcal action spectrum

$$\left(i_{ph} \cdot h\nu / I_0\right)^{\frac{1}{2}} = C\left(h\nu - E_g\right), \tag{2.1}$$

where I_0 and $h\nu$ are the intensity and the photon energy of the incident light, respectively. E_g is the band gap energy of passive film and C is constant. Figure 2-6 shows the photoelectrochemical action spectra obtained from the photocurrent spectra shown in Fig. 2-5. It is clear that each action spectrum shows two regions with different slopes. XPS analysis revealed that passive films formed on pure Ni and Ni-Cr alloys consisted of an inner oxide layer and an outer hydroxide layer[18)]. Strehblow et al. also reported that passive films formed on Ni-Cr alloys consisted of a two-layer with an inner oxide and an outer hydroxide layer[19)]. Therefore, it can be assumed that the photocurrent was generated from both layers, that is, the observed photocurrents were a sum of responses from two components. In the present work the photocurrent spectra were separated into two. The process of spectrum separation is schematically shown in Fig. 2-7. The original spectrum fits with a straight line in the low energy region to obtain the solid line with band gap of E_{g1}. The reminder of spectrum is obtained by subtracting the solid line from the original spectrum. The reminder of spectrum similarly fits with dot line in given E_{g2}. Therefore, this spectrum can be separated into two components using the separation process[20)].

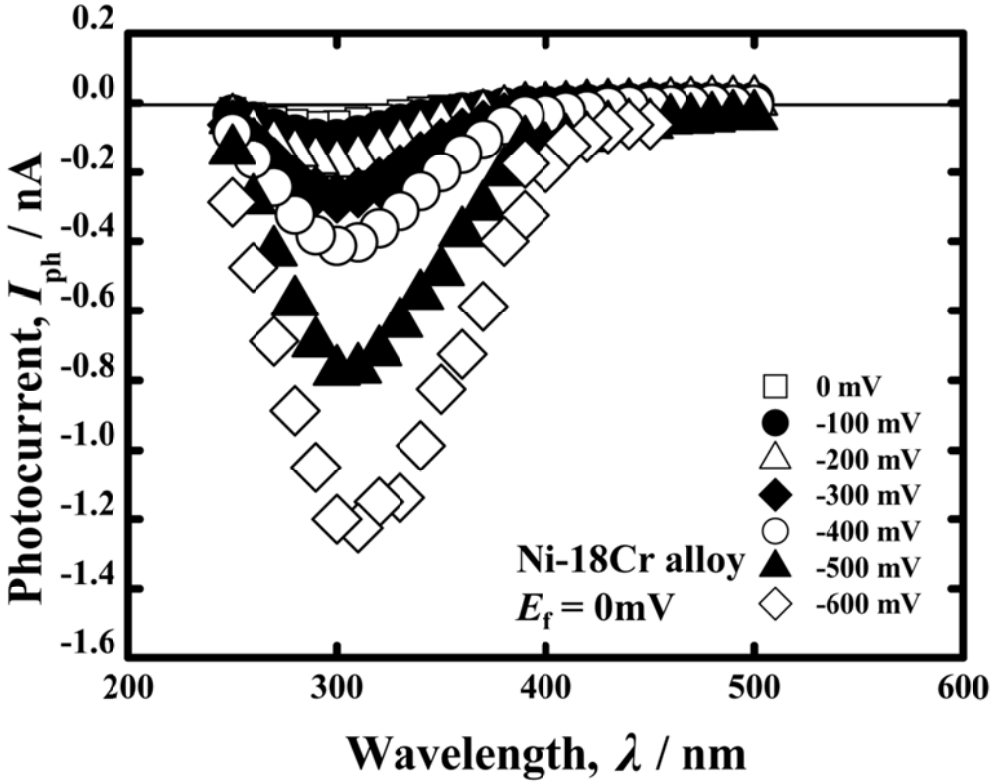

Fig. 2-5 Photocurrent spectra for the passive film formed on Ni-18Cr alloy at 0 mV in pH 8.4 borate buffer solution. The spectra were measured at various potentials.

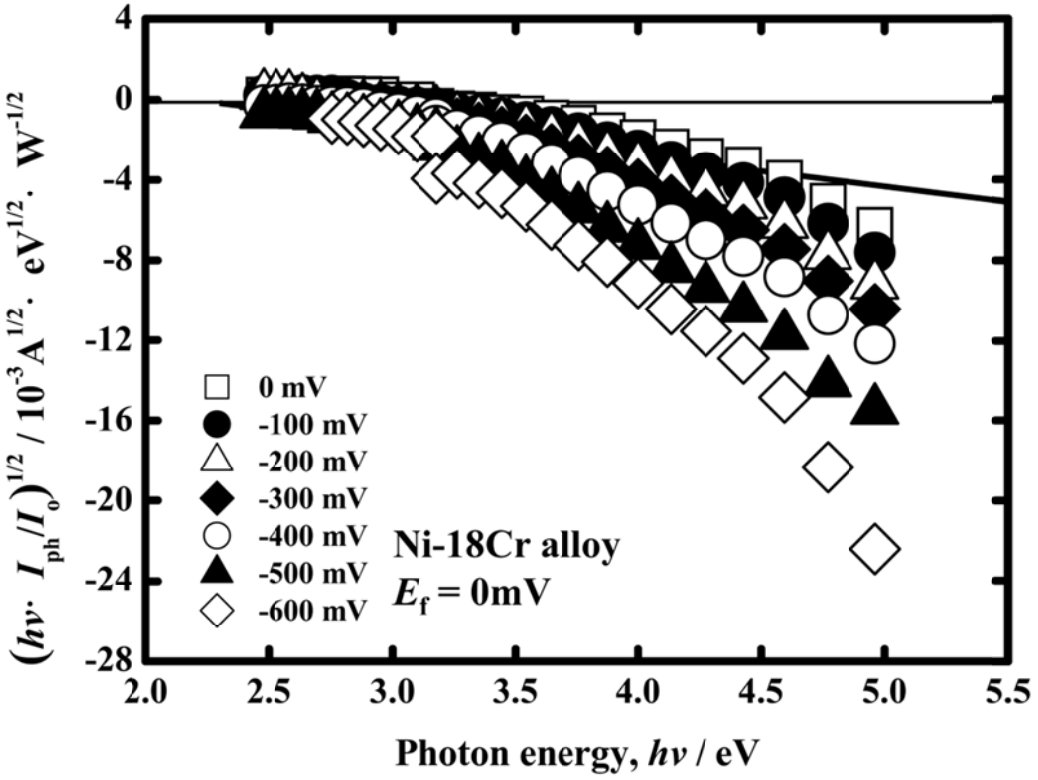

Fig. 2-6 Photoelectrochemical action spectra obtained from the photocurrent spectra shown in Fig. 2-5.

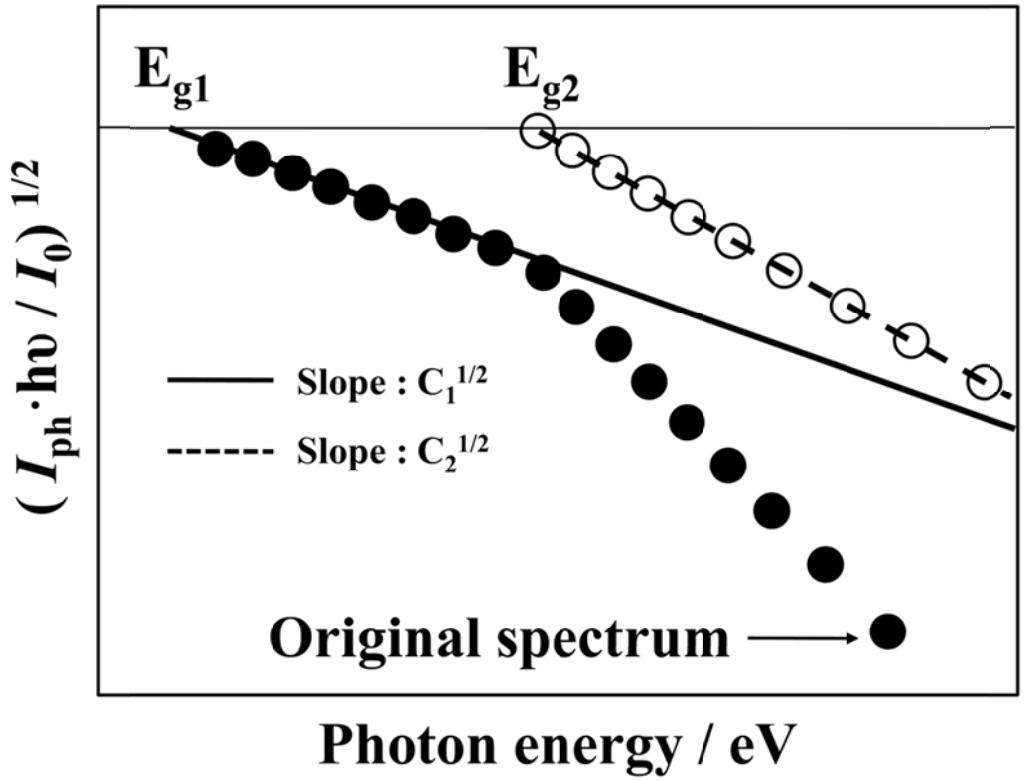

Fig. 2-7 The procedure of photoelectrochemical action spectrum.

Band gap energy was estimated as the photon energy where the $(i_{ph} \cdot h\nu / I_0)^{1/2}$ becomes zero in the photoelectrochemical action spectrum. Band gap energies for the passive film formed on Ni-18Cr alloy at 0 mV were estimated as approximately 2.3 eV and 3.5 eV. Estimated band gap energies were nearly constant for all passivation potentials, measuring potentials, and specimens examined as shown in Fig. 2-8. By referring to previous works on pure Ni[21-24], For pure Ni, the component with the band gap energy of 3.5 eV is NiO whereas that with the energy of 2.3 eV is $Ni(OH)_2$. For Ni-Cr alloys, on the other hand, XPS analysis demonstrated that passive films on Ni-Cr alloys consist mainly of an inner Cr_2O_3 and a covering $Cr(OH)_3$ layer[18] and furthermore, Quarto et al.[25] reported band gap energy of Cr_2O_3 and $Cr(OH)_3$ as approximately 3.5 eV and 2.4 eV, respectively, as shown in Fig. 2-9. Therefore the band gap energies of 3.5 eV and 2.3 eV obtained for Ni-Cr alloys from the photoelectrochemical response are attributed mainly to Cr_2O_3 and $Cr(OH)_3$, respectively. These indicate that passive films formed on pure Ni and Ni-Cr alloys in the pH 8.4 borate buffer solution can be composed of an inner oxide layer with the band gap energy of 3.5 eV and an outer hydroxide layer with 2.3 eV independent of composition of the passive films. Figure 2-10 summarizes the slope of photoelectrochemical action spectrum, *C*, for the passive films formed on pure Ni and Ni-Cr alloys as a function of measuring potential. The passive films were formed at 400 mV in the pH 8.4 borate buffer solution. It is clear that the *C* values for the oxide layers are negative for all potentials examined and the absolute value of the slope increases with decreasing applied potential. This is a typical p-type semiconducting behavior. On the other hand, *C* values obtained for the hydroxide layers are very small and increases almost linearly from negative to positive with applied potential. Such behavior is not typical for semiconductor electrode. Therefore, conduction type of semiconductor cannot be clearly determined for the hydroxide layers

only from the potential dependence of *C* value. It is also apparent from Fig. 2-10 that the *C* values obtained for the hydroxide layers are similar independent of the specimens whereas the *C* value for the oxide layer formed on pure Ni is slightly smaller than those obtained for Ni-Cr alloys. Figure 2-11 shows the potential dependence of *C* value obtained for the passive films on Ni-18Cr alloy formed at various film formation potentials. As apparent, the potential dependences in Fig. 2-11 are essentially similar to those already explained in Fig. 2-10. Therefore, the oxide layer of the passive film exhibits p-type semiconductive behavior independent of the film formation potential. However, the *C* value clearly shows difference in its amplitude, that is, the absolute *C* value increases with increasing the film formation potential. On the other hand, the *C* value is similar for all hydroxide layers formed at the film formation potentials examined. From Fig. 2-10 and 2-11, the flat band potential can be also estimated approximately as 400 mV and 200 mV for inner oxide layer and outer hydroxide layer, respectively.

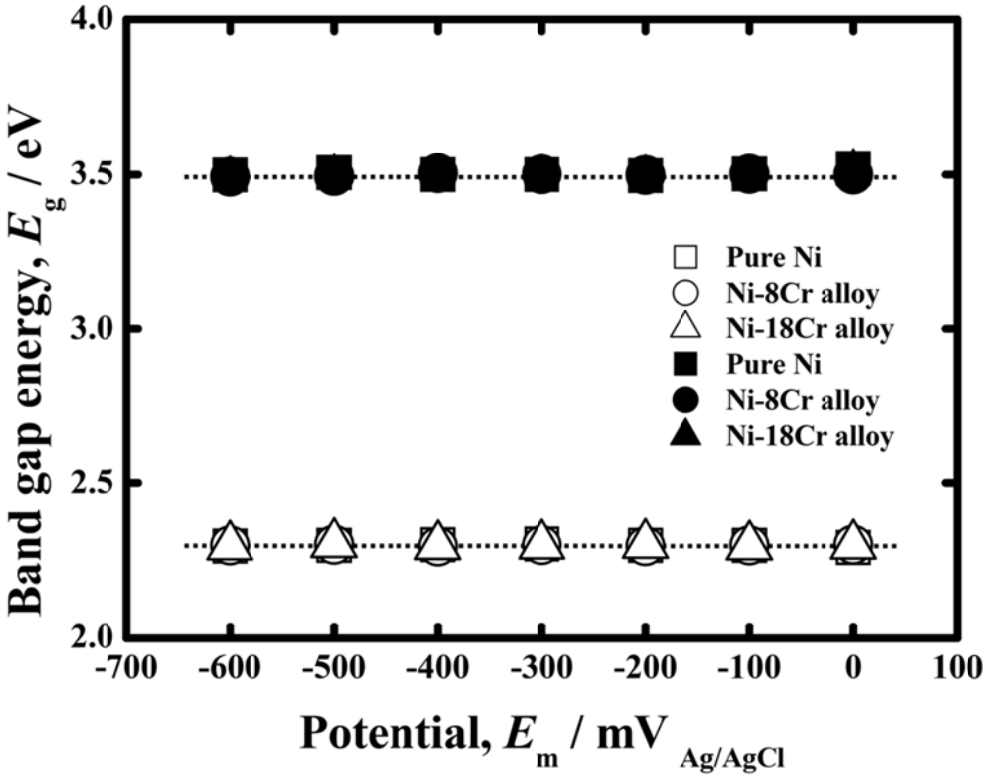

Fig. 2-8 Band gap energies of passive film formed on Ni-based alloys in the borate buffer solution.

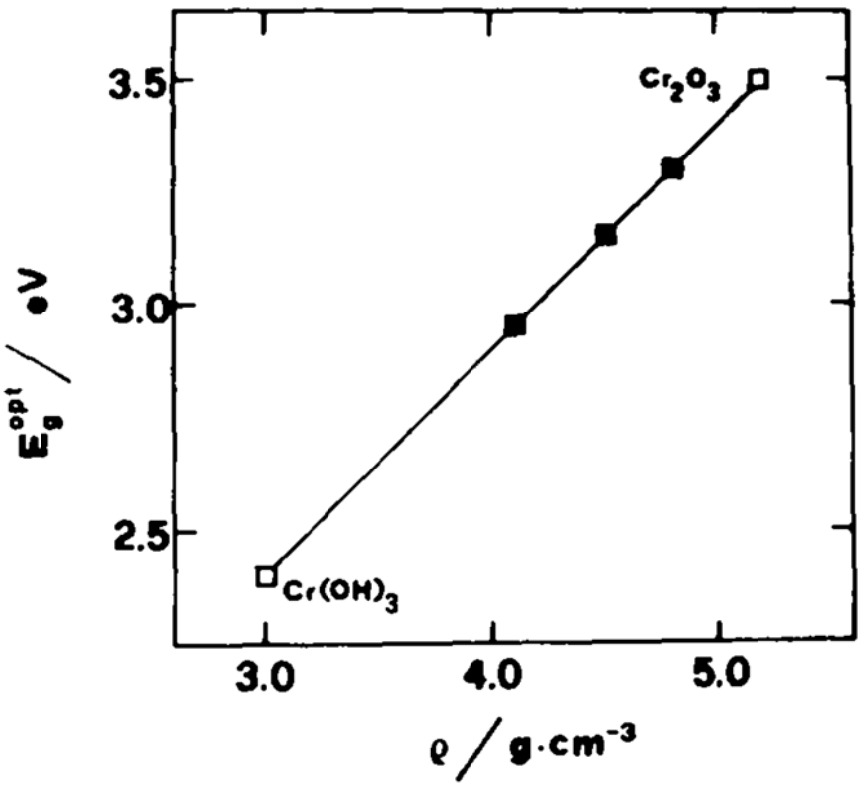

Fig. 2-9 Dependence of the optical band gap of chromium oxi-hydroxides on their density[25].

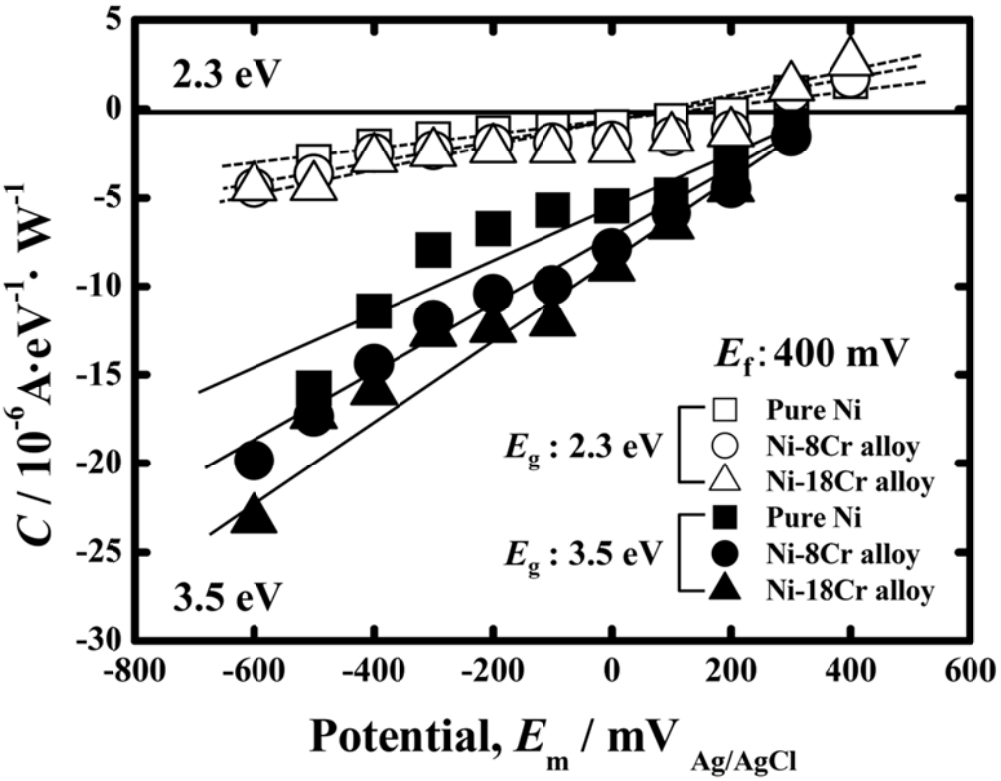

Fig. 2-10 Variations in the slopes of the photoelectrochemical action spectra, *C*, for passive films formed on pure Ni and Ni-Cr alloys in the pH 8.4 borate buffer solution.

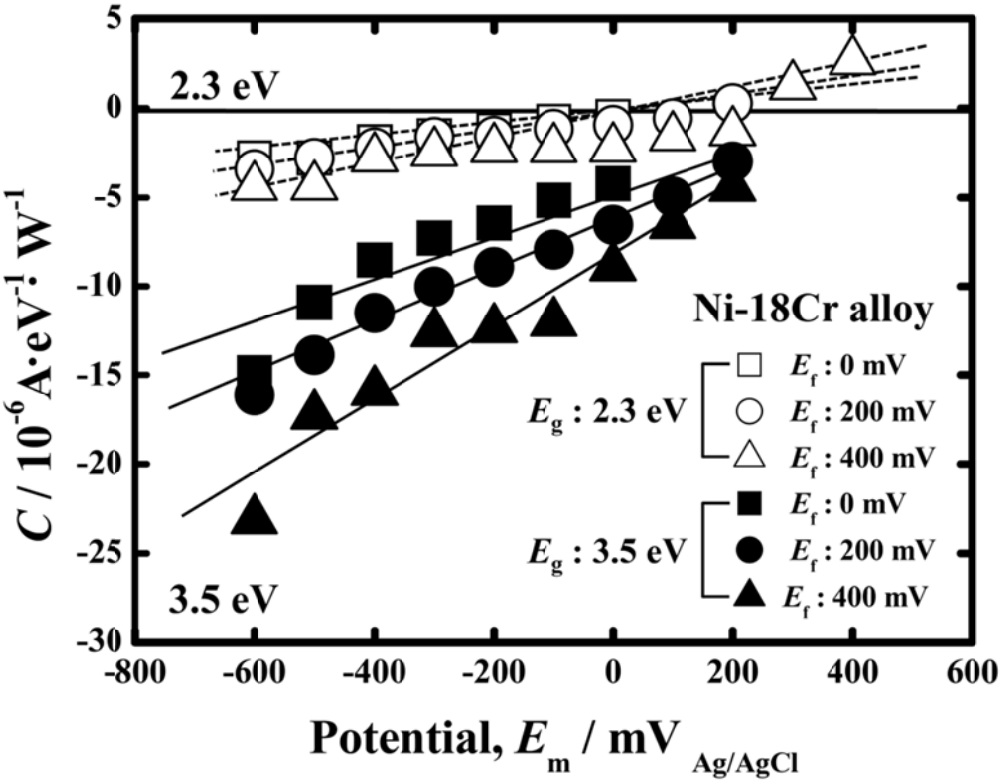

Fig. 2-11 Variations in the slopes of the photoelectrochemical action spectra, *C*, for passive films formed on Ni-18Cr alloy at various potentials in the pH 8.4 borate buffer solution.

2.3.3 Photoelectrochemical response in sulfuric acid solution

Photocurrent spectra were measured also for passive films on pure Ni and Ni-Cr alloys in the sulfuric acid solution. Similar photocurrent spectra and photoelectrochemical action spectra were obtained in the sulfuric acid solution to those in the borate buffer solution as shown Figs. 2-12 and 2-13. In the sulfuric acid solution photoelectrochemical action spectra were also separated into two components, yielding the band gap energies of 3.5 eV and 2.3 eV. Figure 2-14 shows band gap energies for passive films formed on pure Ni and Ni-Cr alloys in the sulfuric acid solution. Similar to the case of the borate buffer solution, band gap energies were independent of applied potentials and composition of the passive films. Figure 2-15 shows potential dependence of the slope of the photoelectrochemical action spectrum, *C*, for passive films formed at 700 mV in the sulfuric acid solution. Similar to the results obtained for the borate buffer solution, in the sulfuric acid solution the slope of the action spectra for oxide layer is negative for all applied potential and the absolute value clearly increases with decreasing potential whereas the slope for hydroxide layer slightly increases from negative to positive with applied potential. From Fig. 2-15, measured flat band potential were approximately as 700 mV and 450 mV for inner oxide layer and outer hydroxide layer, respectively.

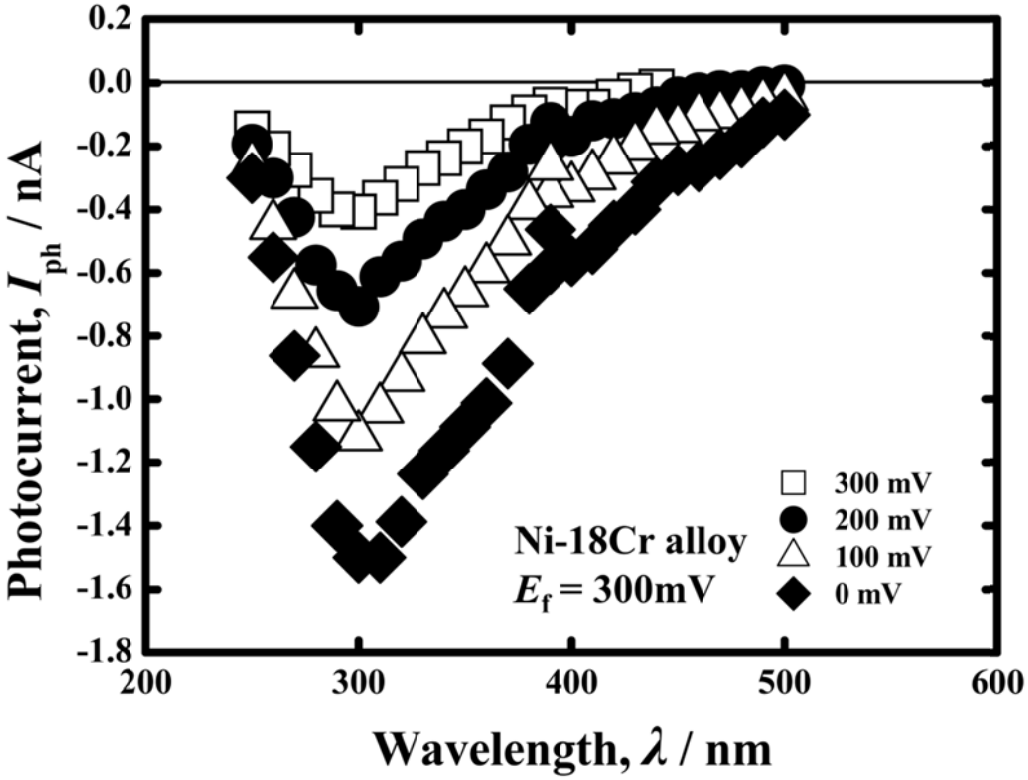

Fig. 2-12 Photocurrent spectra for the passive film formed on Ni-18Cr alloy at 300 mV in the sulfuric acid solution. The spectra were measured at various potentials.

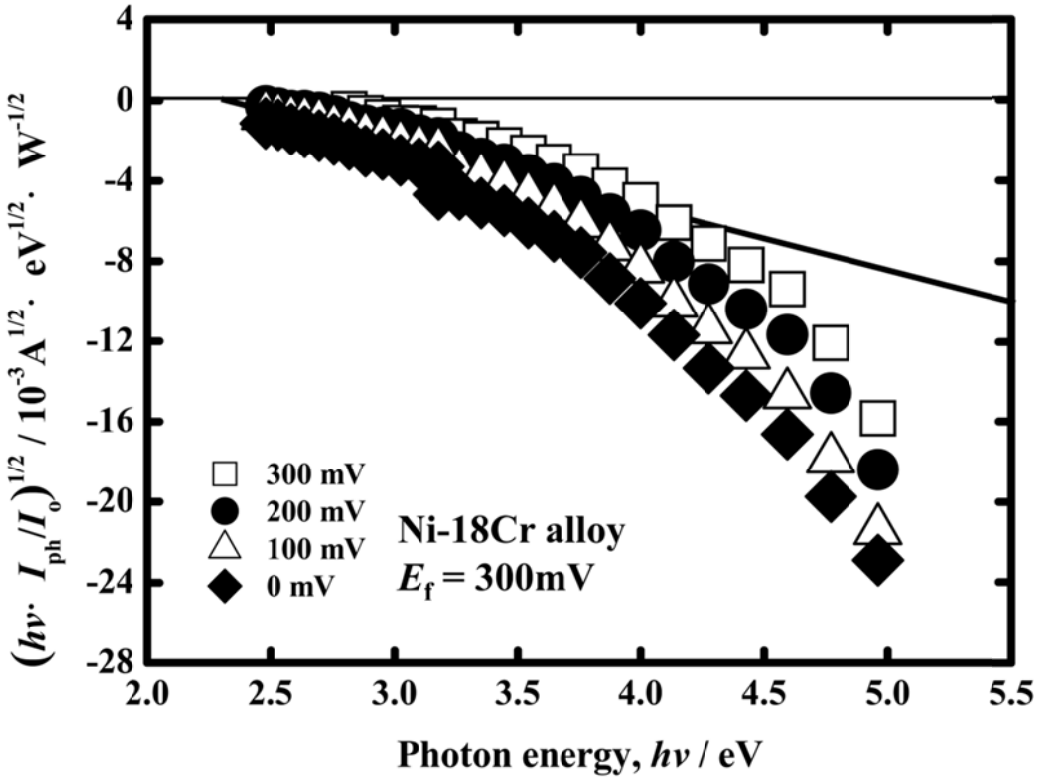

Fig. 2-13 Photoelectrochemical action spectra obtained from the photocurrent spectra shown in Fig. 2-12.

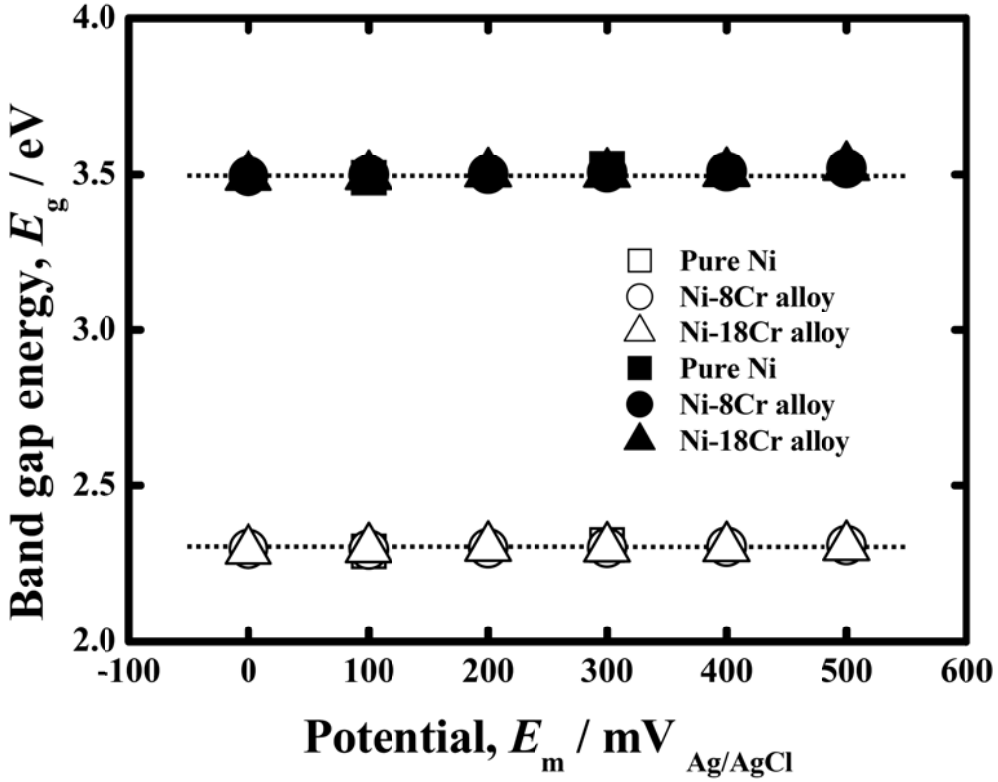

Fig. 2-14 Band gap energies of passive film formed on Ni-based alloys in the sulfuric acid solution.

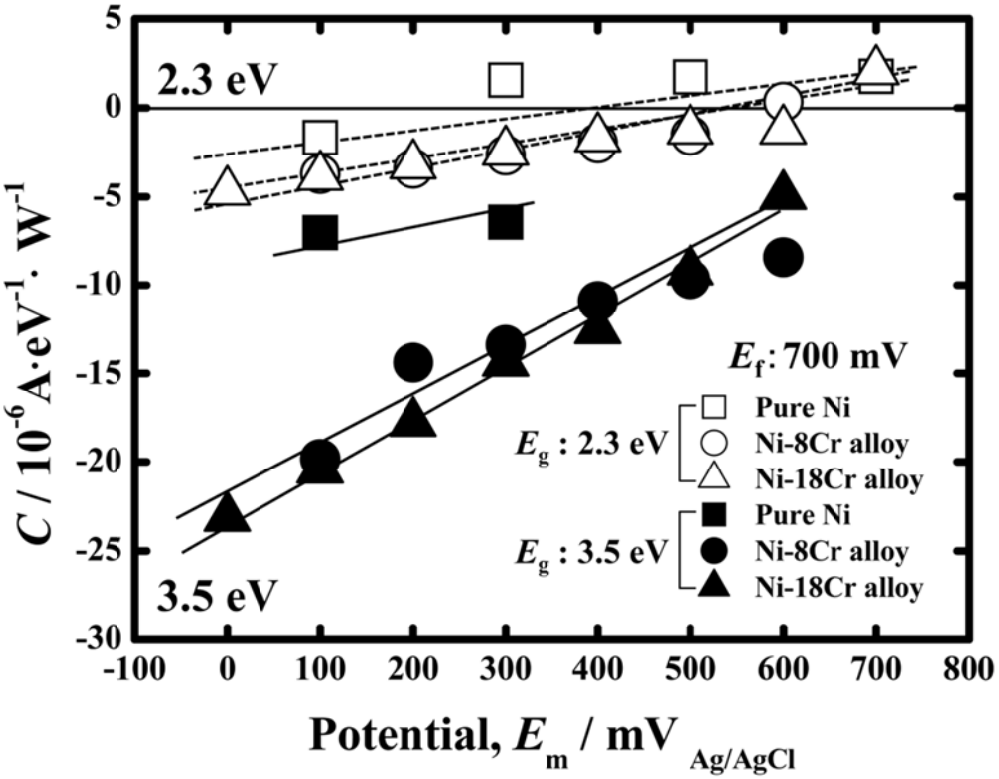

Fig. 2-15 Variations in the slopes of the photoelectrochemical action spectra, *C*, for passive films formed on pure Ni and Ni-Cr alloys in the sulfuric acid solution.

2.3.4 Electrochemical impedance spectroscopy

The electrochemical impedance was measured with similar procedure to the measurement of photocurrent response. The applied potential at which impedance was measured were sequentially shifted in the less noble direction with the interval of 100 mV. The capacitance of space charge layer of passive film was estimated from the impedance at each measuring potential with the frequency of 100 Hz. Mott-Schottky equation expresses the relation between the capacitance space charge layer and the applied potential (Eq. 2.2),

$$\frac{1}{C^2} = \frac{2}{\varepsilon\varepsilon_0 qN}\left(E - E_{fb} - \frac{kT}{q}\right), \tag{2.2}$$

where N represents the carrier density, ε is the dielectric constant of the passive film, ε_0 is the vacuum permittivity, q is the elementary charge, k is the Boltzman constant, T is the absolute temperature and E_{fb} is the flat band potential. Figure 2-16 shows the Mott-Schottky plots for the passive films formed on pure Ni and Ni-Cr alloys. The slope of Mott-Schottky plot was almost horizontal as shown in Fig. 2-16. Therefore, it is difficult to estimate the conduction type of semiconductor, defect density and flat band potential. As described in the previous section, passive films formed on Ni-Cr alloys consist of inner oxide and outer hydroxide part. In case of impedance spectroscopy measurement, the capacitance of outer part of the layer has been basically considered to be revealed. However, the width of space charge layer for outer layer of the passive film formed on Ni-Cr alloy is very thin. The width of space charge layer was not increased enough for the change of potential gradient. Therefore, the semiconductive properties could not be evaluated using Mott-Schottky plot, because capacitance was unchanged.

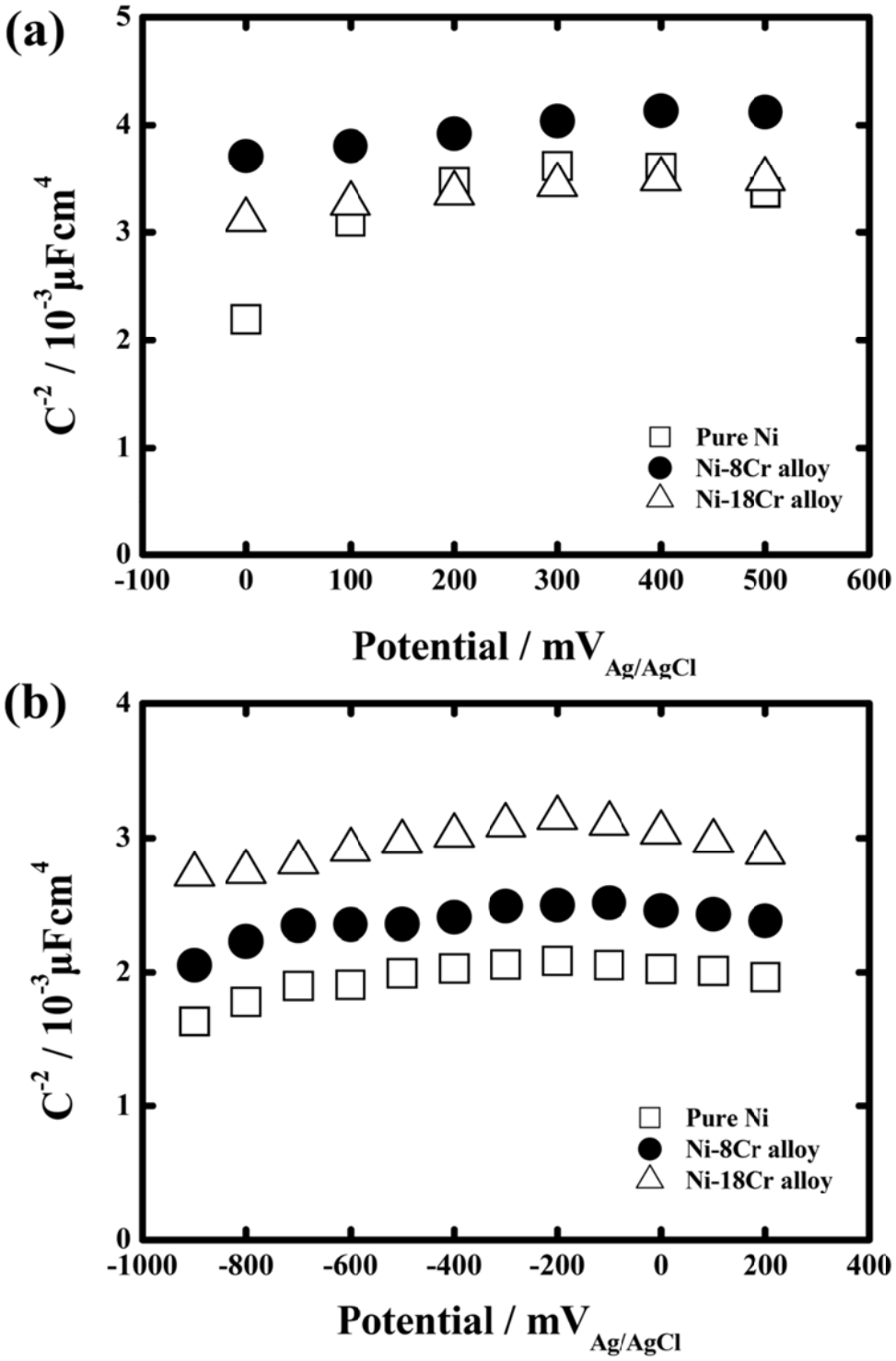

Fig. 2-16 Mott-Schottky plots for passive films formed on Ni-based alloys in (a) the sulfuric acid solution and (b) the borate buffer solution.

2.4 Discussion

2.4.1 Electronic energy band structure model and its correlation with photocurrent transient

As mentioned above, for the passive films formed on pure Ni and Ni-Cr alloys in the pH 8.4 borate buffer and sulfuric acid solutions, the band gap energy of oxide layer was obtained as 3.5 eV whereas that of hydroxide layer was estimated as 2.3 eV. The band gap energies were almost independent of film formation potential, measuring potential, and specimen. Furthermore, similar trend was also observed in the potential dependence of C value in both solutions, that is, C value for oxide layer is negative for all applied potential and its absolute value increases with decreasing potential while C value for hydroxide layer slightly increases from negative to positive with applied potential. Therefore, it is found that the oxide layers formed in the both solutions exhibit p-type semiconducting behavior. As for the hydroxide layer clear potential dependence of the C value was not observed in the both solutions, the conduction type of semiconductor could not be determined. Figure 2-17(a) and 2-17(b) summarize directions of steady state photocurrent in the potential range where the photocurrent measurements were performed in the borate buffer solution and the sulfuric acid solution, respectively. In the figure, "larger $h\nu$" means that the photo excitation occurs in both oxide and hydroxide layers whereas on "smaller $h\nu$" the excitation takes place in only hydroxide layer. It is clear that the potential range can be classified into three types; (I) only positive photocurrent is obtained independent of photon energy, (II) negative and positive photocurrents are obtained for larger and smaller photon energy, respectively, (III) only negative photocurrent is obtained. Assuming that the passive films formed on pure Ni and Ni-Cr alloys in both solutions consist of the inner p-type oxide layer with the band gap energy of 3.5 eV and the covering n-type hydroxide layer with 2.3 eV, the photocurrent transients obtained for passive films on pure Ni and

Ni-Cr alloys can be reasonably explained using an electronic band structure model. The proposed electronic band structure model is illustrated as shown in Fig. 2-18(a). In the system, there are three interfaces; (I) substrate/inner oxide layer, (II) inner oxide layer/outer hydroxide layer, (III) outer hydroxide layer/solution. The band structure varies with applied potential as shown in Fig. 2-18(b) - 2-18(e). In the potential range examined the space charge layer formed at the interface (III) is in the depleted state, and the width of the space charge layer decreases with decreasing applied potential as the outer hydroxide layer behaves as n-type semiconductor. At the interface (II) a p/n heterojunction is created as two semiconductive components with different band gap energies are connected at the interface; p-type oxide layer with the band gap energy of 3.5 eV and n-type hydroxide layer with 2.3 eV. The space charge layers created inside the p-type oxide layer (denoted as SCL(II_a) in Fig. 2-18(a)) and inside the n-type hydroxide layer (denoted as SCL(II_b) in Fig. 2-18(a)) are both in the depleted state. The width of both space charge layers increases with decreasing applied potential. At the interface(I), ohmic contact is considered to be formed. In this model, the conduction band edge and the valence band edge are assumed to be pinned at the passive film/solution interface and the potential applied to a substrate appears at space charge layers.

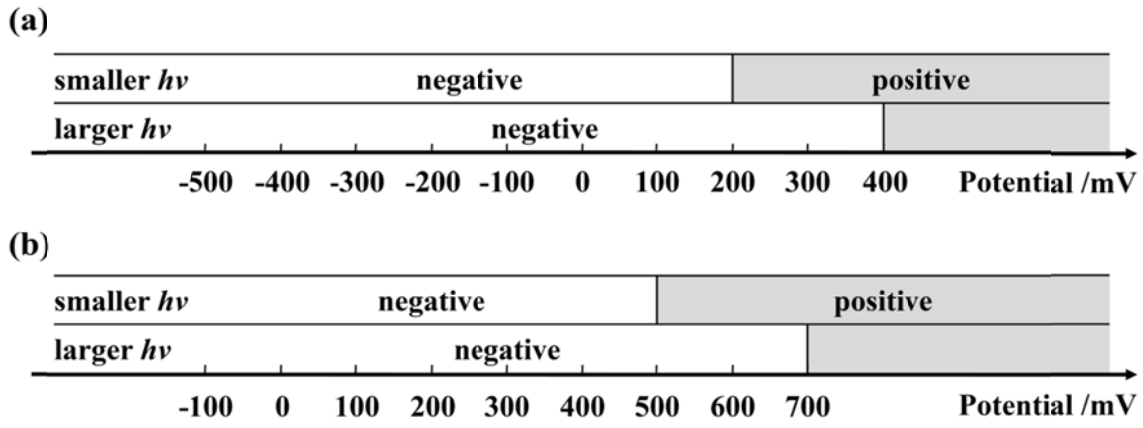

Fig. 2-17 Diagrams of the potential regions exhibiting the direction of photocurrent generated for oxide and hydroxide layers formed in (a) the pH 8.4 borate buffer solution and (b) the sulfuric acid solution.

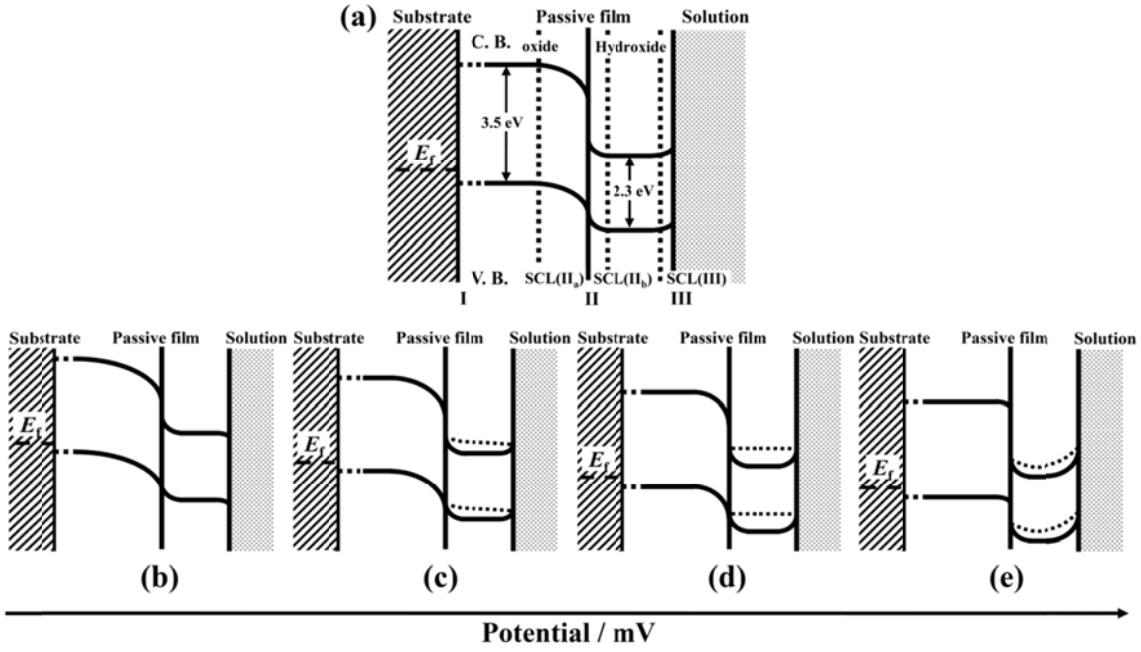

Fig. 2-18 Schematic drawings of (a) an electronic band structure model of passive films on pure Ni and Ni-Cr alloys and (b-e) changes of the band structure with the applied potential in the noble direction.

Photo excitation takes place only in the outer hydroxide layer, that is, the SCL(II_b) and the SCL(III) when the photon energy of the light is ranged from 2.3 eV to 3.5 eV (denoted as "smaller $h\nu$" in Fig. 2-17(a) and 2-17(b)). The holes generated in the hydroxide layer move into the inner oxide layer (SCL(II_b)) and also towards solution (SCL(III)) along the potential gradients whereas the photo-excited electrons might be accumulated in the conduction band in the hydroxide layer as potential barriers exist at both interfaces (II) and (III). Although most of photo-excited electrons will be recombined with holes, some accumulated electrons in the conduction band might modify the energy band as shown with dashed lines in Fig. 2-18(c) - 2-18(e). The net photocurrent generated just after photo irradiation commences is determined by the balance of inward and outward migration of holes. Therefore, at higher potential, photocurrent is generated mainly as anodic current because the SCL(III) is wider compared to the SCL(II_b). Then, the energy band in the hydroxide layer is changed as shown in Fig. 2-18(e) due to the accumulation of electrons in the conduction band in the hydroxide layer. This modification might increase the width of the SCL(III), leading to the gradual increase of photocurrent after the rapid increase of anodic current as shown in Fig. 2-4(b). By decreasing applied potential the width of the SCL(III) decreases whereas that of the SCL(II_b) increases. Therefore, at a certain potential (for examples 200 mV in the borate buffer solution, 500 mV in the sulfuric acid solution; see Fig. 2-17(a) and 2-17(b)), the contributions of the SCL(III) and the SCL(II_b) to photocurrent become equivalent. As a result, the net photocurrent becomes zero. Further decrease of applied potential results in the opposite situation as shown in Fig. 2-4(c), that is, the width of the SCL(II_b) is larger than that of the SCL(III). This might lead to the rapid increase of the current in the cathodic direction just after photo irradiation commences. Furthermore the subsequent band modification will cause gradual increase of the current as shown in Fig. 2-4(a).

Photo irradiation with larger photon energy than 3.5 eV leads to the generation of electron-hole pairs in both oxide and hydroxide layers. Holes generated in the SCL(II_a) migrate towards substrate along the potential gradient in the oxide layer. Photo-excited electrons, on the other hand, move to the conduction band in the hydroxide layer. This charge separation generates negative photocurrent. At higher applied potential, however, the SCL(II_a) formed in oxide layer is very narrow and the contribution of the layer to the photocurrent is very small. Therefore, the net photocurrent is determined by the balance of inward and outward migration of holes in the hydroxide layer. When the SCL(III) is wider compared to the SCL(II_b), therefore positive photocurrent is generated also by photo irradiation with larger energy than 3.5 eV with current transient in Fig. 2-18(b). Slight potential shift in the less noble direction cause the SCL(II_a) wider and therefore its contribution to photocurrent becomes larger, resulting in net negative photocurrent even when the photocurrent generated by photo irradiation with the smaller energy is positive. In the situations shown in Fig. 2-18(c) and 2-18(d), the photo-excited electrons created in the oxide layer can migrate through the hydroxide layer due to the band modification explained above and reach the interface of the hydroxide layer/solution to be consumed by some cathodic reaction. Therefore negative photocurrent is observed at lower applied potential.

As the photocurrent transient shown in Fig. 2-4(c) is observed at higher applied potential, the process of photocurrent generation can be essentially similar to that explained above. Cathodic and anodic peaks just after photo irradiation commences and is terminated, respectively, are observed on Ni-Cr alloys when polarized around the transpassive region of chromium. Therefore, they might be related to the traspassive dissolution of chromium, but the details are not clear at the moment.

2.4.2 Comparison of passive films on Ni-Cr alloy with passive films on Fe-Cr alloy

From the results on the photoelectrochemical response we proposed that the passive films formed on pure Ni and Ni-Cr alloys consist of inner p-type oxide layer with the band gap energy of 3.5 eV and outer n-type hydroxide layer with 2.3 eV. Although the electronic energy band structure is similar independent of the specimens, differences can be observed in the slope of the photoelectrochemical action spectrum, that is, the *C* value depending on the specimens.

In the pH 8.4 borate buffer solution, as shown in Fig. 2-9 and 2-10, the *C* value for hydroxide layer is very similar among the specimens whereas there is a clear difference in the *C* value between pure Ni and Ni-Cr alloys for oxide layer. The difference becomes more apparent in the sulfuric acid solution (see Fig. 2-14). Furthermore, in the sulfuric acid solution, the *C* value even for hydroxide layer formed on pure Ni is different compared with those on Ni-Cr alloys. It is clear from Figs. 2-9 and 2-14, on the other hand, that the *C* values for oxide and hydroxide layers on Ni-8Cr alloy are quite similar to those on Ni-18Cr alloy in both solutions. These can be attributed to the chemical compositions of passive films formed on the specimens. As mentioned above, the passive films formed on Ni-Cr alloys consist mainly of an inner Cr_2O_3 layer and a covering $Cr(OH)_3$ layer, indicating that chemical composition of passive films formed on Ni-Cr alloys is totally different from that on pure Ni, This difference in composition can change the electronic properties of both layers, leading to the change in the *C* value from the value obtained for pure Ni. In the pH 8.4 borate buffer solution, however, significant amount of Ni is incorporated into hydroxide layer. Therefore, the *C* values for hydroxide layer formed on Ni-Cr alloys did not change compared to those obtained for pure Ni. On the other hand, Cr enrichment occurs in both layers of passive films formed on Ni-Cr alloys in the sulfuric acid solution due to enhanced dissolution of nickel and as a result the *C* values in both

oxide and hydroxide layers are different from those obtained for pure Ni. As even in the sulfuric acid solution, chromium content in passive films on Ni-8Cr is similar to that on Ni-18Cr, however, the *C* values obtained for both alloys are almost same in all experimental conditions. It is well known that chromium enrichment is significantly facilitated on Fe-Cr alloys in acid solutions compared to in neutral solutions. Therefore, the chromium enrichment in acid solutions can drastically affect the electronic band structure of passive films on Fe-Cr alloys. Fujimoto et al. mentioned that the passive film formed on Fe-18Cr alloy in a borate buffer solution consists of an inner n-type oxide layer and an outer n-type hydroxide layer whereas in a sulfuric acid solution, the passive film formed on Fe-18Cr alloy is composed of an inner p-type oxide layer and an outer n-type hydroxide layer[10,12)]. Therefore, it is found that chromium content in passive films can affect the electronic properties of passive films formed on Fe-Cr and Ni-Cr alloys, and when the chromium content in passive films is beyond critical amount even electronic band structure can be modified.

2.5 Conclusion

Semiconductive properties of passive films formed on pure Ni and Ni-Cr alloys in a 0.1M sulfuric acid and a pH 8.4 borate buffer solutions were investigated by the photoelectrochemical response. Observed photocurrents were strongly affected by various parameters such as the film formation potential, pH of solution and Cr content whereas flat band potentials were affected only by pH. From detailed analysis of the photoelectrochemical response, we proposed a heterogeneous structure with p/n junction – the inner p-type oxide layer with the band gap energy of 3.5 eV and the outer n-type hydroxide layer with 2.3 eV – for the passive films formed on pure Ni and Ni-Cr alloys. The band structure model can be applied for the passive films formed on pure Ni and Ni-Cr alloys in both solutions, different from the passive films of Fe-Cr alloys for which different electronic band structure models were proposed depending on pH of solutions.

References:

1. K. Hashimoto and K. Asami, Corros. Sci., **19** (1979) 427.

2. N.S. Mclntyre, D.G. Zetaruk and D. Owen, J. Electrochem. Soc., 126 (1979) 750.

3. A. Kawashima, K. Asami and K. Hashimoto, Corros. Sci., **25** (1985) 1103.

4. S.S. Hwang, U.C. Kim and Y.S. Park, J. Nucl. Mater., **246** (1997) 77.

5. C. Sunseri, S. Piazza, Di Paola and F. Di Quarto, J. Electrochem. Soc., **134** (1987) 2410.

6. H. Gerischer, Corros. Sci., **31** (1990) 81.

7. H. Tsuchiya, S Fujimoto and T Shibata, J. Electrochem. Soc., **151** (2004) B39.

8. M. J. Carmezim, A. M. Simões, M. F. Montemor and M. Da Cunha Belo, Corros. Sci., **4** (2005) **7**581.

9. T. L. Sudesh, L. Wijesinghe and Daniel John Blackwood, Corros. Sci., **50** (2008) 23.

10. H. Tsuchiya, S. Fujimoto and T. Shibata, J. Electrochem. Soc., **151** (2004) B39.

11. N. Sato, Corros. Sci., **42** (2000) 1957.

12. H. Tsuchiya, S. Fujimoto, O. Chihara and T. Shibata, Electrochim. Acta, **47** (2002) 4357.

13. N.T.C. Oliveira, S.R. Biaggio, P.A.P. Nascente, S. Piazza, C. Sunseri and F. Di Quarto, Electrochim. Acta, **51** (2006) 3506.

14. H.-J. Jang and H.-S. Kwon, J. Electroanal. Chem., **590** (2006) 120-125.

15. T.L. Sudesh, L. Wijesinghe and D.J. Blackwood, Appl. Surf. Sci., **253** (2006) 1006.

16. N.E. Hakiki, J. Appl. Electrochem., **38** (2008) 679.

17. L. Marchetti, S. Perrin, Y. Wouters, F. Martin and M. Pijolat, Electrochim. Acta, **55** (2010) 5384.

18. W.-S. Kim, H. Tsuchiya and S. Fujimoto, submitted to Materials Transactions.

19. T. Jabs, P. Borthen and H.-H. Strehblow, J. Electrochem. Soc., **144** (1997) 1231.

20. S. Fujimoto, O. Chihara and T. Shibata, Mater. Sci. Forum, **289-292** (1998) 989.

21. S.M. Wilhelm and N. Hackerman, J. Electrochem. Soc., **128** (1981) 1668.

22. Y. Mito, M. Ueda and T. Ohtsuka, Corros. Sci., **51** (2009) 1540.

23. C. Sunseri, S. Piazza and F. Di Quarto, Mater. Sci. Forum, **185-188** (1995) 435.

24. H.-J. Jang, C.-J. Park and H.-S. Kwon, Electrochim. Acta, **50** (2005) 3503.

25. F. Di Quarto, S. Piazza and C. Sunseri, Corros. Sci., **31** (1990) 721.

Chapter 3 Semiconductive Properties of Passive Films Formed on Alloy 600 and Alloy 690; Influence of Alloy Composition

3.1 Introduction

Alloy 600 and Alloy 690 have been used as structural materials of chemical plants and equipments of power generator etc. because of their high corrosion resistance. The high corrosion resistance is attributed to passive films on the materials and strongly depends on the structures, compositions and properties of passive films[1), 2)]. Therefore, the analysis of passive films has been considered to be prerequisite and carried out with various analytical techniques.

As already mentioned, semiconductive properties of passive films formed on Ni-based alloys have been studied using the photoelectrochemical response and the electrochemical impedance technique[3)-9)]. In the chapter 2, the author also examined semiconductive properties of passive films formed on pure Ni and Ni-Cr alloys and proposed the electronic band structure model of the passive films.

In the present chapter, semiconductive properties of passive films formed on Alloy 600 and Alloy 690 in a 0.1 M sulfuric acid solution and a pH 8.4 borate buffer solution were studied using the photoelectrochemical response. Especially how chemical composition of passive films affects semiconductive properties is focused.

3.2 Experimental

Materials examined were Alloy 600, Alloy 690 and high-purity Alloy690. The chemical compositions of the alloys were listed in Table 3-1. The surfaces of the materials were polished mechanically with SiC abrasive paper and mirror finished with alumina pastes, then cleaned with ethanol, methanol and distilled water, successively. Solutions used in the present work were a 0.1M H_2SO_4 and a pH 8.4 borate buffer solution. Both were deaerated for more than 12 hours with N_2 gas prior to experiments. Electrochemical measurements were carried out in a conventional three-electrode cell with a platinum plate and Ag/AgCl electrode as a counter electrode and a reference electrode, respectively.

The polarization curves were measured from -600 to 2000 mV in the sulfuric acid solution and from -1000 to 2000 mV in the borate buffer solution with a scan rate of 1 mV/s. Photoelectrochemical response was examined around passive regions of the materials in the solutions. A specimen was polarized at a desired film formation potential, E_f, in a passive region for 24 hours before photoelectrochemical response measurement commences. In the measurement the monochromatic light obtained using a 150 W Xenon arc lamp with a grating monochromator was irradiated on the specimen in the electrochemical cell through a quarts window. A current change caused during the photoirradiation for 15 s was recorded as photocurrent transient at the film formation potential. Then the applied potential was changed stepwise with the interval of 100 mV in the less noble direction. Photocurrent transient was measured at each measuring potential, E_m, with changing the wavelength of the incident light from 250 to 500 nm. The XPS analysis was also carried out using a Rigaku XPS-7000 spectrometer equipped with x-ray source of Al-Kα without any sputtering techniques. The composition of passive films was quantitatively computed from the integrated peak intensities of the $Ni2p_{3/2}$, $Cr2p_{3/2}$, $Fe2p_{3/2}$, O1s and C1s spectra.

Table 3-1 Chemical compositions of specimens. (wt%)

	C	Si	Mn	Co	Ni	Cr	Fe	Mo	Ti	Al	P	S	B
Alloy 600	0.010	0.310	0.360	-	75.010	15.710	7.350	-	-	-	0.009	<0.001	-
Alloy 690	0.020	0.120	0.260	0.030	Bal	29.550	9.610	0.020	0.110	0.90	90.00*	20.00*	<10*
High-purity Alloy 690	0.0019	0.01	<0.01	0.02	Bal	28.92	10.0	0.01	0.09	0.09	0.0009	0.0008	<0.0001

(* ppb)

3.3 Results

3.3.1 Polarization curves of Alloy 600 and Alloy 690

Figures 3-1 and 3-2 show potentiodynamic polarization curves of Alloy 600 and Alloy 690 in the sulfuric acid solution and the borate buffer solution, respectively. Polarization curves measured for Ni-18Cr alloy and Ni-30Cr alloy are also included as comparison. It is clear that in the sulfuric acid solution the polarization curves of Alloy 600 and Alloy 690 were similar to those obtained for Ni-18Cr alloy and Ni-30Cr alloy, respectively, except for passive current density. The passive current densities obtained for Alloy 600 and Alloy 690 were slightly lower compared to those for Ni-18Cr alloy and Ni-30Cr alloy. From the figure the passive region in the sulfuric acid solution was determined from 100 to 900 mV for Alloy 600 and Alloy 690. In the borate buffer solution, on the other hand, the passive region and the transpassive region was located between -400 and 400 mV and between 400 and 900 mV, respectively, for both specimens. Photoelectrochemical response measurements were performed around the passive regions.

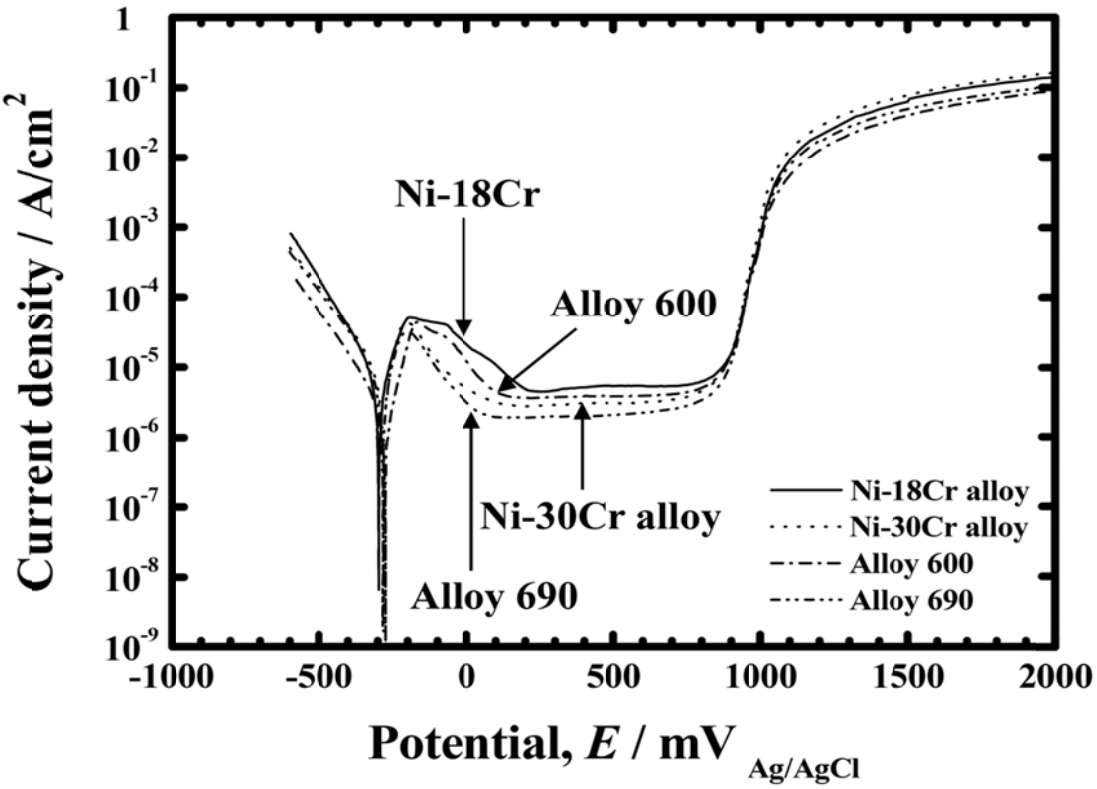

Fig. 3-1 Polarization curves of Alloy 600 and Alloy 690 measured in the sulfuric acid solution.

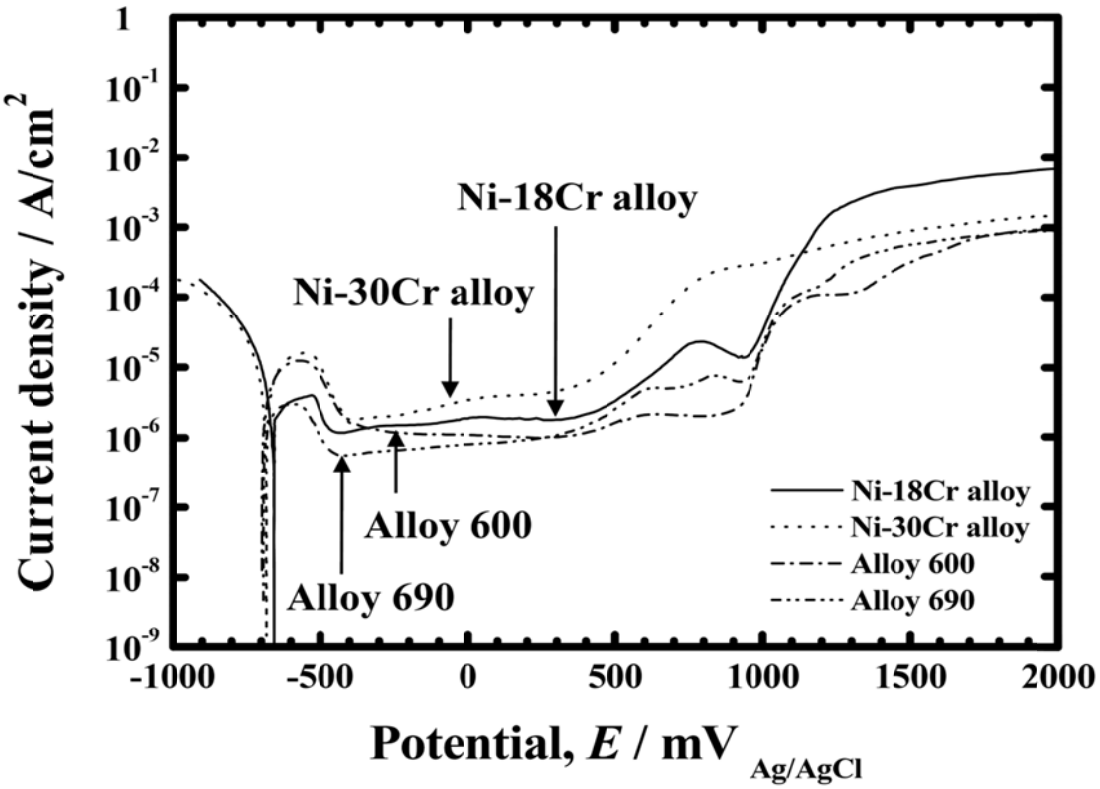

Fig. 3-2 Polarization curves of Alloy 600 and Alloy 690 measured in the borate buffer solution.

3.3.2 Photoelectrochemical response for passive films formed on Alloy 600 and Alloy 690 in sulfuric acid solution

Figure 3-3 shows typical photocurrent transients recorded for passive films formed on Alloy 600 and Alloy 690. As apparent, the photocurrent transient is not constant, but varies during photoirradiation. Therefore, in the present work the difference between current recorded just before photoirradiation and after 15 s was defined as photocurrent and analyzed also in the present work.

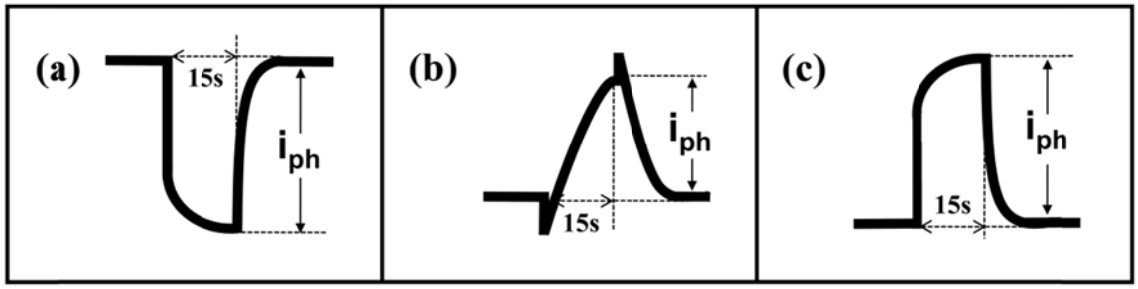

Fig. 3-3 Example of photocurrent transients obtained for passive films formed on Alloy 600 and Alloy 690 in the sulfuric acid solution and the borate buffer solution.

Figure 3-4 presents photocurrent spectra obtained at various measuring potentials for the passive film formed on Alloy 690 at 500 mV for 24 hours in the sulfuric acid solution. It is clear that photocurrent varies depending on applied potential as well as the wavelength of incident light. As the intensity of the light is different depending on wavelength, photocurrent spectra were normalized for further analyses also in the present work. Assuming that the photo excitation takes place as an indirect transition [1), 10)-13)], photocurrent spectra can be normalized as photoelectrochemical action spectrum

$$\left(i_{ph} \cdot h\nu / I_0\right)^{\frac{1}{2}} = C\left(h\nu - E_g\right) \tag{3.1}$$

where I_0 and $h\nu$ are the intensity and the photon energy of incident light, respectively, and E_g is the band gap energy of passive film. C is the slope of photoelectrochemical

action spectrum and reflects the amplitude of photocurrent generated. By replotting the photocurrent spectra in Fig. 3-4, photoelectrochemical action spectra are obtained as shown in Fig. 3-5. As clear from the figure, the photoelectrochemical action spectra do not exhibit one straight line, but two regions with different slopes. Furthermore it is noticeable that the spectrum obtained at 500 mV exhibits both positive and negative values depending on the photon energy. When photocurrent is generated from a single layer, the photocurrent should not change its direction at a fixed potential even if the wavelength of incident light is changed. Angle-resolved XPS analysis revealed that passive films formed on Alloy 600 and Alloy 690 in the sulfuric acid solution consist of duplex layers, that is, an inner oxide layer and a covering outer hydroxide layer. Chemical compositions of the passive films formed on both alloys in the sulfuric acid solution are summarized in Table 3-2. Therefore one may deduce that photocurrent obtained for passive film is considered as sum of two components originated from an oxide layer and a hydroxide layer. In the present work, therefore, the photoelectrochemical action spectra were separated into two components and then band gap energy and slope of photoelectrochemical action spectrum were estimated. Band gap energy, E_g, is obtained as the photon energy at which the $(i_{ph} \cdot h\nu / I_0)^{1/2}$ equals to zero in photoelectrochemical action spectra. Details of the separation process were reported in the chapter 2. From the photoelectrochemical action spectra shown in Fig. 3-5, the band gap energies for the passive film formed on Alloy 600 at 500 mV in the sulfuric acid solution were estimated as approximately 3.5 eV and 2.3 eV. The band gap energies were independent of alloy composition and measuring potential as shown in Fig. 3-6. Referring to the literatures[8),14)], the band gap energy of both NiO and Cr_2O_3 was reported as approximately 3.5 eV while the band gap energy of $Ni(OH)_2$ and $Cr(OH)_3$ was estimated as approximately 2.3 eV. This is in line with results obtained

from the XPS analysis. Figures 3-7 and 3-8 show variations in the slope of the photoelectrochemical action spectrum, *C*, for passive films formed on Alloy 600 and Alloy 690 in the sulfuric acid solution, respectively. It is clear that *C* values for oxide layer are negative for all applied potentials and the absolute values increases with decreasing applied potential. On the other hand, slopes obtained for hydroxide layer increases from negative to positive with increasing applied potential although the *C* values are very small compared to those for oxide layer.

Table 3-2 Cation fractions in passive films formed on Alloy 600 and Alloy 690.

		Hydroxide layer			Oxide layer		
		Ni(hyd)	Cr(hyd)	Fe(hyd)	Ni(ox)	Cr(ox)	Fe(ox)
Surfuric acid solution	Alloy 600	0.197	0.571	0.232	0.115	0.698	0.187
	Alloy 690	0.094	0.682	0.224	0.067	0.823	0.110
Borate buffer solution	Alloy 690	0.206	0.588	0.206	0.159	0.502	0.339

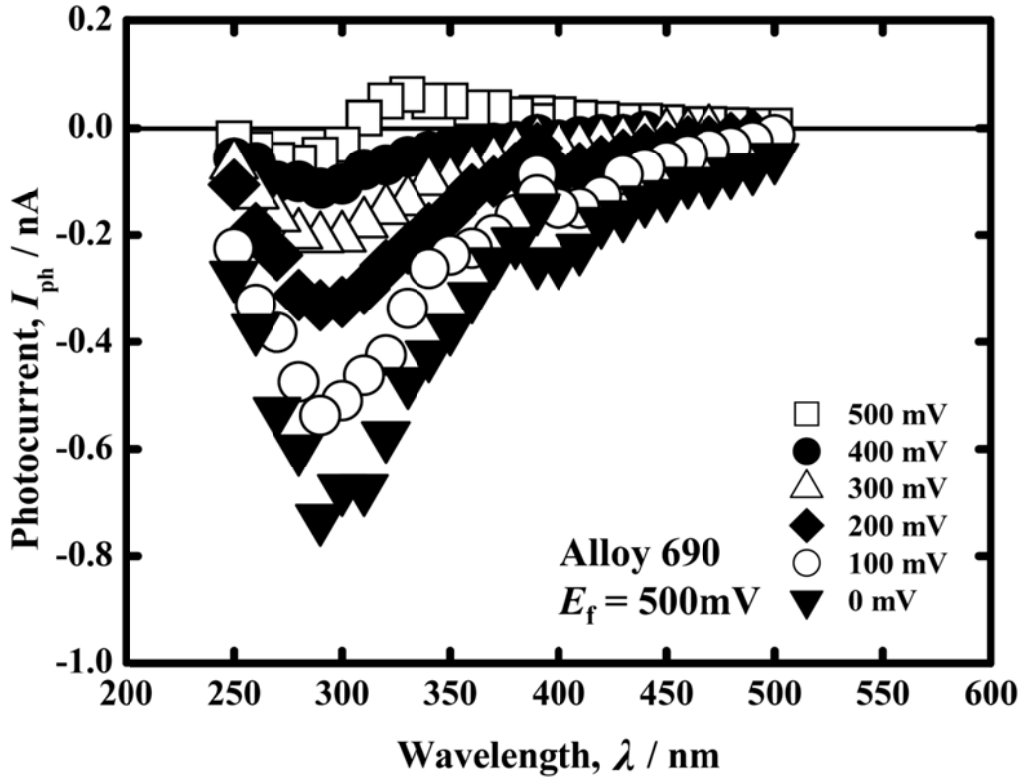

Fig. 3-4 Photocurrent spectra for the passive film formed on Alloy 690 at 500 mV in the sulfuric acid solution. The spectra were obtained at various measuring potentials.

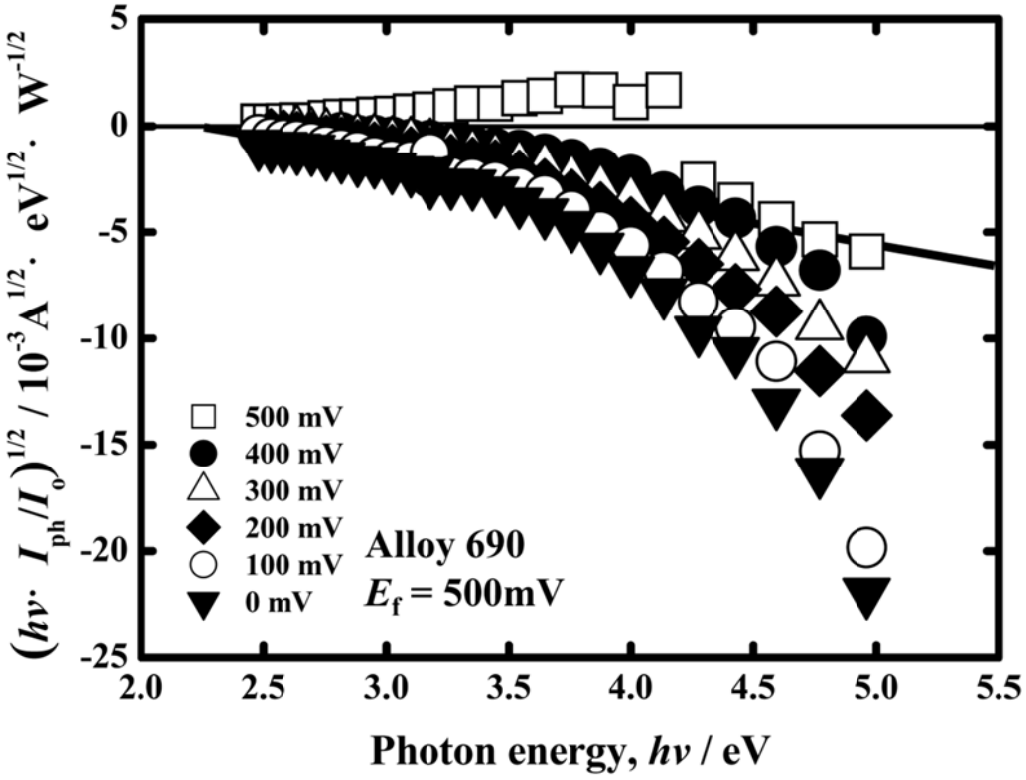

Fig. 3-5 Photoelectrochemical action spectra calculated from the photocurrent spectra shown in Fig. 3-4.

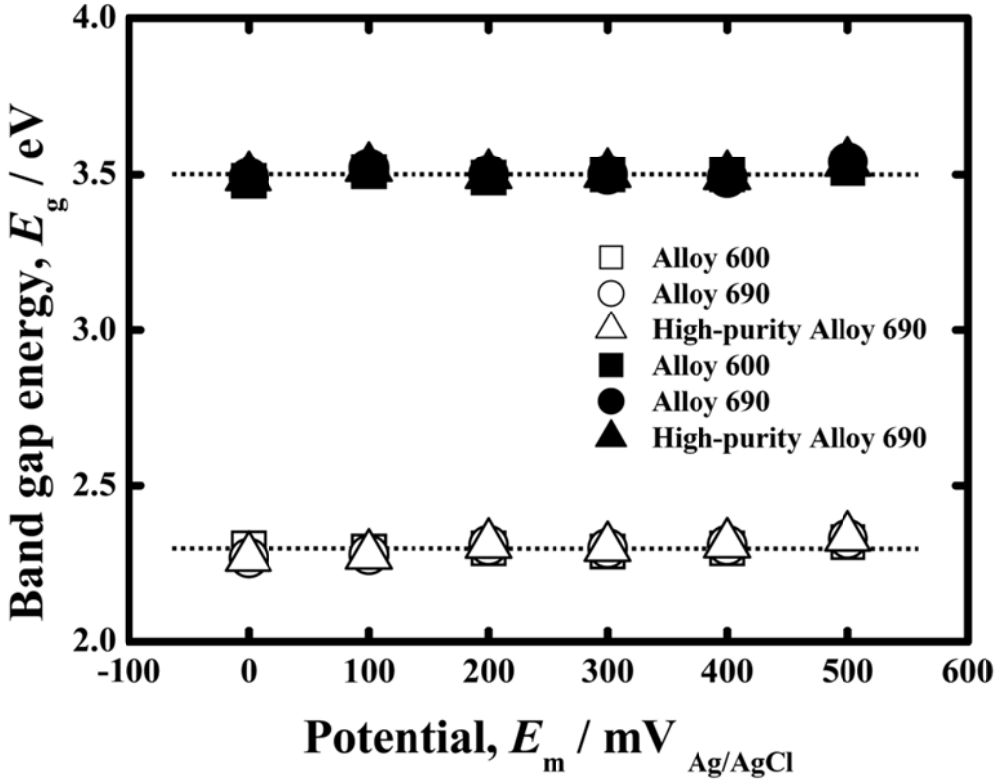

Fig. 3-6 Band gap energies of passive film formed on Alloy 600, Alloy 690 and high-purity Alloy 690 in the sulfuric acid solution.

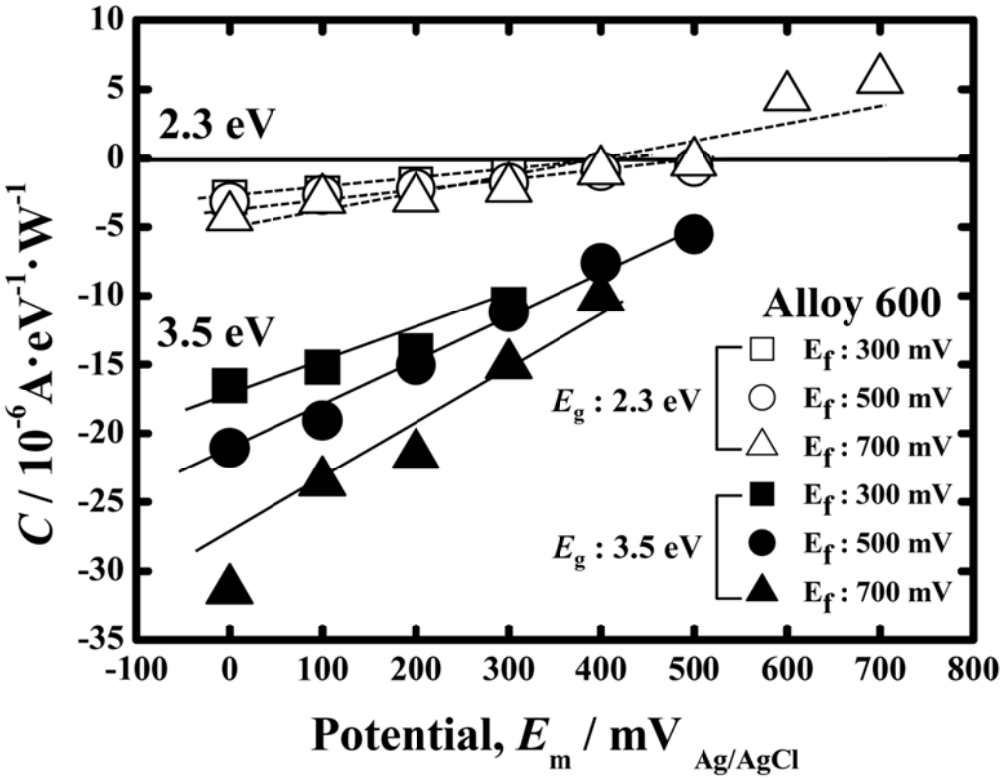

Fig. 3-7 Variations in the slopes of the photoelectrochemical action spectra, *C*, obtained for passive films formed on Alloy 600 at several potentials in the sulfuric acid solution.

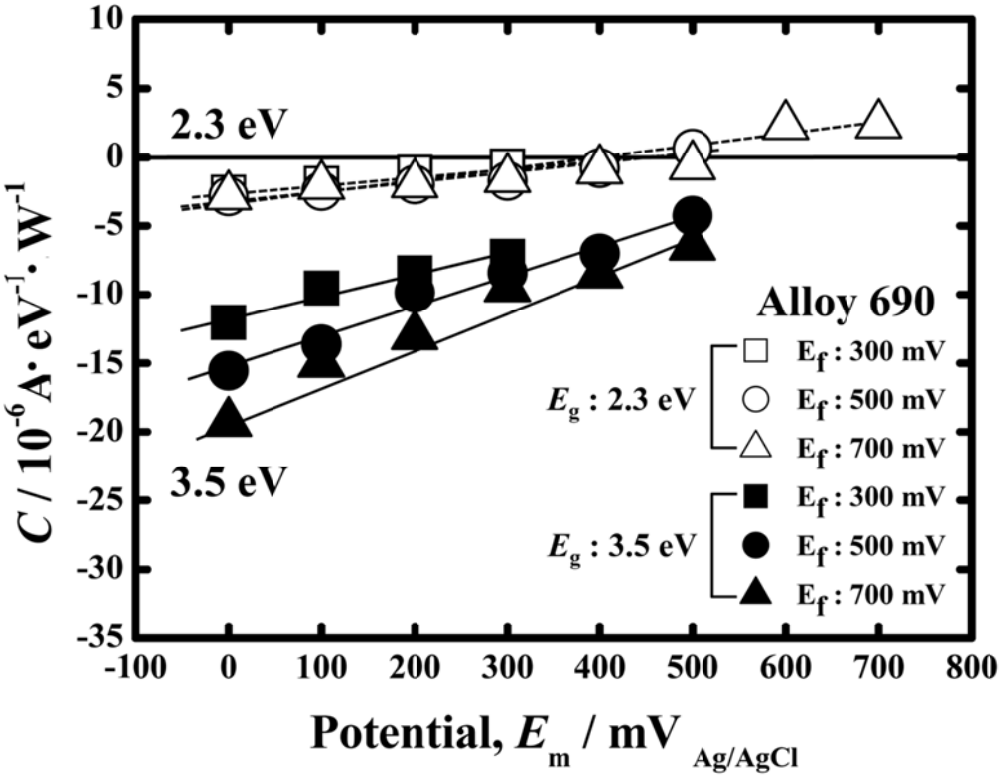

Fig. 3-8 Variations in the slopes of the photoelectrochemical action spectra, *C*, obtained for passive films formed on Alloy 690 at several potentials in the sulfuric acid solution.

3.3.3 Photoelectrochemical response for passive films formed on Alloy 600 and Alloy 690 in borate buffer solution

Photocurrent spectra were measured also for passive films formed on Alloy 600 and Alloy 690 in the borate buffer solution as shown in Figs. 3-9. In Fig. 3-10, similar photoelectrochemical action spectra obtained from Fig. 3-9 were obtained in the borate buffer solution to those in the sulfuric acid solution. Therefore photoelectrochemical action spectra in the borate buffer solution were also separated into two components, yielding the band gap energies of 3.5 eV and 2.3 eV. Figure 3-11 summarizes the band gap energies for passive films on alloy 600 and Alloy 690 in the borate buffer solution. The band gap energies are almost constant independent of alloy composition, applies potentials and solutions. Figure 3-12 shows potential dependence of the slope of the photoelectrochemical action spectrum, *C*, for passive films formed at 0 mV in the borate buffer solution. Similar to the results obtained for the sulfuric acid solution, in the borate buffer solution the slope of the action spectra for oxide layer is negative for all applied potential and the absolute value clearly increases with decreasing potential whereas the slope for hydroxide layer slightly increases from negative to positive with applied potential. However, different from the result for the sulfuric acid solution, the *C* value for oxide layer on Alloy 600 is similar to that on Alloy 690.

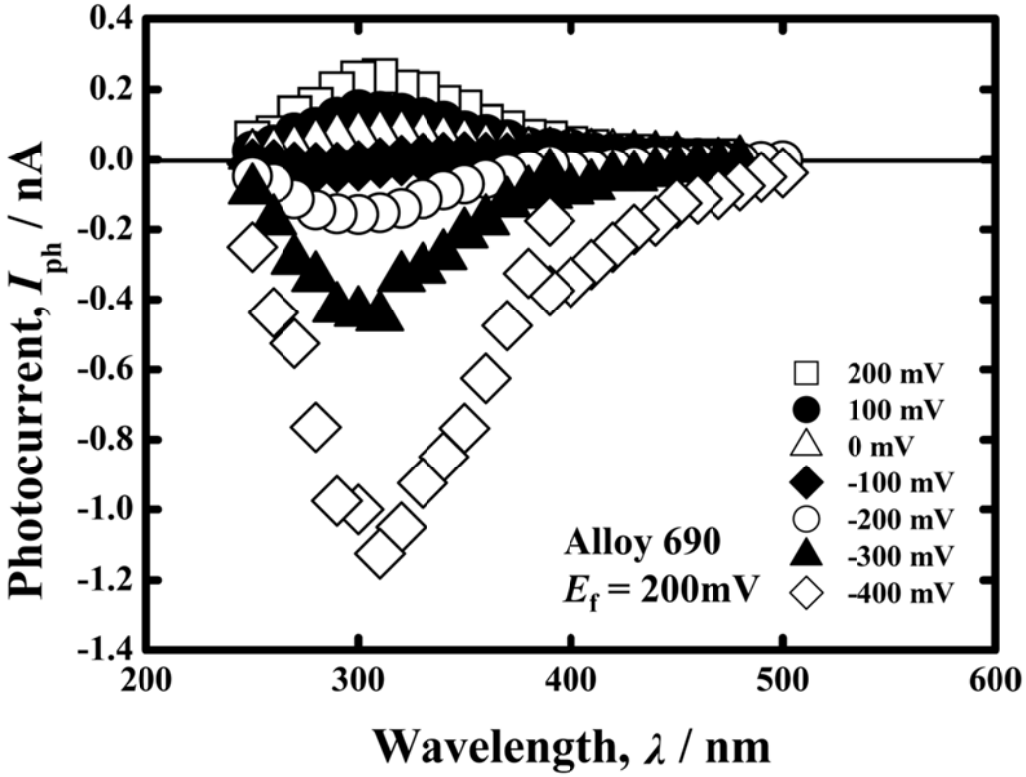

Fig. 3-9 Photocurrent spectra for the passive film formed on Alloy 690 at 200 mV in the borate buffer solution. The spectra were obtained at various measuring potentials.

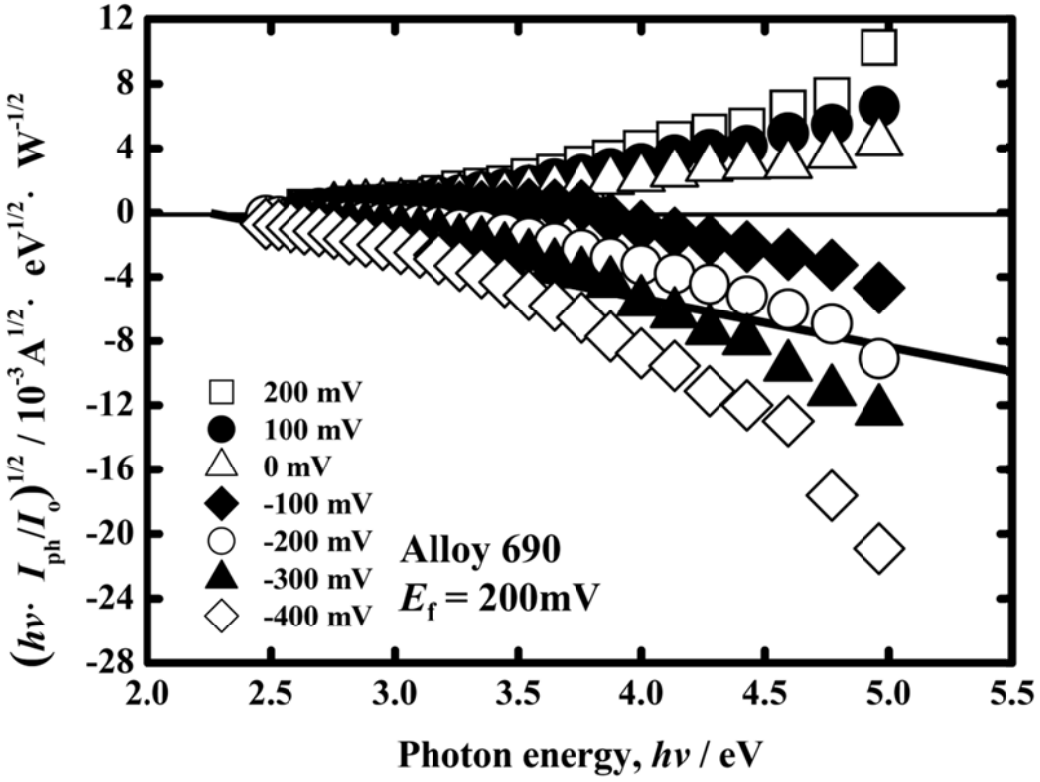

Fig. 3-10 Photoelectrochemical action spectra calculated from the photocurrent spectra shown in Fig. 9.

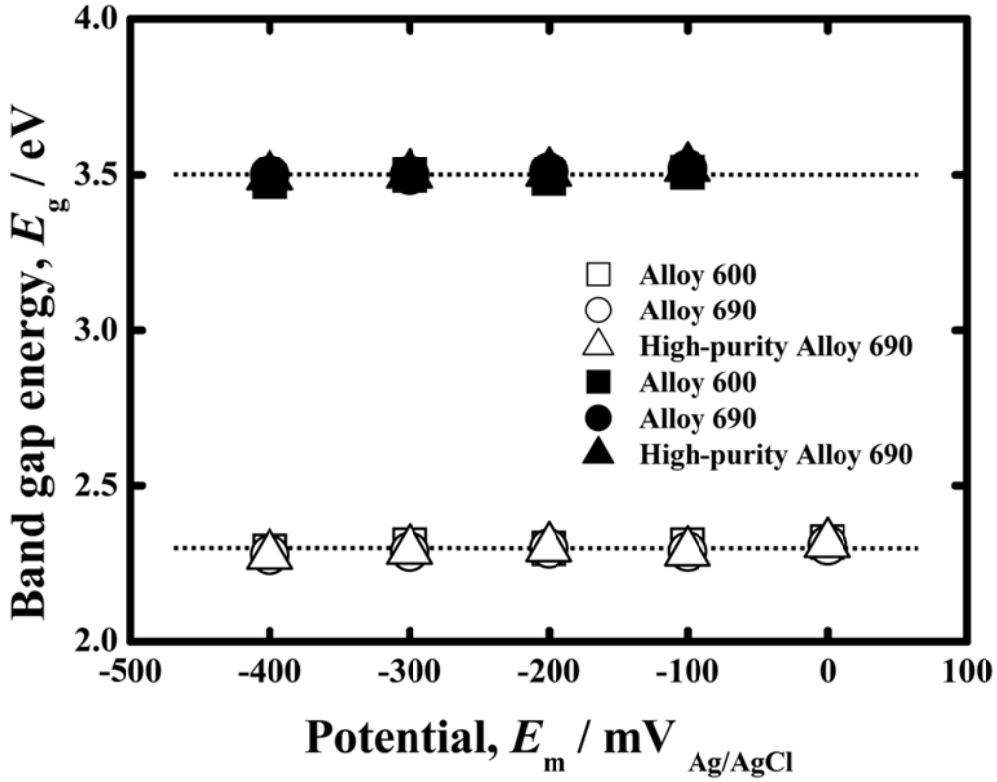

Fig. 3-11 Band gap energies of passive film formed on Alloy 600, Alloy 690 and high-purity Alloy 690 in the borate buffer solution.

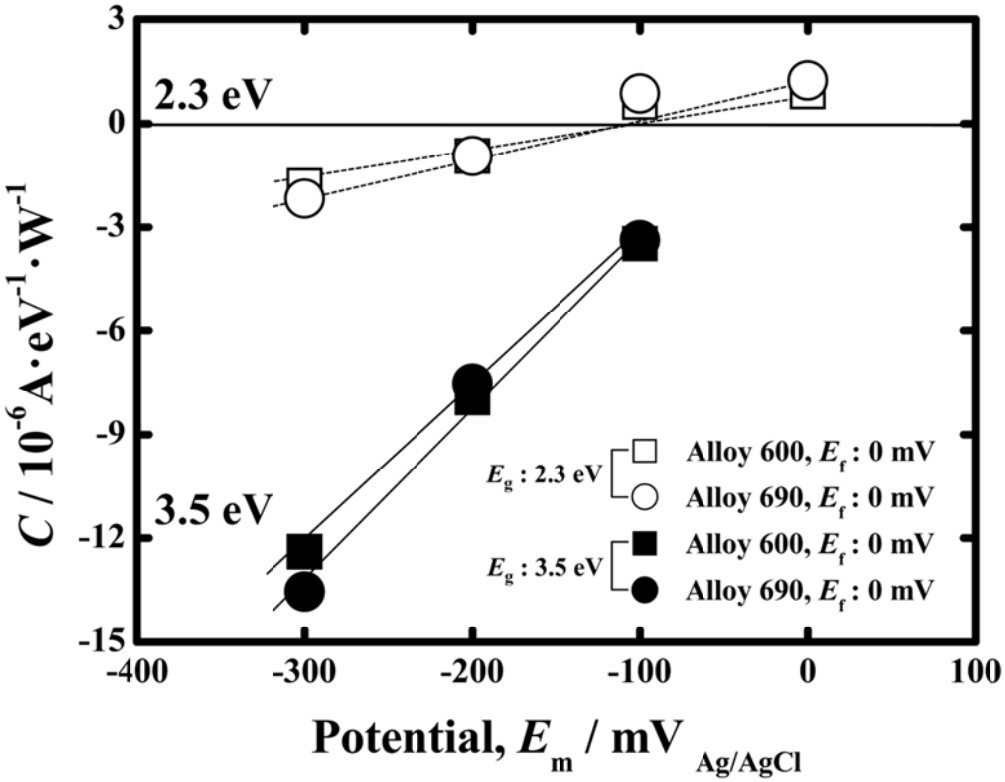

Fig. 3-12 Variations in the slopes of the photoelectrochemical action spectra, *C*, obtained for passive films formed on Alloy 600 and Alloy 690 at several potentials in the borate buffer solution.

3.4 Discussion

3.4.1 Electronic band structure of passive films formed on Alloy 600 and Alloy 690

In the chapter 3 semiconductive properties of passive films on Alloy 600 and Alloy 690 in the sulfuric acid solution and the borate buffer solution were examined by the photoelectrochemical response. As illustrated in Fig. 3-3 photocurrent exhibited three types of transient for passive films on both alloys. These transients were observed also for pure Ni and Ni-Cr alloys in the solutions. Furthermore, the potential dependence of the slope of the photoelectrochemical action spectrum shown in Figs. 3-7 and 3-8 were quite similar to those obtained for pure Ni and Ni-Cr alloys, that is, the *C* values for oxide layer were negative for all applied potentials and the *C* values increase with decreasing applied potential whereas the *C* values for hydroxide layer are very small compared to those for oxide layer and increase from negative to positive with applied potential. Therefore the electronic band structure of passive films formed on Alloy 600 and Alloy 690 is considered to be similar to that proposed for pure Ni and Ni-Cr alloys – passive films on Alloy 600 and Alloy 690 consist of p-type inner oxide layer with the band gap energy of 3.5 eV and n-type outer hydroxide layer with the band gap energy of 2.3 eV[14)].

3.4.2 Influence of chemical composition of passive films on semiconductive properties

As described above, the electronic band structure of passive films on Alloy 600 is same as that for Alloy 690. However, a difference can be observed in the amplitude of photocurrent. It is clear from Figs. 3-7 and 3-8 that in the sulfuric acid solution, the *C* values obtained for Alloy 600 are slightly larger than those for Alloy 690. The difference in the amplitude of photocurrent was observed also between pure Ni and Ni-Cr alloys in the chapter 2. Table 3-2 indicates chemical compositions of passive films formed on Alloy 600 and Alloy 690 in the sulfuric acid solution, quantitatively examined with the XPS. The XPS result clearly indicates that passive films formed both on Alloy 600 and Alloy 690 in the sulfuric acid solution consist mainly of an inner chromium oxide and an outer chromium hydroxide layer. However, more chromium is enriched in the passive film formed on Alloy 690 than that on Alloy 600. It is found, therefore, that this chemical composition difference can affect the amplitude of photocurrent.

It is well known that the chemical composition of a passive film can be affected not only by the chemical composition of a substrate but also by environment. An example is found in Table 3-2. In the sulfuric acid solution, as mentioned above, a passive film formed on Alloy 690 consists mainly of an inner chromium oxide layer and a covering chromium hydroxide layer, that is, less iron is incorporated in the passive film due to the selective dissolution. On the other hand, in the borate buffer solution, such selective dissolution of iron is suppressed, meaning that a certain amount of iron is incorporated in the passive film on Alloy 690. In order to examine the effect of iron incorporation into passive film, the photoelectrochemical response for the passive film formed on Alloy 690 in the borate buffer solution was examined. The photoelectrochemical response for the passive film formed on Ni-30Cr alloy was also investigated as comparison. Note that

Ni-30Cr alloy contains almost same amount of chromium as Alloy 690, but does not contain iron. Figures 3-13 and 3-14 show variations of the slope of the photoelectrochemical action spectrum of passive films on Alloy 690 and Ni-30Cr alloy in the sulfuric acid solution and the borate buffer solution, respectively. It is apparent that in the sulfuric acid solution which dissolves iron from a passive film on Alloy 690, the *C* values are more or less similar for oxide layer as well as hydroxide layer between the specimens whereas in the case of the borate buffer solution in which a passive film formed on Alloy 690 incorporates a certain amount of iron, the *C* values obtained for oxide layer on Alloy 690 are clearly different from those on Ni-30Cr alloy. This indicates that the incorporation of iron in passive films can affect semiconductive properties. For further investigation, the photoelectrochemical response were examined for passive films formed on high-purity Alloy 690 and compared to those on conventional Alloy 690. Results are summarized in Figs. 3-15 and 3-16. As apparent, impurities that are included in conventional Alloy 690 exhibit no effects on semiconductive properties of passive films of Alloy 690. Therefore, it can be concluded that when a certain amount of impurity is incorporated into passive films, semiconductive properties can be affected.

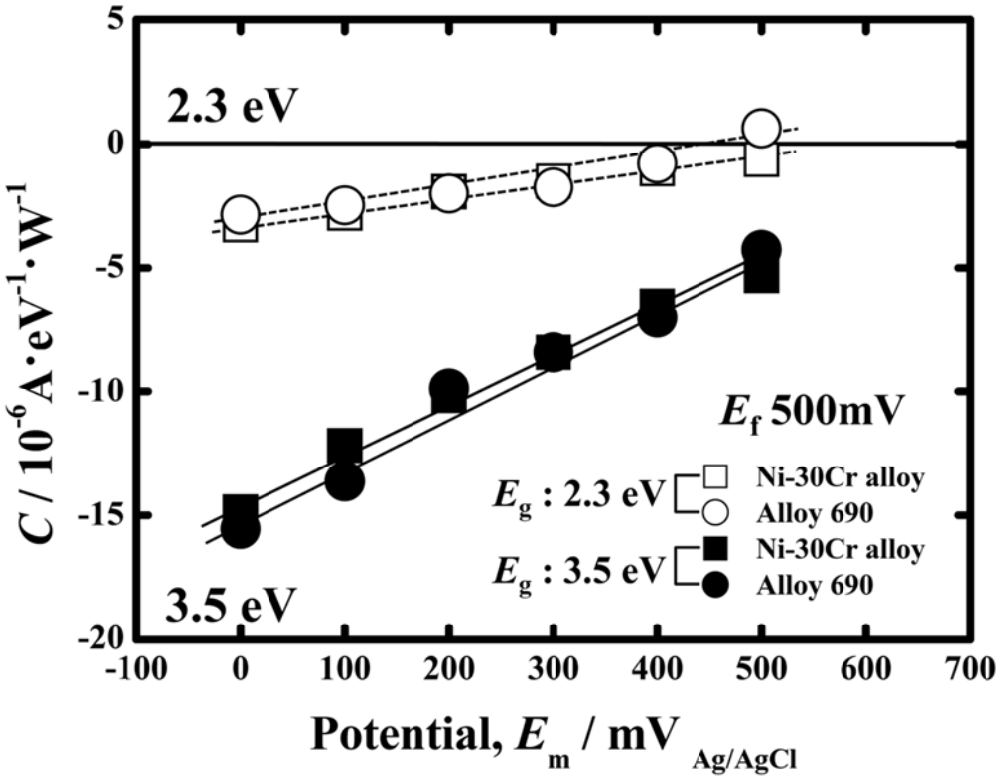

Fig. 3-13 Variations in the slopes of the photoelectrochemical action spectrum, *C*, obtained for passive films formed on Alloy 690 and Ni-30Cr alloy in the sulfuric acid solution.

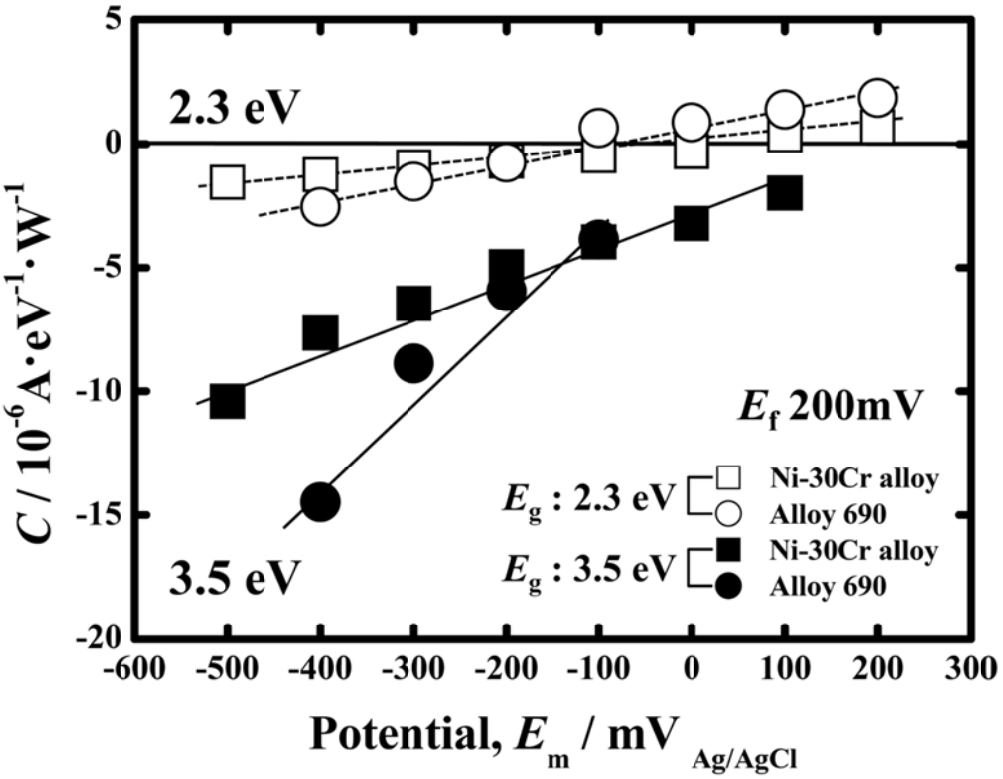

Fig. 3-14 Variations in the slopes of the photoelectrochemical action spectrum, *C*, obtained for passive films formed on Alloy 690 and Ni-30Cr alloy in the borate buffer solution.

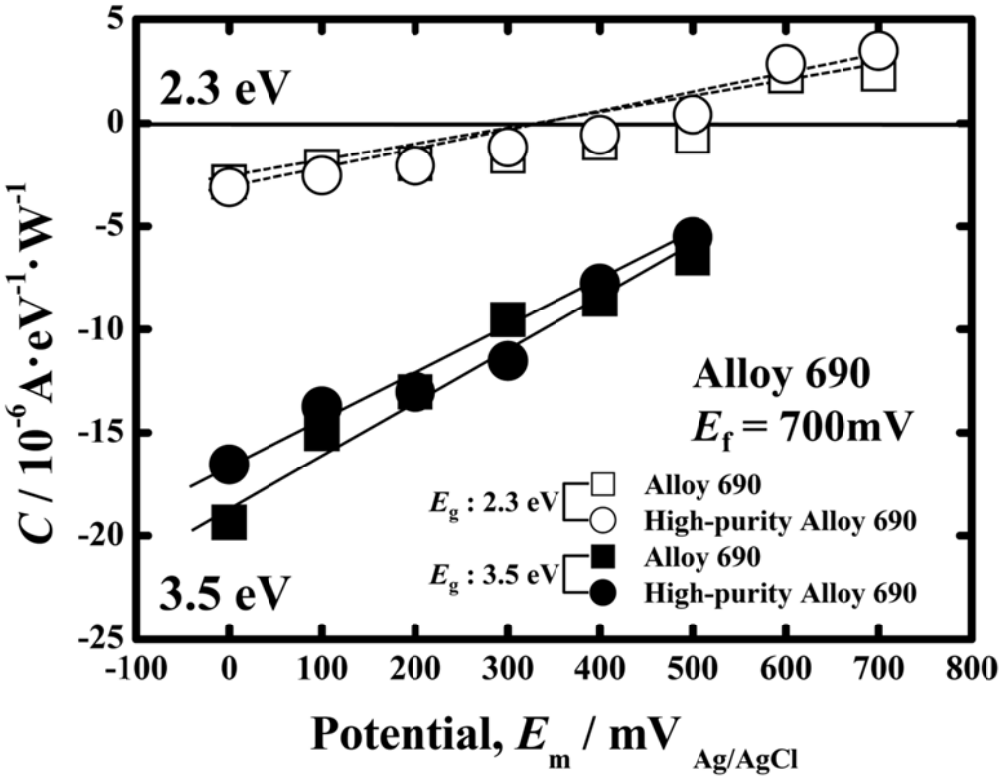

Fig. 3-15 Variations in the slopes of the photoelectrochemical action spectrum, *C*, obtained for passive films formed on conventional and high-purity Alloy 690 in the sulfuric acid solution.

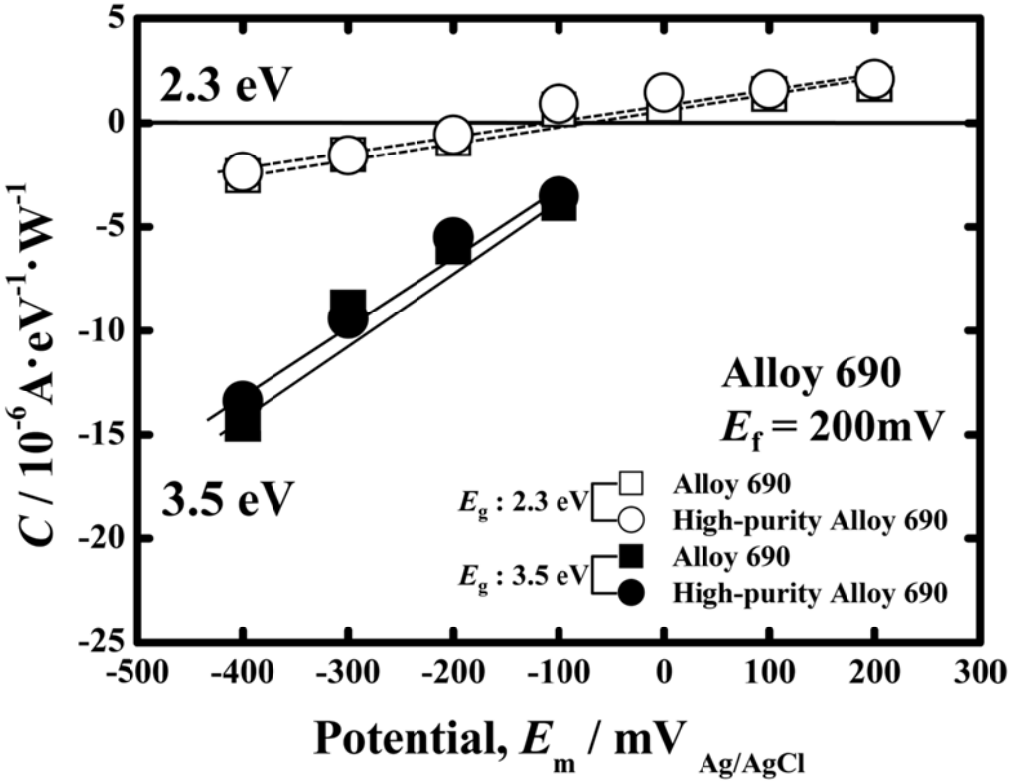

Fig. 3-16 Variations in the slopes of the photoelectrochemical action spectrum, *C*, obtained for passive films formed on conventional and high-purity Alloy 690 in the borate buffer solution.

3.5 Conclusion

Semiconductive properties of passive films formed on Alloy 600 and Alloy 690 in a 0.1M sulfuric acid solution and a pH 8.4 borate buffer solution were examined by the photoelectrochemical response. Duplex structure consisting of a p-type inner oxide layer with the band gap energy of 3.5 eV and an n-type outer hydroxide layer with the band gap energy of 2.3 eV was proposed as an electronic band structure model for the passive films. In the case of sulfuric acid solution, the slopes of the photoelectrochemical action spectrum, *C*, for Alloy 690 were similar to those for Ni-30Cr alloy while in borate buffer solution, the slopes of the photoelectrochemical action spectrum, *C*, for Alloy 690 were quite different from those for Ni-30Cr alloy. These behaviors were attributed to the modification of semiconductive properties by the incorporation of Fe into passive films. In the borate buffer solution, more Fe was doped into passive films, which leads to the change in photoelectrochemical response. However, impurities included in commercial Alloy 690 did not cause any changes in semiconductive properties of passive films.

References:

1. H. Tsuchiya, S. Fujimoto and T. Shibata, J. Electrochem. Soc., **151** (2004) B39.

2. N. Sato, Corr. Sci., **42** (2000) 1957.

3. M. Da Cunha Belo, N. E. Hakiki and M. G. S. Ferreira, Electrochim. Acta, **44** (1999) 2473.

4. M. Bojinov, G. Fabricius, P. Kinnunen, T. Laitinen, K. Mäkelä, T. Saario and G. Sundholm, J. Electroanal. Chem., **504** (2001) 29.

5. M. F. Montemor, M. G. S. Ferreira, N. E. Hakiki and M. Da Cunha Belo, Corros. Sci., **42** (2000) 1635.

6. S. M. Wilhelm and N. Hackerman, J. Electrochem. Soc., **128** (1981) 1668.

7. Y. Mito, M. Ueda and T. Ohtsuka, Corros. Sci., **51** (2009) 1540.

8. C. Sunseri, S. Piazza and F. Di Quarto, Mater. Sci. Forum, **185-188** (1995) 435.

9. H. J. Jang, C. J. Park and H. S. Kwon, Electrochim. Acta, **50** (2005) 3503.

10. C. Sunseri, S. Piazza, Di Paola and F. Di Quarto, J. Electrochem. Soc., **134** (1987) 2410.

11. S. Fujimoto, O. Chihara and T. Shibata, Mater. Sci. Forum, **289-292** (1998) 989.

12. H. Tsuchiya, S. Fujimoto, O. Chihara and T. Shibata, Electrochim. Acta, **47** (2002) 4357.

13. S. Fujimoto and H. Tsuchiya, Corros. Sci., **49** (2007) 195.

14. F. Di Quarto, S. Piazza and C. Sunseri, Corros. Sci., **31** (1990) 721.

Chapter 4 Photoelectrochemical Response of Passive Films Formed on Alloy 600 and Alloy 690 in High Temperature and High Pressure Water; Influence of Dissolved Hydrogen and Cold Working

4.1 Introduction

As corrosion resistance of metallic materials is ascribed to passive film on surface, the structure and properties of passive films have been examined. Semiconductive property is one of the most investigated properties of passive films and can be studied by photoelectrochemical response and electrochemical impedance spectroscopy[1-4]. In particular, extensive efforts have been paid to reveal semiconductive properties of passive films on stainless steels in various environments[5-13]. Pure Ni and Ni-Cr alloys have been also often studied. For examples, Wilhelm et al. examined that semiconductive properties of passive film formed on pure Ni in a pH8.4 borate buffer solution by the photoelectrochemical response and found that the passive film exhibited p-type semiconductive nature with the band gap energy of 3.1 eV[14]. Jang et al. investigated effects of Cr on the structure and electronic properties of passive films formed on Ni-Cr alloys and reported that electronic properties were affected by composition of passive films formed on the surfaces[15]. Sunseri et al. proposed a duplex structure consisting of inner anhydrous layer with the band gap energy of approximately 3.45 eV and the outer hydrated oxide layer with the band gap energy of 3.0 eV as an band structure model of passive films formed on pure Ni in pH 8.4 and pH 8.9 borate buffer solutions[16]. Belo et al. suggested a p-n heterjunction structure consisting of an inner p-type region, consisting mainly of chromium oxide, and an

outer n-type region containing iron-nickel oxide as an electronic band structure model of the passive films formed on Ni-based alloys type Alloy 600 in acidic solution and borate buffer solution.[17),18)]. The present authors also examined semiconductive properties of passive films formed on pure Ni, Ni-Cr alloys, Alloy 600 and Alloy 690 in acidic and neutral solutions at room temperature[19)].

Alloy 600 and Alloy 690 have been used as a structural material for steam generator in pressure water reactor (PWR). Therefore, it is important to examine semiconductive properties of passive films formed on the alloys not only at room temperature but also at elevated temperature. Marchetti et al.[20)] studied semiconductive properties of the passive films formed on Ni-30Cr alloy, Alloy 600 and Alloy 690 in high temperature and high pressure water. They separated photoelectrochemical response into three components, that is, three band gap energies of 2.2, 3.5 and 4.1~4.5 eV were estimated. The band gap energy of 2.2 eV was attributed to Ni hydroxide and/or Ni ferrite and that of 3.5 eV was ascribed to Cr_2O_3. Furthermore, it was reported that the spinel phase $Ni_{1-x}Fe_xCr_2O_4$ exhibited the band gap energy of 4.1 ~ 4.5 eV. Kim et al.[21)] examined effects of the solution temperature and the pH on the electrochemical properties of oxide films on Alloy 600. They reported that the oxide formed in 0.5 M H_3BO_3(pH 4.4) at 300 °C showed the p-type semiconducting property unlike the n-type oxide films up to 250 °C. In higher pH solutions (pH 6.5 or pH 13.4) Ni-rich oxide films of the p-type were formed.

The present chapter reports semicondutive property of passive films formed on Alloy 600 and Alloy 690 in high temperature and high pressure water with the focus on influences of cold working and dissolved hydrogen level.

4.2 Experimental

Specimens used were Alloy 600 and Alloy 690. Chemical compositions are listed in Table 4-1. Both alloys were mill-annealed and then subjected to cold working with the reduction rates of 10 and 20 % (denoted as 0, 10 and 20%CW). The surfaces of specimens were mechanically ground with SiC abrasive papers and then polished with alumina pastes. After the polishing, specimens were ultra-sonically cleaned in ethanol, methanol and distilled water, successively. In the present work, prior to electrochemical measurements, polished specimens were passivated in diluted aqueous solution containing 500 ppm B and 2 ppm Li under high temperature and high pressure (360 ^{o}C, 20 MPa). The dissolved oxygen in the solution was maintained at less than 1 ppb and the concentration level of the dissolved hydrogen was controlled as 0, 0.5 and 2.75 ppm.

The electrochemical measurements conducted in the present work were polarization curve measurement and photoelectrochemical response. Both were carried out in a three-electrode cell with a platinum counter electrode and an Ag/AgCl reference electrode in a pH 8.4 borate buffer solution at room temperature. The buffer solution was deaerated with nitrogen gas for more than 12 hours prior to measurements.

Polarization curves of specimens were measured from -1000 mV to 2000 mV with a sweep rate of 1 mV/s in a pH 8.4 borate buffer solution at room temperature. In the photoelectrochemical response measurement, passivated surface of specimens was irradiated by monochromatic light generated using a 150 W Xenon arc lamp and a grating monochromatorin the electrochemical cell through a quartz window, which results in transient of current. The current transient was recorded as photocurrent for 60

s as the wavelength was varied from 250 to 500 nm. The photoelectrochemical response measurements were carried out at 200 mV. Then the applied potential was changed with the interval of 100 mV in the less noble direction and the photoelectrochemical response was measured at each potential.

Table 4-1 Chemical compositions of specimens. (wt%)

	C	Si	Mn	Co	Ni	Cr	Fe	Mo	Ti	Al	P	S	B
Alloy 600	0.010	0.310	0.360	-	75.010	15.710	7.350	-	-	-	0.009	<0.001	-
Alloy 690	0.020	0.120	0.260	0.030	Bal	29.550	9.610	0.020	0.110	0.90	90.00*	20.00*	<10*

(* ppb)

4.3 Results

4.3.1 XPS analysis of passive films

The structure and composition of passive films formed on Alloy 690 and Alloy 600 in high temperature and high pressure water for 24 hours were analyzed by Hard X-ray photoelectron spectroscopy (HAX-PES). Figure 4-1 presents typical Ni2p and Cr2p spectra obtained for passive films formed on Alloy 600 in high temperature and high pressure water with the dissolved hydrogen (DH) level of 2.75 ppm at elevated temperatures. Those obtained from an as-polished sample is included as comparison As shown in Fig. 4-1, the spectra can be decomposed into three peaks, that is, metallic, oxide and hydroxide. From angle resolved HAX-PES it becomes clear that passive films formed on the alloy for 24 hours consist of an inner oxide layer and a covering hydroxide layer. The clear metallic peaks in the spectra ensure that the thickness and composition of passive films on the alloy in the elevated temperature can be calculated from the decomposed spectra. Thicknesses of passive films formed on the alloys were a few tens of nm, affected by dissolved hydrogen level. The passive film formed on the alloys without dissolved hydrogen (DH = 0 ppm) was thicker than those formed with DH of 2.75 ppm. Furthermore, dissolved hydrogen affected Cr fraction in passive films. Without dissolved hydrogen, the Cr fraction in passive films was significantly smaller compared to that in passive films formed with DH of 2.75 ppm in which the Cr fraction in passive films was equivalent to alloy compositions.

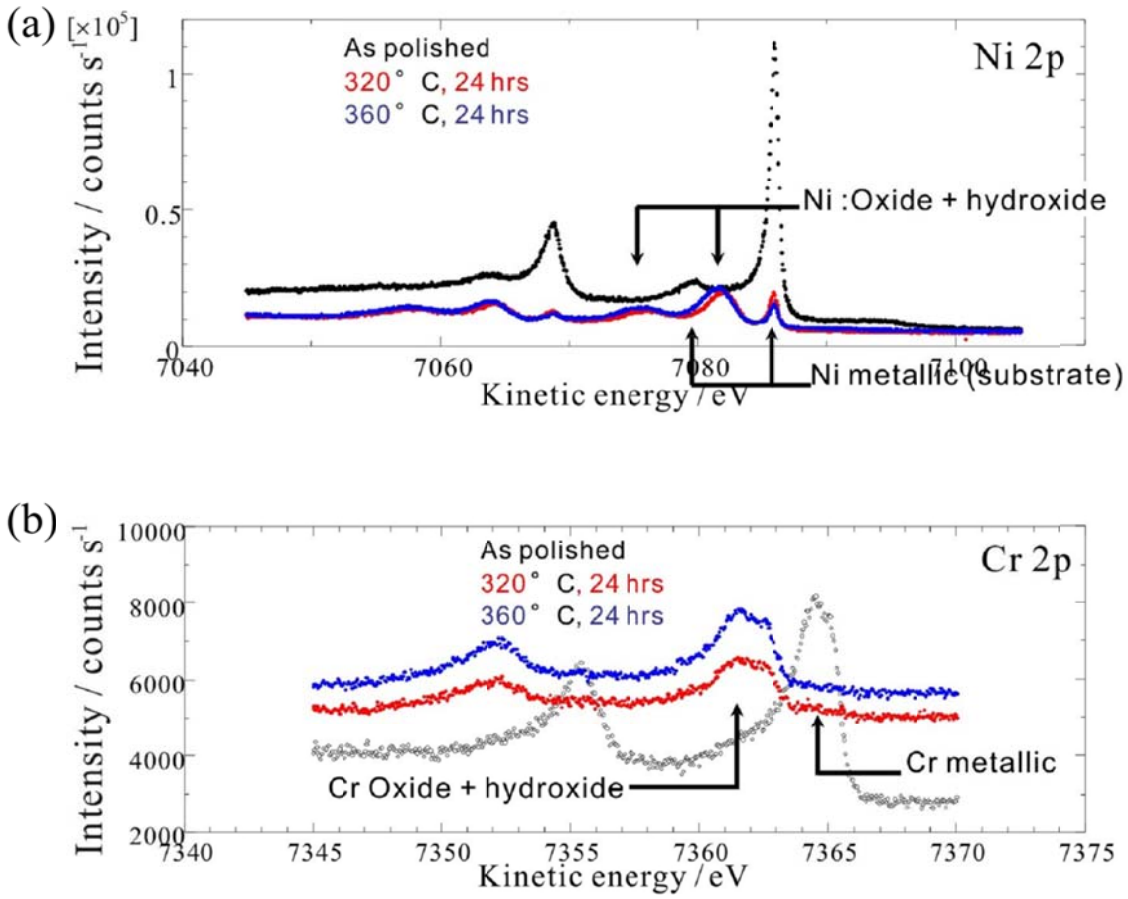

Fig. 4-1 XPS spectra (a) Ni2p and (b) Cr2p detected for the passive films formed on Alloy 600 in high temperature and high pressure water. Spectrum obtained for an as-polished sample was included as comparison.

4.3.2 Polarization curves

Figures 4-2 and 4-3 show polarization curves of Alloy 690 and Alloy 600, respectively, in pH8.4 borate buffer solution at room temperature. Polarization curves shown in Figs. 4-2(a) and 4-3(a) were measured just after polishing the specimens while curves in Figs. 4-2(b) and 4-3(b) were measured for passivated specimens in high temperature and high pressure water for 24 hours with the dissolved hydrogen level of 2.75 ppm. In the case of Alloy 690 as shown in Fig. 4-2, the passivation in high temperature and high pressure water clearly decreases current in the potential range examined and shifts the corrosion potential to the noble direction. It is also apparent that cold working does not affect polarization behavior of as-polished and passivated Alloy 690. On the other hand, cold working significantly changes polarization behavior of passivated Alloy 600, in particular, passive current density drastically increases with increasing the degree of cold working although the polarization behavior of as-polished Alloy 600 is not affected by cold working.

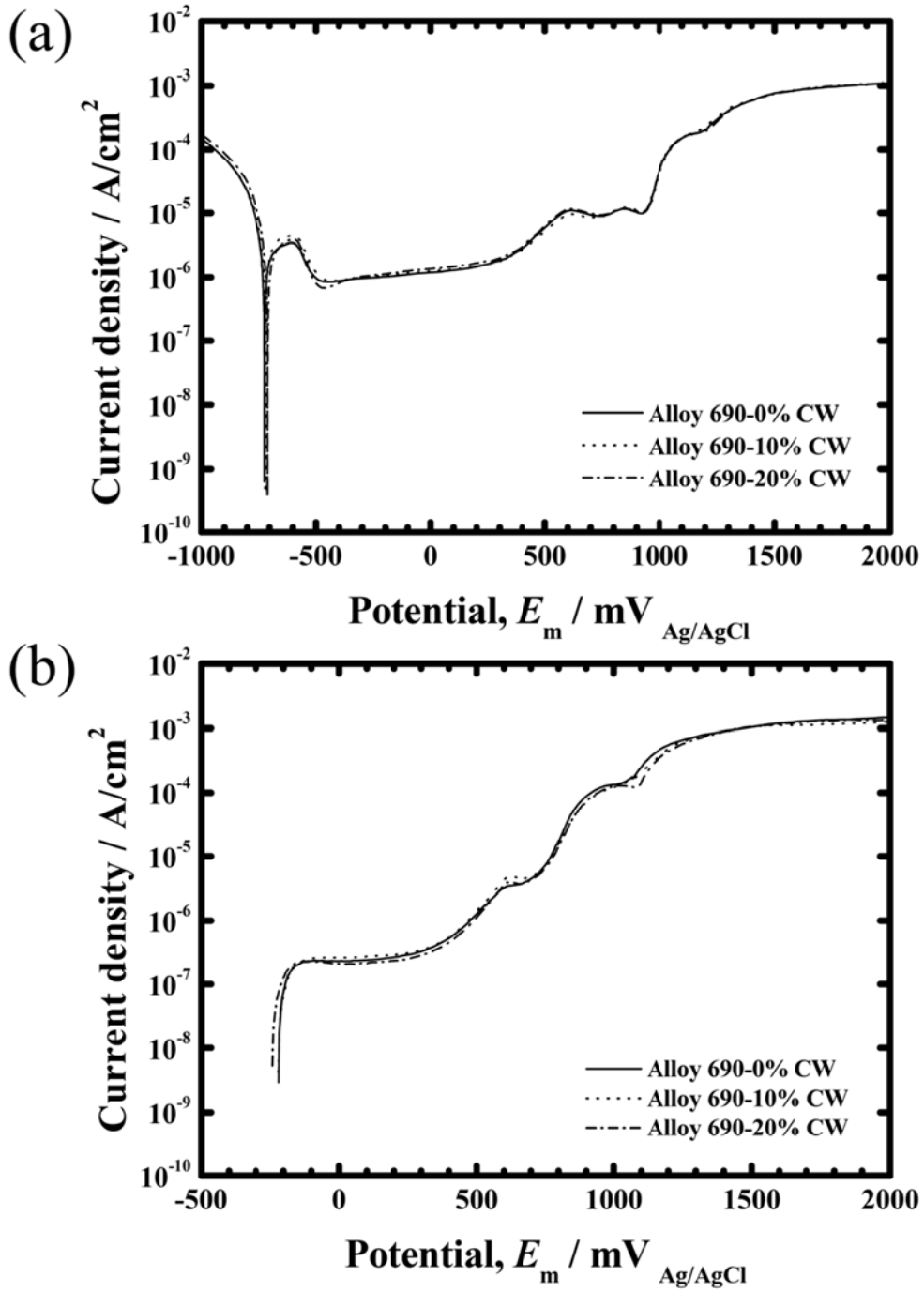

Fig. 4-2 Polarization curves of (a) as-polished and (b) passivated Alloy 690. The passivation was carried out in high temperature and high pressure water for 24 hours with the dissolved hydrogen level of 2.75 ppm.

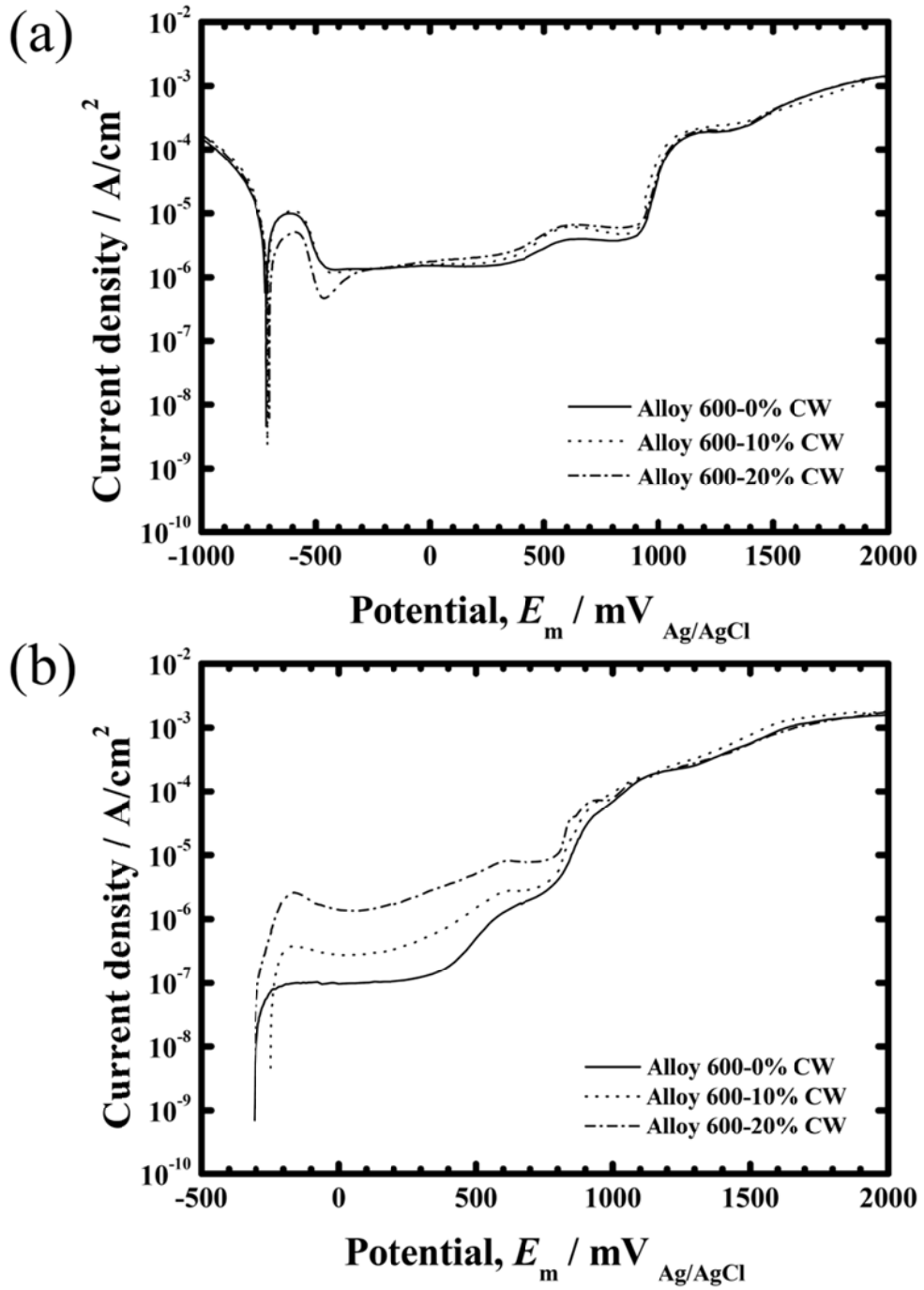

Fig. 4-3 Polarization curves of (a) as-polished and (b) passivated Alloy 600. The passivation was carried out in high temperature and high pressure water for 24 hours with the dissolved hydrogen level of 2.75 ppm.

4.3.3 Photoelectrochemical response

The photoelectrochemical response measurement was carried out in pH8.4 borate buffer solution. Figure 4-4 shows typical photocurrent obtained for passive films formed on Alloy 600 and Alloy 690 in high temperature and high pressure water at the dissolved hydrogen level of 2.75 ppm. It is clear that photocurrent exhibits some transient. The shape of the photocurrent transients obtained from passive films formed on the alloys in high temperature and high pressure water is quite different from that from passive films formed at room temperature (as shown Fig. 3-3)[19]. In the present work the difference between current recorded just after photo irradiation and after 60 s was defined as steady photocurrent and analyzed.

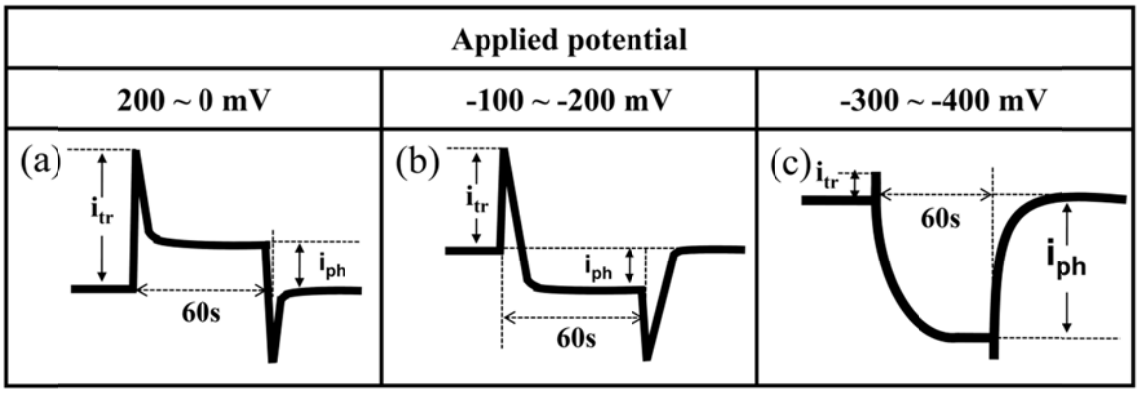

Fig. 4-4 Example of photocurrent transients obtained for passive films formed on Alloy 600 and Alloy 690 in high temperature and high pressure water.

Figure 4-5(a) shows photocurrent spectra obtained for passive films formed on Alloy 600 and Alloy 690 in high temperature and high pressure water with the dissolved hydrogen of 2.75 ppm. It is apparent that higher photocurrent was obtained for the passive film formed on Alloy 690. Furthermore, the photocurrent varied depending on

the wavelength of incident light. As the light intensity is not constant for each wavelength, the photocurrent spectra were normalized for further analyses. Assuming indirect transition for the photo-excitation, photocurrent spectrum can be normalized as photoelectrochemical action spectrum,

$$\left(i_{ph} \cdot h\nu / I_0\right)^{\frac{1}{2}} = C\left(h\nu - E_g\right) \tag{1}$$

where I_0 and $h\nu$ are the intensity and the photon energy of the incident light, respectively. E_g is the band gap energy of passive film and C is constant. Figure 4-5(b) exhibits an example of photoelectrochemical action spectra obtained from Fig. 4-5(a). It is obvious that the photoelectrochemical action spectra do not exhibit one straight line, the slope of the photoelectrochemical action spectra changes around at the photon energy of 3.5eV. As mentioned in 4.3.1, passive films formed on Alloy 600 and Alloy 690 in the present work are duplex structure consisting of an inner oxide layer and a covering hydroxide layer although the compositions of the films are different depending on the dissolved hydrogen level in the environment. Therefore, it is found that photocurrent obtained from the passive films is sum of two responses originated from duplex layers with different band gap energies, which results in the change of the slope in the photoelectrochemical action spectra in Fig. 4-5(b). In the present work, the photoelectrochemical action spectra were separated into two components and then the band gap energy of each layer was estimated. Band gap energy, E_g, was obtained as the photon energy at which the $(i_{ph} \cdot h\nu/I_0)^{1/2}$ equals to zero in photoelectrochemical action spectrum. The separation process of photoelectrochemical action spectrum was previously reported in details. From the photoelectrochemical action spectra shown in Fig. 4-5(b), the band gap energies for the passive films formed on Alloy 600 and Alloy

690 at the elevated temperature were estimated as approximately 2.3 eV and 3.5 eV. Band gap energies of chromium oxide and nickel oxide were reported as approximately 3.5 eV while those of chromium hydroxide and nickel hydroxide were reported as around 2.3 – 2.5 eV[16),22),23)]. The band gap energies estimated in the present work are similar to those in the literatures. Therefore, it is found that the obtained band gap energy of 3.5 eV is derived from chromium and nickel oxides whereas that of 2.3 eV is from chromium and nickel hydroxides. These results are in line with the structure of passive films formed on the alloys, which was determined by the XPS analysis. Figure 4-6 summarizes the band gap energies for passive films formed on the alloys in high temperature and high pressure water. The band gap energies obtained for passive films formed on the alloys were almost constant independent of the degree of cold working and the dissolved hydrogen level. However, the amplitude of photocurrent was affected by cold working and dissolved hydrogen that will be described in the following sections.

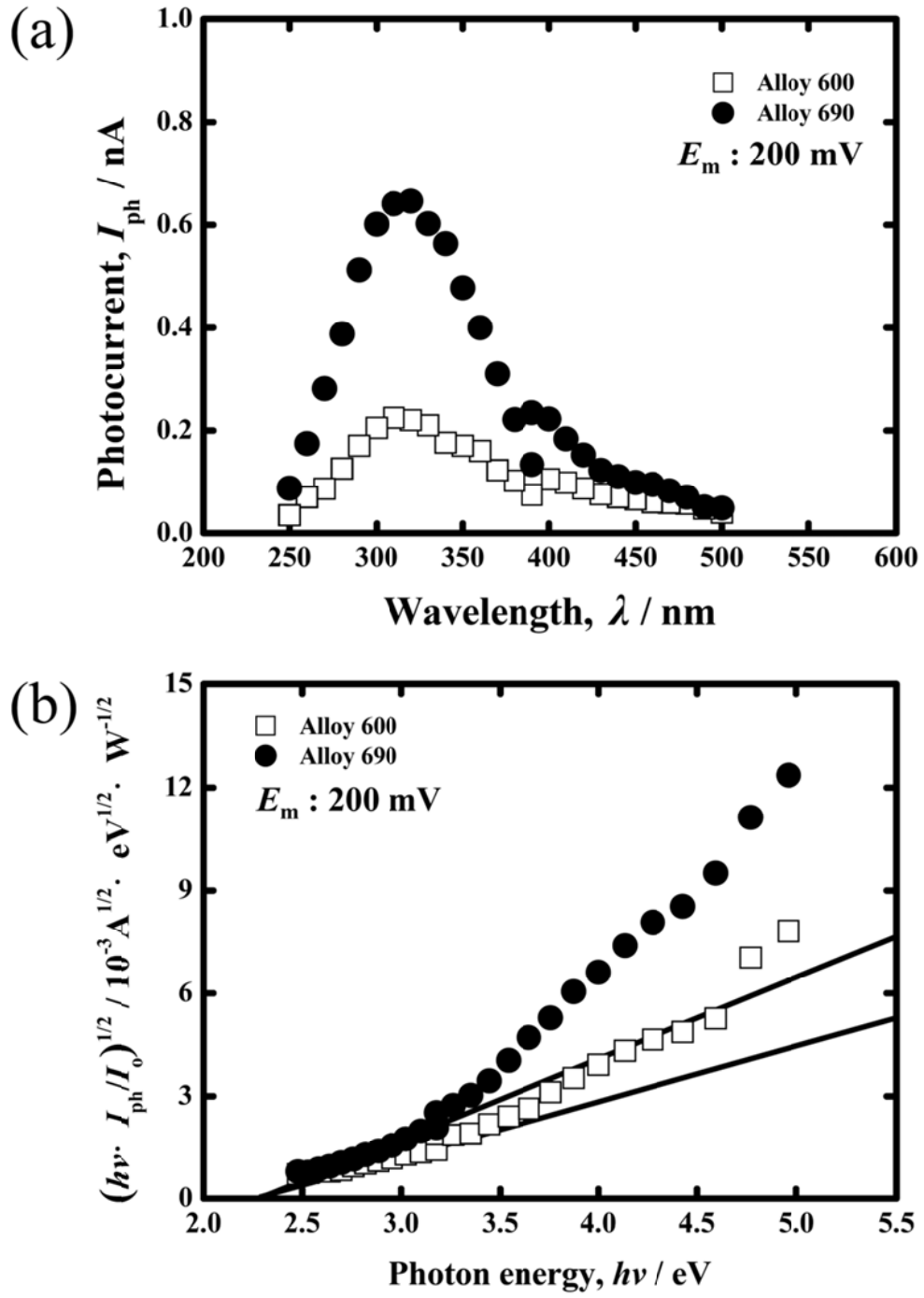

Fig. 4-5 (a) Photocurrent spectra for the passive film formed on Alloy 600 and Alloy 690 in high temperature and high pressure water with the dissolved hydrogen level of 2.75 ppm. (b) Photoelectrochemical action spectra calculated from the photocurrent spectra shown in Fig. 5(a).

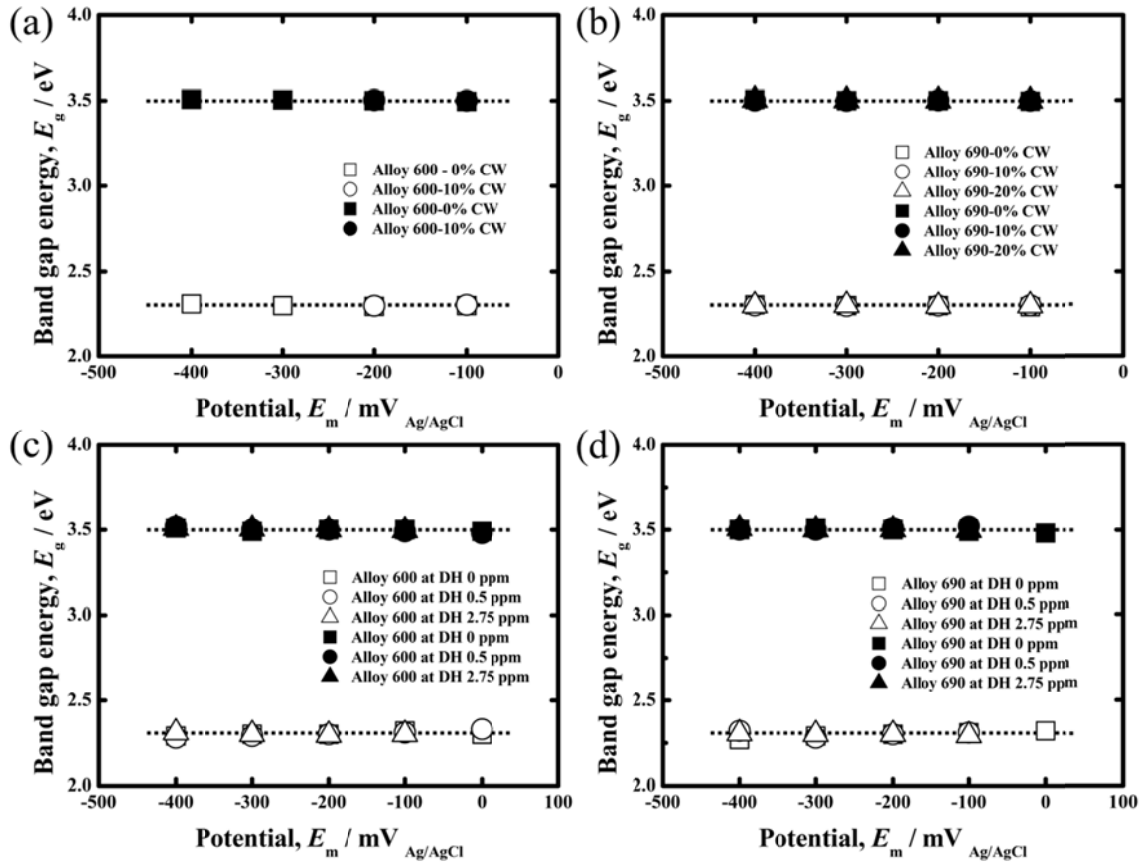

Fig. 4-6 Band gap energies of passive film formed on Alloy 600 and Alloy 690 in high temperature and high pressure water with (a) and (b) the degree of cold working and (c) and (d) the dissolved hydrogen level.

4.3.3.1 Effect of dissolved hydrogen on photoelectrochemical response

Potential dependence of photocurrent was examined also for passive films formed on Alloy 600 and Alloy 690 in high temperature and high pressure water with different dissolved hydrogen levels and was summarized in Figs. 4-7 and 4-8, respectively. Selected wavelengths of incident light were 460 nm and 310 nm, corresponding to the photon energies of approximately 2.7 eV and 4.0 eV, respectively. The former is larger than the band gap energy of outer hydroxide layers, meaning that the photo-excitation takes place only on hydroxide layer. On the other hand, the latter is larger than that of both layers. Therefore, the photo-excitation occurs on both layers. As apparent, photocurrent obtained for passive films formed on Alloy 600 varied depending on the dissolved hydrogen level at which the passive films were formed, that is, photocurrent became smaller with increasing the dissolved hydrogen level independent of photon energy of the incident light. In the case of Alloy 690, on the other hand, photocurrent observed for the passive film formed under the dissolved hydrogen level of 2.75 ppm was similar to that for the passive film formed under the dissolved hydrogen of 0.5 ppm. However, photocurrent obtained for the passive film formed without dissolved hydrogen was larger compared to those obtained for the passive films formed under the dissolved hydrogen of 2.75 and 0.5 ppm. Therefore, it becomes clear that semiconductive properties of passive films were affected also by the dissolved hydrogen.

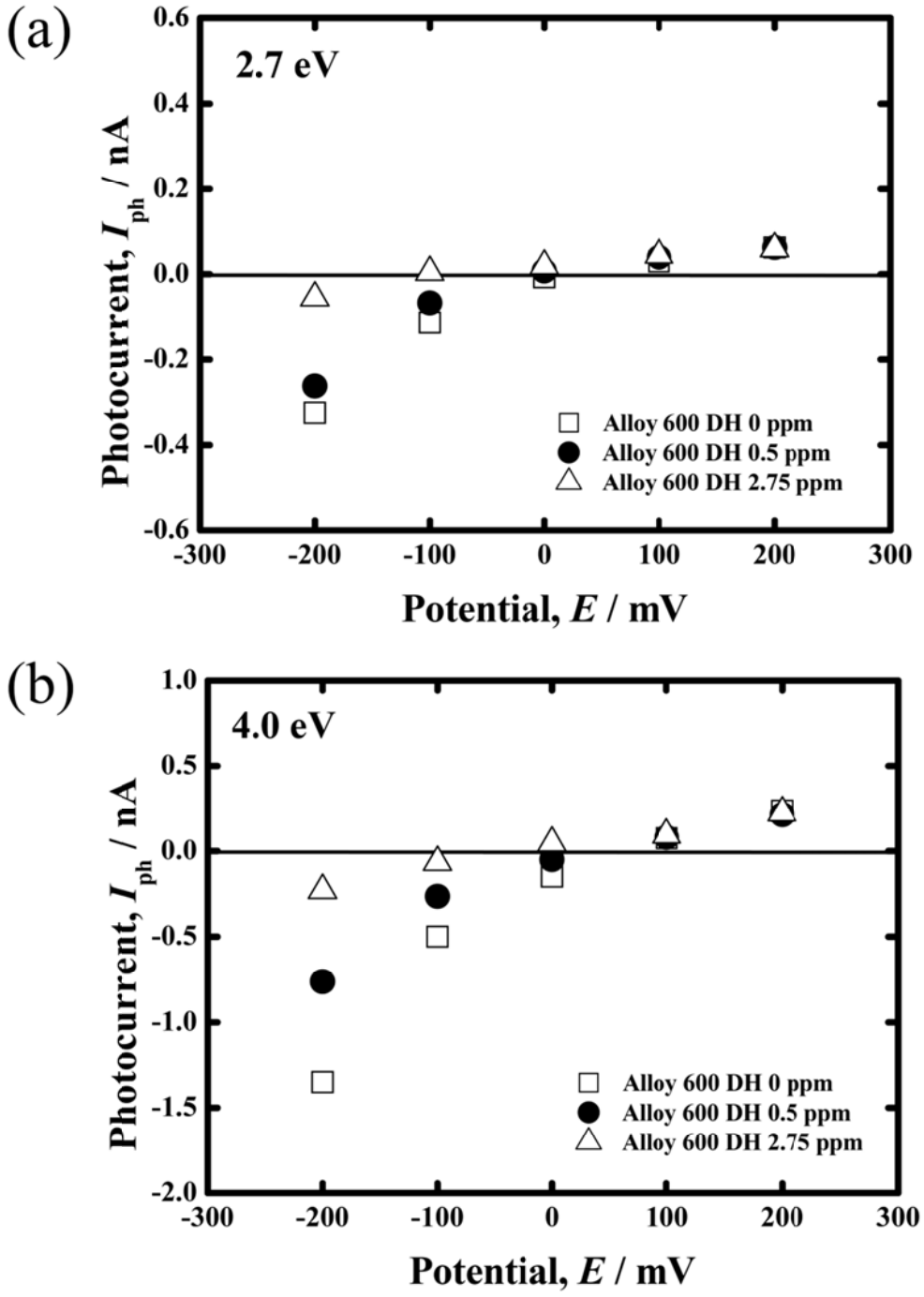

Fig. 4-7 Potential dependence of photocurrent for passive films formed on Alloy 600 in high temperature and high pressure water with different dissolved hydrogen levels at photon energies used for the photocurrent measurement were (a) 2.7 eV and (b) 4.0 eV.

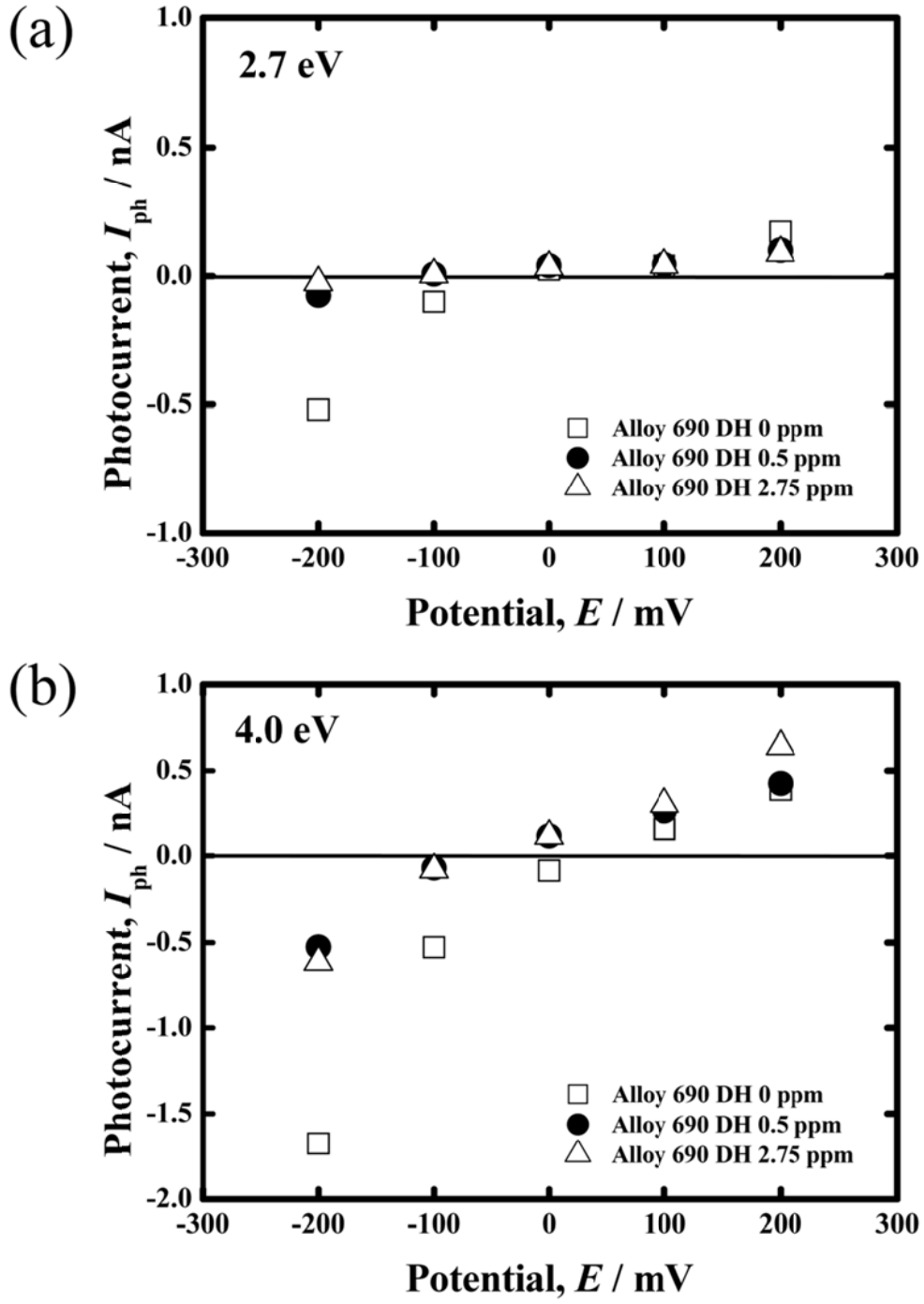

Fig. 4-8 Potential dependence of photocurrent for passive films formed on Alloy 690 in high temperature and high pressure water with different dissolved hydrogen levels at photon energies used for the photocurrent measurement were (a) 2.7 eV and (b) 4.0 eV.

4.3.3.2 Effect of cold working on photoelectrochemical response

Figures 4-9 and 4-10 show potential dependence of photocurrent measured for passive films formed on Alloy 600 and Alloy 690 with different degree of cold working, respectively. Also in this figure, selected wavelengths of incident light were 460 nm and 310 nm because the band gap energies obtained for the passive films were similar independent of the dissolved hydrogen level. It is clear that the potential dependence of photocurrent obtained on Alloy 690 is independent of the degree of cold working and quite similar to each other for both photon energies while potential dependence of photocurrent obtained on Alloy 600 is clearly different depending on the degree of cold working. Furthermore, for 20%CW specimen, photocurrent could not be measured due to the relatively high passive current density as shown in Fig. 4-3(b). These results imply that semiconductive properties of passive films formed on Alloy 600 were strongly affected by cold working although no obvious influence of cold working on semiconductive properties of passive films were confirmed on Alloy 690.

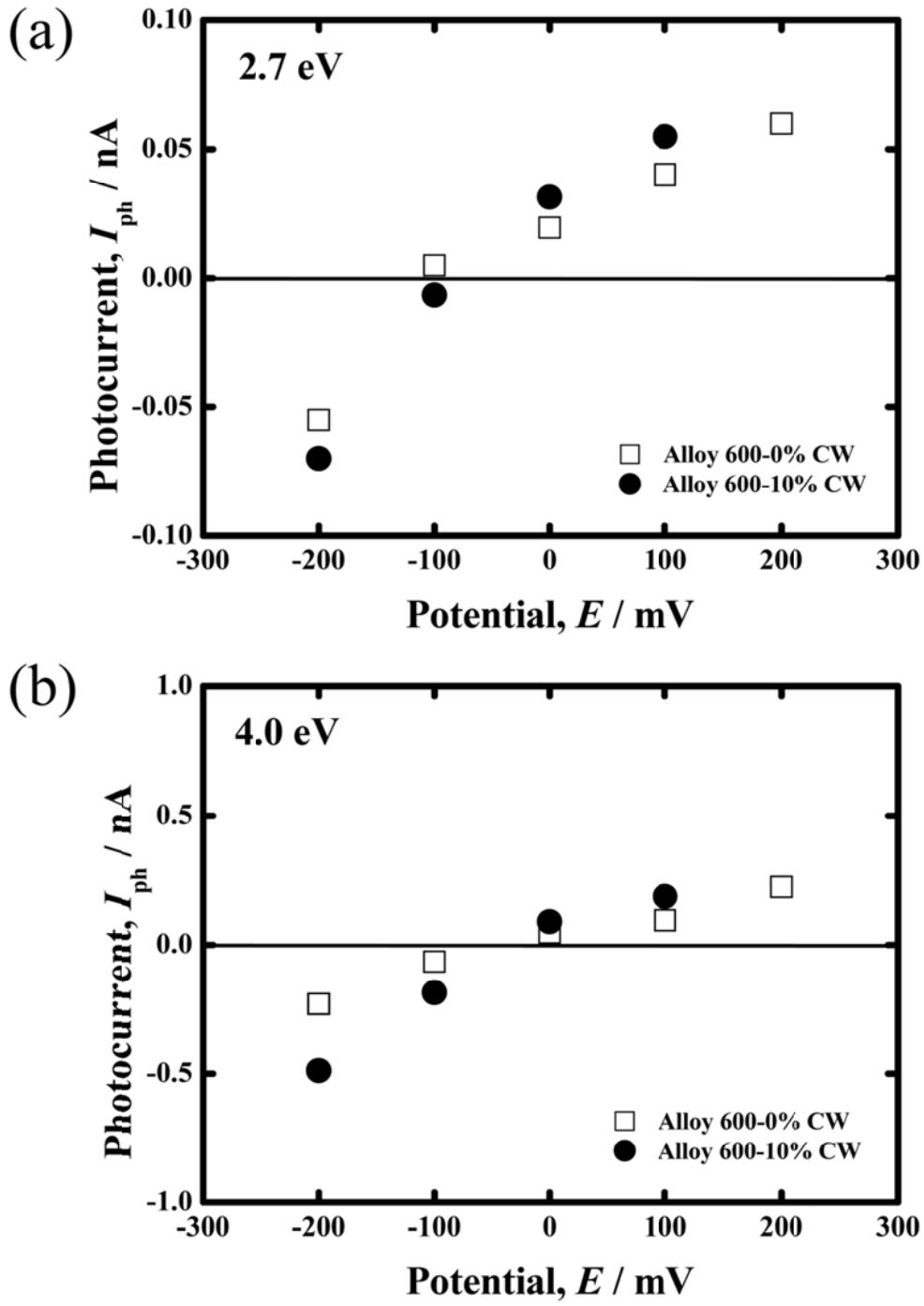

Fig. 4-9 Potential dependence of photocurrent for passive films formed on Alloy 600 in high temperature and high pressure water with different degree of cold working at photon energies used for the photocurrent measurement were (a) 2.7 eV and (b) 4.0 eV.

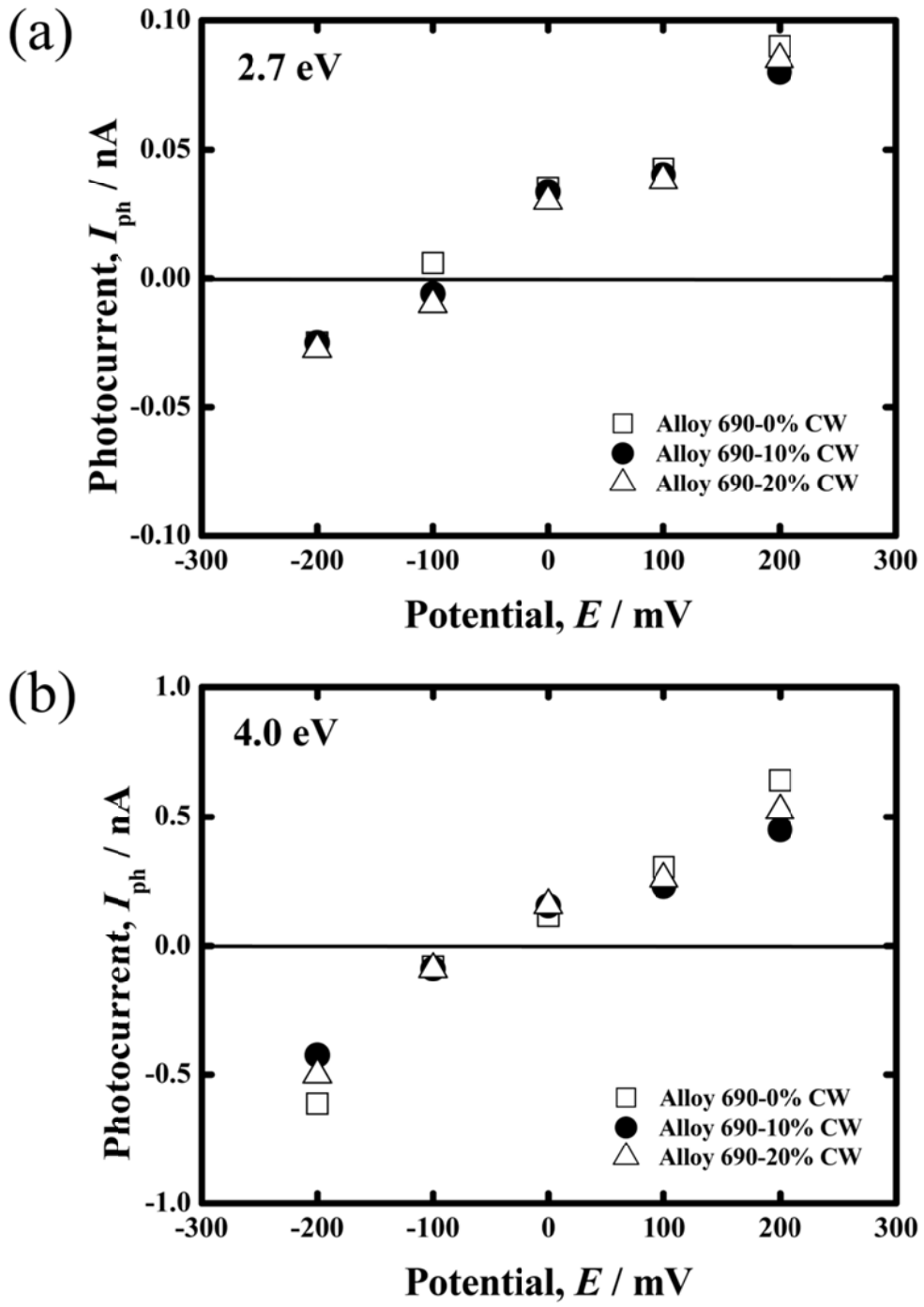

Fig. 4-10 Potential dependence of photocurrent for passive films formed on Alloy 690 in high temperature and high pressure water with different degree of cold working at photon energies used for the photocurrent measurement were (a) 2.7 eV and (b) 4.0 eV.

4.4 Discussion

4.4.1 Photocurrent transients and electronic band structure

Passive films formed on Alloy 600 and Alloy 690 exhibited three types of photocurrent transients in the present work as shown in Fig. 4-4. The photocurrent transient of Fig. 4-4(a) is observed at high measured potential above flat band potential. The anode photocurrent was generated rapidly just after photo irradiation by increasing the separation of the electron-hole pairs[24), 25)]. The hole and the electron migrate toward the electrolyte interface and the alloy, respectively. During photo irradiation, migration of holes is very difficult because the hole is accumulated in the electrolyte interface. And then photocurrent decreases to a steady state value. After photo irradiation is terminated, in contrast to photo irradiation, an opposite transient current is obtained. The photocurrent transient of the Fig. 4-4(b) was occurred similar to that of the Fig. 4-4(a). However, the cathodic current generated during the photo irradiation. It is that the hole migrate toward the alloy in the SCL(II_a) and the SCL(II_b) which are used both in the depleted state. In case of Fig. 4-4(c), the SCL(III) decreases due to the accumulation of electrons in the conduction band at low measured potential. Both the SCL(II_a) and the SCL(II_b) are also used in the depleted state. Typically, the width of the accumulated region as SCL(III) is very thin compared to that of the depleted region as SCL(II). Therefore, the accumulated region should not affect the photocurrent. And the transient current did not occur at low measured potential because the width of the SCL(III) is attributed to the transient current. The photocurrent is rapidly changed in the cathodic direction just after photo irradiation commenced, and then the photocurrent slowly approached a steady state value. After photo irradiation is terminated the photocurrent turns back to the original value by the opposite method of photo irradiation.

As mentioned in the results, the band gap energy of p-type inner oxide layer for the passive film formed on Alloy 600 and Alloy 690 in high temperature and high pressure water was shown as 3.5 eV whereas the band gap energy of n-type outer hydroxide layer for that was obtained as 2.3 eV. In the present work, the electronic band structure model of the passive film formed on Alloy 600 and Alloy 690 in high temperature and high pressure water was proposed as shown in Fig. 4-11.

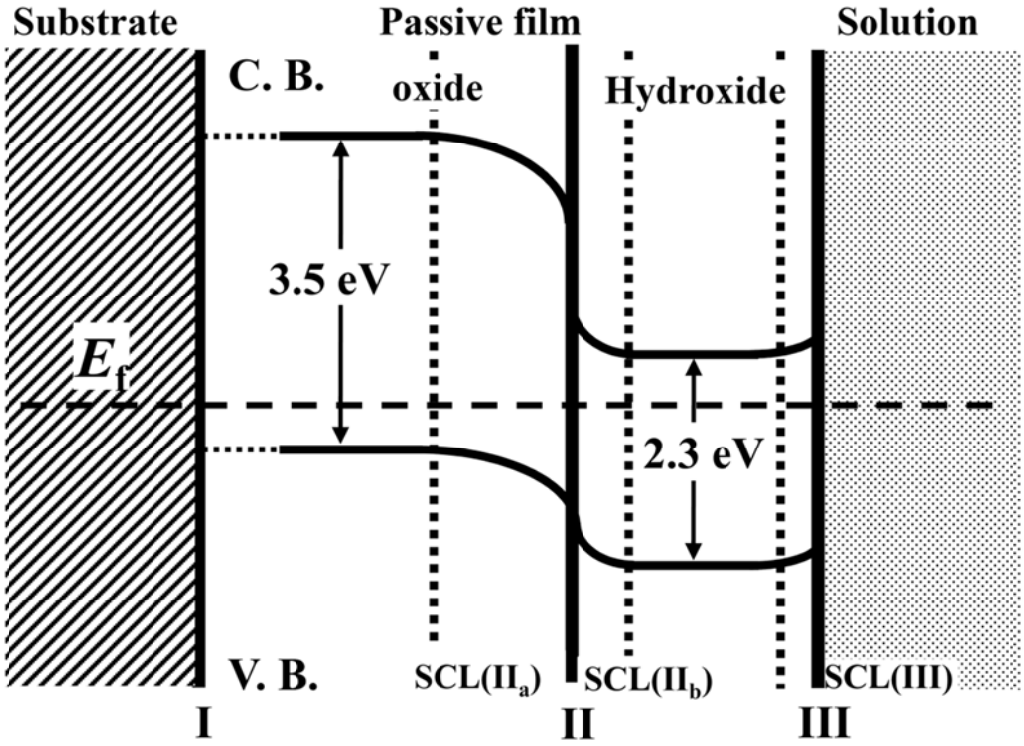

Fig. 4-11 The electronic band structure model of passive films formed on Alloy 600 and Alloy 690 in high pressure and high temperature.

4.4.2 Effect of dissolved hydrogen and cold working

In the present work, the photoelectrochemical response for passive films formed on Alloy 600 and Alloy 690 was examined. The results indicated that band gap energies of passive films on the alloys were similar independent of cold working and dissolved hydrogen. However, cold working and dissolved hydrogen clearly affected the amplitude of photocurrent as shown in Figs. 4-7, 4-8, 4-9 and 4-10. The present section discusses how cold working and dissolved hydrogen affect photocurrent generated from passive films on the alloys in high temperature and high pressure water.

4.4.2.1 Effect of dissolved hydrogen

As shown in Fig. 4-7, the amplitude of photocurrent obtained for the passive films formed on Alloy 600 was affected by dissolved hydrogen. In particular, clear changes can be observed in the amplitude of photocurrent when the incident light with the photon energy of 4.0 eV was used. Photo irradiation with the energy of 4.0 eV causes photo-excitation on both inner oxide and outer hydroxide layers while with the photon energy of 2.7 eV photo-excitation takes place only on outer hydroxide layer. It is clear from Fig. 4-7(a) that the photocurrent generated for outer hydroxide layer is small. Therefore, in the photocurrent generated for both oxide and hydroxide layers shown in Fig. 4-7(b), contribution from hydroxide layer can be relatively smaller compared to that from oxide layer. That is, changes in photocurrent in Fig. 4-7(b) reflect properties of inner oxide layer. The stability of oxides in high temperature water can be affected by dissolved hydrogen, especially, the stability of NiO is strongly affected by dissolved hydrogen among the constituent of Alloy 600. It is reported that the dissolved hydrogen level at the Ni/NiO phase boundary varies with temperature of water[26),27)]. At the

defined temperature in the present work, Ni is stable with the dissolved hydrogen of 2.75 ppm while in the case of 0 and 0.5 ppm, NiO is more stable phase compared to Ni. Therefore, the chemical composition of passive films formed on Alloy 600 can change depending on dissolved hydrogen level, that is, passive film formed under the dissolved hydrogen of 2.75 ppm can be considered to contain certain amounts of Cr oxide while passive films formed under 0 and 0.5 ppm contain mainly Ni oxide compared to passive film formed under 2.75 ppm. This is in line with results obtained by XPS analysis of passive films formed. Therefore, it is concluded that the changes in photocurrent depending on dissolved hydrogen can be attributed to the variation of the chemical composition of oxide layer on Alloy 600. For Alloy 690, similar trend was observed to Alloy 600, that is, the amplitude of photocurrent decreased with increasing dissolved hydrogen. However, photocurrent observed for the passive film formed under the dissolved hydrogen of 2.75 ppm was almost similar to that for the passive film formed under 0.5 ppm, which is different from the case of Alloy 600. Cr content in Alloy 690 is almost twice larger than that in Alloy 600. Therefore, passive films on Alloy 690 contain more Cr compared to those on Alloy 600 when the passive films are formed under the same dissolved hydrogen level. This results in the difference observed between Alloy 600 and Alloy 690.

4.4.2.2 Effect of cold working

Photocurrent generated from passive films formed on Alloy 600 was strongly affected by cold working, depending on the degree of cold working, as shown in Fig. 4-9, that is, electronic properties of the passive films formed on the alloy can be varied by cold working. Barbucciet al. reported that a much more defective oxide was formed due to defects in a bulk material introduced by cold working[28]. Therefore, also in the present work, it can be considered that the defects that were introduced by cold working affected a defective structure and electronic properties of passive films. In the present work, the defects in materials were qualitatively examined by Electron Back Scatter Diffraction (EBSD). Figure 4-12 shows the kernel average misorientation (KAM), as represented by the degree of coloring, obtained by analyzing EBSD data. The KAM exhibits local misorientation defined as an average misorientation of a point against all of its neighbors and therefore can estimate qualitatively the residual strain distribution. In Figures 4-12(a) and 4-12(b), the KAM distributions obtained for mill-annealed Alloy 600 and Alloy 690 are presented as an example. As apparent, the KAM distribution is uniform for mill-annealed specimens. Figures 4-12(c) and 4-12(d) show the KAM distribution obtained for 20%CW Alloy 690 and 20%CW Alloy 600, respectively. It is clear that cold working introduces strain, in particular, near grain boundaries the strain level is higher compared to that in grains. Obviously more sever strain is introduced for Alloy 600 compared to Alloy 690. Therefore, one can deduce that strain introduced by cold working affects electronic properties of passive films and resulting photocurrent generated in the present work, That is, strain was introduced into Alloy 690 by cold working, but its amount was not high enough to change electronic properties of the passive films formed on the alloy. On the other hand, as shown in Fig. 4-12(c), in the

case of Alloy 600, more strain introduced affect electronic properties of passive films and resulting photocurrent generated.

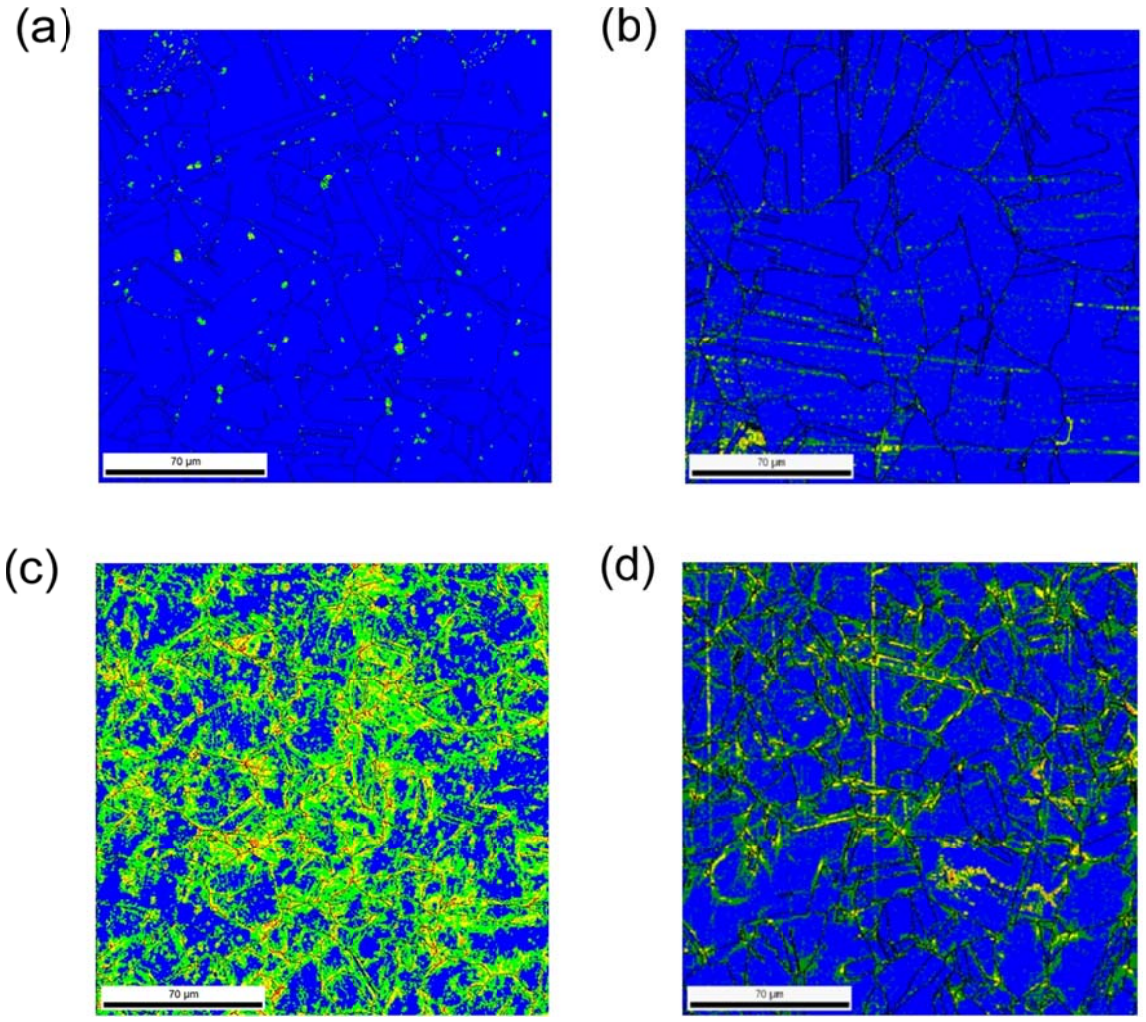

Fig. 4-12 Kernel average misorientation maps for (a) mill-annealed and (c) 20% cold worked Alloy 600, and (b) mill-annealed and (d) 20% cold worked Alloy 690.

4.5 Conclusion

Passive films formed on Alloy 600 and Alloy 690 in high temperature and high pressure water were examined by a surface analytical technique and electrochemical techniques. XPS revealed that passive films formed on Alloy 600 and Alloy 690 consisted of an outer hydroxide layer and an inner oxide layer. The chemical compositions of the passive films significantly changed depending on the dissolved hydrogen level, that is, passive films consisted mainly of nickel oxide and hydroxide when the dissolved hydrogen level was low while larger amounts of chromium was incorporated into passive films when the hydrogen level was higher, like 2.75 ppm. The change of chemical composition in passive films affected photocurrent. Photocurrent obtained for the passive films formed under low concentration of the dissolved hydrogen was large compared to that for the films formed under high concentration of the dissolved hydrogen. Cold working also affected the electrochemical behavior, especially for Alloy 600. Polarization curves and photocurrent obtained for Alloy 690 were similar independent of the degree of cold working. However, polarization curves and photocurrent for Alloy 600 were significantly affected by cold working. This was attributed to larger amounts of local strain introduced to Alloy 600 by cold working compared to Alloy 690.

References

1. U. Stimming, Electrochim. Acta **31** (1986) 415.

2. S. Piazza, M. Santamaria, C. Sunseri and F. Di Quarto, Electrochim. Acta **48** (2003) 1105.

3. T. Ohtsuka and T. Otsuki, Corros. Sci. **40** (1998) 951.

4. J.R. Vilche, K. Jüttner, W.J. Lorenz, W. Kautek, W. Paatsch, M.H. Dean and U. Stimming, J. Electrochem. Soc. **136** (1989) 3773.

5. H. Tsuchiya, S. Fujimoto and T. Shibata, J. Electrochem. Soc. **151** (2004) B39.

6. A.M.P. Simoes, M.G.S. Ferreira, B. Rondot and M. Da Cunha Belo, J. Electrochem. Soc., **137** (1990) 82.

7. P. Schmuki and H. Böhni, J. Electrochem. Soc. **139** (1992) 1908.

8. H. Tsuchiya, S. Fujimoto, O. Chihara and T. Shibata, Electrochim. Acta **47** (2002) 4357.

9. A. Fattah-alhosseini, F. Soltani, F. Shirsalimi, B. Ezadi and N. Attarzadeh, Corros. Sci. **53** (2011) 3186.

10. N.E. Hakiki, Corros. Sci. **53** (2011) 2688.

11. H.-H. Ge, X.-M.Xu, L. Zhao, F. Song, J. Shen and G.-D. Zhou, J. Appl. Electrochem. **41** (2011) 519.

12. N.E. Hakiki, S. Boudin, B. Rondot and M. Da Cunha Belo, Corros. Sci. **37** (1995) 1809.

13. H. Jang and H. Kwon, J. Electroanal. Chem. **590** (2006) 120.

14. S.M. Wilhelm and N. Hackerman, J. Electrochem. Soc. **128** (1981) 1668.

15. H. Jang and H. Kwon, ECS Transactions **3** (2007) 1.

16. C. Sunseri, S. Piazza and F. Di Quarto, Mater. Sci. Forum **185-188** (1995) 435.

17. M. Da Cunha Belo, N.E. Hakiki and M.G.S. Ferreira, Electrochim. Acta **44** (1999) 2473.

18. L.A.S. Ries, M. Da Cunha Belo, M.G.S. Ferreira and I.L. Muller, Corros. Sci. **50** (2008) 676.

19. W.-S. Kim, H. Tsuchiya and S. Fujimoto (submitted to Materials Transactions).

20. L. Marchetti, S. Perrin, Y. Wouters, F. Martin and M. Pijolat, Electrochim. Acta **55** (2010) 5384.

21. D.-J. Kim, H.-C. Kwon and H.P. Kim, Corros. Sci. **50** (2008) 1221.

22. F. Di Quarto, M.C. Romano, M. Santamaria, S. Piazza and C. Sunseri, Russ. J. Electrochem. **36** (2000) 1203.

23. F. Di Quarto, S. Piazza and C. Sunseri, Corros. Sci. **31** (1990) 721.

24. P. Salvador, Surface Science **192** (1987) 36.

25. P. Salvador, C. Gutiėrrez, J. Electranal. Chem. **160** (1984) 117.

26. P.L. Andresen, J. Hickling, A. Ahluwalia and J. Wilson, Corros. **54** (2008) 707.

27. Q. Peng, J. Hou, K. Sakaguchi, Y. Takeda and T. Shoji, Electrochim. Acta **56** (2011) 8375.

28. A. Barbucci, G. Cerisola and P.L. Cabot, J. Electrochem. Soc. **149** (2002) B534.

Chapter 5 Characterization of Oxide Films Formed on Alloy 600 and Alloy 690 in Simulated PWR Primary Water by Using Hard X-ray Photoelectron Spectroscopy (HAX-PES)

5.1 Introduction

Ni based alloys are widely used in various energy and chemical plants such as light water nuclear reactors. For examples, Alloy 600 and Alloy 690 have been used for the materials of steam generator (SG) tubing of pressurized water reactor (PWR). However, intergranular stress corrosion cracking (IGSCC) has been frequently reported for SG tubing of mill-annealed Alloy 600[1)-3)]. Therefore, this material has been replaced successively by Alloy 690[4)] as IGSCC of SG tubing on Alloy 690 has not led to a significant failure in practical use. On the other hand, in laboratory tests cracks that could propagate as IGSCC have been confirmed on cold-worked Alloy 690 in the PWR primary water environment[5)-6)]. Therefore, IGSCC of Alloy 690 employed in the primary side of PWR environment can be of a significant importance, and numerous efforts to understand IGSCC behavior on the Ni-based alloys have been paid. As several properties of oxide films formed on metals and alloys, for examples, chemical composition, thickness and electrochemical properties, may be related to the corrosion process including SCC, many authors have studied oxide films formed on Ni based alloys also in high temperature and high pressure aqueous environments[7)-21)].

The properties of passive films have been examined using several electrochemical techniques[22)-24)] and also using various surface analytical techniques[25-26)]. Among the analytical techniques, X-ray photoelectron spectroscopy (XPS) and Auger electron spectroscopy (AES) have been extensively applied for passivity study. XPS is

applicable for characterization of passive films formed on corrosion resistant alloys including stainless steels and Ni based alloys as the inelastic mean free path of photoelectrons is comparable with the thickness of passive films formed on the materials. This indicates that the photoelectrons yielded over the entire thickness of passive films can be detected without any destructive process such as sputtering; hence, the thickness, composition, and chemical states of passive films formed on various materials have been successfully studied[27)-31)]. However, as oxide films formed even on such materials in high temperature aqueous solutions are very thick, it is difficult for conventional XPS to analyze the thick oxide films. Therefore, passive films on Ni based alloys exposed to high temperature water environments has been characterized using sputtering technique in AES[8)] or XPS[7), 10)]. On the other hand, as hard X-ray photoelectron spectroscopy (HAX-PES) can provide large energy of incident X-ray, the kinetic energy of photo electrons becomes large, meaning that much larger inelastic mean free path can be realized. This enables the characterization of much thicker passive films.

The present chapter describes surface analysis on oxide films of Alloy 600 and Alloy 690 formed in high temperature and high pressure water with the focus on influences of cold working and dissolved hydrogen level. Passive films of Alloy 600 and Alloy 690 were formed in simulated PWR primary water, and were then characterized by hard X-ray photoelectron spectroscopy using high energy X-rays generated by a synchrotron radiation facility.

5.2 Experimental

Materials examined were mill-annealed Alloy 600 and Alloy 690, chemical compositions of which are listed in Table 5-1. The alloys were cut into small coupon specimens with the size of approximately 3×8×3 mm^3. The specimens were ground using SiC paper, mirror-finished using submicron alumina paste, and then degreased in acetone, methanol and distilled water successively in an ultra-sonic bath. Specimens were immersed in a high temperature and high pressure aqueous solution containing 500 ppm B and 2 ppm Li (0.046 M H_3BO_3 + 2.9×10^{-4} M LiOH) for 24 hours at 320 °C or 360 °C using an autoclave with a solution-circulating facility. The concentration of oxygen (DO) was maintained less than 2ppb during the immersion while dissolved hydrogen (DH) was controlled to be 0 or 2.75ppm.

The immersed specimens were characterized using a HAX-PES apparatus at Spring-8, a large synchrotron radiation facility in the Harima Science Park City, Hyogo, Japan. The SCIENTA R-4000 hemispherical electron energy analyzer at BL46XU was used in the present work. The photon energy of the incident X-rays was around 7940 eV and the energy resolution of the system was 225 meV estimated by the measurement of the Fermi edge of Au at pass energy of 200 eV. The photoelectron take-off angle adopted in the present work was 80° and was occasionally changed to 30°.

Table 5-1 Chemical compositions of specimens. (wt%)

	C	Si	Mn	Co	Ni	Cr	Fe	Mo	Ti	Al	P	S	B
Alloy 600	0.010	0.310	0.360	-	75.010	15.710	7.350	-	-	-	0.009	<0.001	-
Alloy 690	0.020	0.120	0.260	0.030	Bal	29.550	9.610	0.020	0.110	0.90	90.00*	20.00*	<10*

(* ppb)

5.3 Results

5.3.1 XPS analysis of passive films

Figure 5-1 shows typical photoelectron spectra obtained for Alloy 600 and Alloy 690. The alloys were exposed to the simulated PWR primary water with 2.75 ppm DH at 360 °C for 24 hours. It is clear from the figure that the spectrum of each element can be separated into some chemical states. The binding energy, E_b, of each component obtained is summarized in Table 5-2. These values are determined by referring to those reported in the literatures[14), 29), 30)-33)]. Some of separated spectra can be identified to photoelectrons of the metallic states of Ni, Cr, and Fe for both Alloy 600 and Alloy 690. As photoelectrons of metallic states are yielded from the substrate alloy, it can be deduced that the photoelectrons pass through oxidized layer formed on the substrate, and are detected by an analyzer. Therefore, it is confirmed that photoelectrons yielded over the entire thickness of the oxide layer are successfully detected for further analysis. It is apparent that in Ni spectra shown in Fig. 5-1(a), the intensity of the oxide, Ni^{ox}, is quite small compared to that of the hydroxide, Ni^{hyd} whereas spectra of both oxide and hydroxide of Cr and Fe are clearly recognized for both Alloy 600 and Alloy 690. This result indicates that the amount of Ni is quite small in the oxide layers formed on Alloy 600 and Alloy 690 in this high temperature and high pressure water environment.

Figure 5-2 shows the spectra obtained for Alloy 600 immersed in the solution with 2.75 ppm DH and without DH at 320 °C for 24 h. More hydroxides and oxides of Ni and Fe are formed when exposed to the solution without DH compared to the case with DH. On the other hand, more Cr is included in the hydroxides and oxides of the oxide layer formed on Alloy 600 exposed to the solution with DH.

Table 5-2 Binding energy of various states of elements examined in the present study.

Element	Chemical state	Binding energy (eV)
Ni	Ni^0 $2p_{3/2}$ (metal)	852.8
	$Ni^{2+}2p_{3/2}$ (oxide)	854.9
	$Ni^{2+}2p_{3/2}$ (hydroxide)	856.7
Fe	Fe^0 $2p_{3/2}$ (metal)	706.8
	$Fe^{2+}2p_{3/2}$ (oxide)	709.5
	$Fe^{3+}2p_{3/2}$ (oxide)	711.2
	$Fe^{3+}2p_{3/2}$ (hydroxide)	713.2
Cr	Cr^0 $2p_{3/2}$ (metal)	574.1
	$Cr^{3+}2p_{3/2}$ (oxide)	576.4
	$Cr^{3+}2p_{3/2}$ (hydroxide)	577.6
O	O^{2-} 1s (oxide)	530.1
	OH^- 1s (hydroxide)	531.7
	O^{2-} 1s (H_2O)	533.3
C	C 1s	285.0

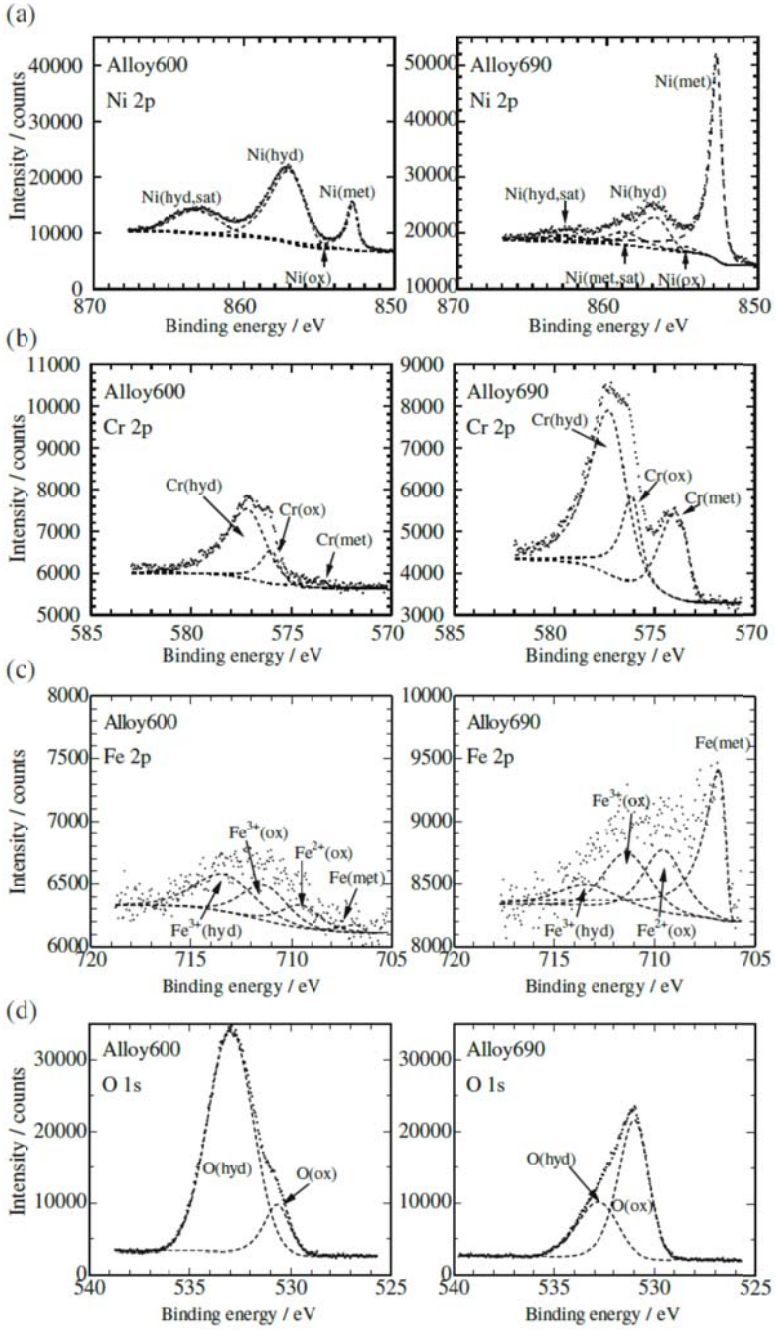

Fig. 5-1 HAX-PES spectra of (a) Ni2p, (b) Cr2p, (c) Fe2p, and (d) O**1**s measured for Alloy 600 and Alloy 690 immersed in the simulated PWR primary system at 360 ºC with 2.75ppm DH for 24 h.

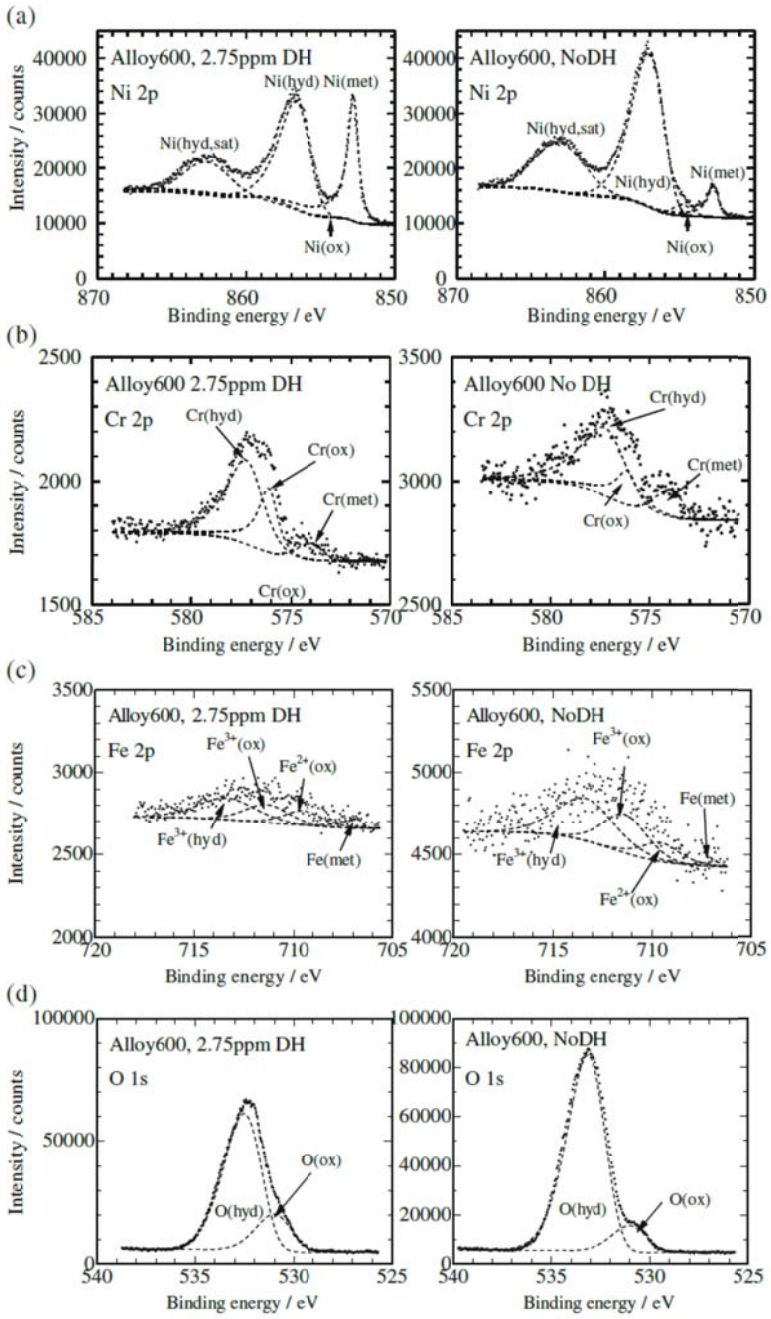

Fig. 5-2 HAX-PES spectra of (a) Ni2p, (b) Cr2p, (c) Fe2p, and (d) O1s measured for Alloy 600 immersed in the simulated PWR primary system at 320 ºC with 2.75ppm DH and without DH for 24 h.

5.3.2 Surface morphology

Figure 5-3 shows the morphology of some oxidized specimens formed on Alloy 600 and Alloy 690 was observed by field emission scanning electron microscopy (FE-SEM). It is noticeable that needle-like corrosion products are formed and distributed on the surfaces and the amount of the products is larger for Alloy 600 than for Alloy 690. Furthermore, the amount of these products is larger in the solution without DH than in the solution with 2.75ppm DH. Although some granular deposits are also visible, their morphologies are not found to be similar to those of granular oxides commonly observed on stainless steels immersed in a high temperature and high pressure water.

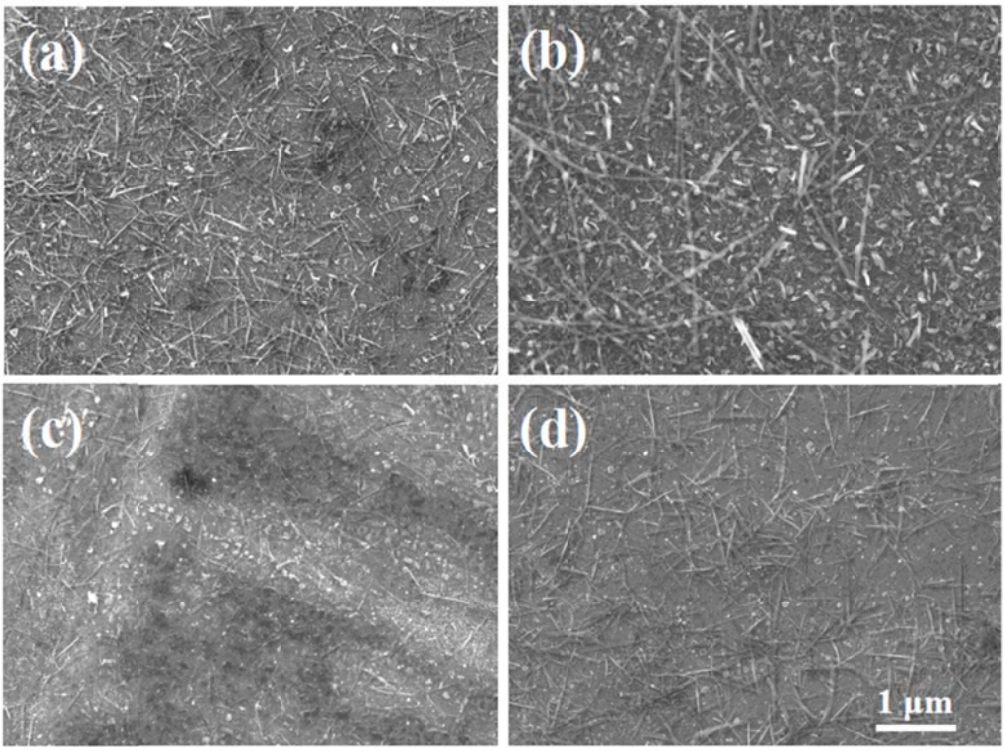

Fig. 5-3 SEM imagess of the surface of specimens immersed in simulated PWR primary water at 360 ºC for 24 h. (a) Alloy 600 with 2.75ppm DH, (b) Alloy 600 without DH, (c) Alloy 690 with 2.75ppm DH, and (d) Alloy 690 without DH.

5.3.3 Parameters for quantitative analysis on XPS spectra

Passive films are characterized quantitatively using the integrated intensity of each component of XPS spectra. For quantification, photoionization cross section, σ, and inelastic mean free path, λ, that denote the sensitivity to yield photoelectrons and the escape length of photoelectrons, respectively, are required. In the present study, the photoelectron spectra of as-received Alloy 600 are also measured. The photoionization cross-section of an element, *z*, in an alloy, σ_z, is described by the following equation, assuming that the alloy surface is covered with a thin passive film and a contaminant layer:

$$I_z = (\Psi X C_z \sigma_z \lambda_z^{met}) \exp(-d^{layer}/\lambda_z^{layer} \sin\theta) \exp(-t^{con}/\lambda_z^{con} \sin\theta) \quad (5.1)$$

where I_z indicates the integrated intensity of photoelectrons that yielded from element *z* in an alloy, then passed through both passive film and contaminant layer; Ψ and X means apparatus constant and intensity of incident X-rays, respectively; C_z is the molar concentration of element *z* for a unit volume of an alloy; d^{layer} and t^{con} express thicknesses of the passive film and contaminant layer, respectively; λ_z^{met}, λ_z^{layer}, and λ_z^{con} are the inelastic mean free paths of photo electrons yielded from element *z*, some layer (passive film in the present study), and contaminant layer, respectively; and θ is the take-off angle of the photoelectrons. Since in the present study the take-off angle of 80° is applied, that is, θ = 80°, sinθ provides 0.985. Therefore sinθ can be assumed as unity and then ignored for the calculation. The inelastic mean free paths of the elements in metal, oxide and/or hydroxide, and contaminant hydrocarbon ($C_{12}H_{12}$) are estimated in the present study using Quases-IMFP-TPP2M Ver. 2.2 software,

developed by Tougaard[34] according to the formula proposed by Tanuma etal.[35]. Table 5-3 summarizes the results. The thicknesses of the naturally formed passive film and contaminant layer that covers the passive film are assumed to be 1.5 nm and 2 nm, respectively, by referring to our previous study[31]. The photoionization cross-sections of Ni, Cr, and Fe are also computed to 23.88×10^4, 6.26×10^4 and 10.23×10^4, respectively, provided that ΨX can be treated as unity and unchanged throughout the present study.

Table 5-3 List of inelastic mean free paths for photoelectrons employed in the present study

(nm)

	E_K**	in Metal	in NiO	in Cr_2O_3	in $C_{14}H_{14}$
Ni	(7100)	7.40	8.40	9.53	14.1
Cr	(7350)	8.53	8.65	9.81	14.6
Fe	(7250)	7.99	8.55	9.69	14.4
O	(7650)	-	8.70	10.14	15.1
C	(7400)	15.14*	8.95	9.86	14.7

** approximate kinetic energy

* in graphite

5.3.4 Numerical characterization of oxide layer

The thickness of the oxide layer, d^{layer}, on the Ni based alloys were in the present work estimated by intensity attenuation of the Ni metallic spectrum from the substrate alloy by using eq. (5.1) described below:

$$I_{Ni}^{met} = (C_{Ni}\sigma_{Ni}\lambda_{Ni}^{met}) \exp(-d^{layer}/\lambda_{Ni}^{layer}) \exp(-t^{con}/\lambda_{Ni}^{con}) \quad (5.1)$$

$$d^{layer} = \lambda_{Ni}^{layer} \{\ln(C_{Ni}\sigma_{Ni}\lambda_{z}^{met}/I_{Ni}^{met}) - t^{con}/\lambda_{Ni}^{con}\}, \quad (5.2)$$

where C_{Ni} expresses the molar concentration of Ni (0.108 and 0.0828 mol/cm^3 for Alloy 600 and Alloy 690, respectively). The initially obtained thickness of the oxide layer is calculated, assuming that the Ni content in the substrate alloy remains unchanged during the exposure to high temperature water environment. The alloy composition underneath the oxide layer is also estimated from I_{Ni}^{met}, I_{Cr}^{met} and I_{Fe}^{met} by eq. (5.1) using the roughly estimated thickness of the oxide layer, d^{layer}, obtained above. Then, d^{layer} is re-calculated again using the estimated Ni content. After the steps of the calculation were repeated several times, d^{layer} and alloy composition underneath the oxidized layer were obtained. Figures 5-4 and 5-5 shows the calculated results, that is, thickness evolution and Cr concentration in the substrate alloy, respectively. As shown in Fig. 5-4, the thickness increases with solution temperature and furthermore oxide layers formed on Alloy 600 are thicker compared to those on Alloy 690. It is also noticeable that a much thicker oxide layer is grown on Alloy 600 when exposed to the solution without DH. Figure 5-5 clearly indicates that the Cr content in the substrate alloy beneath the oxide layer becomes smaller after the immersion in elevated temperatures.

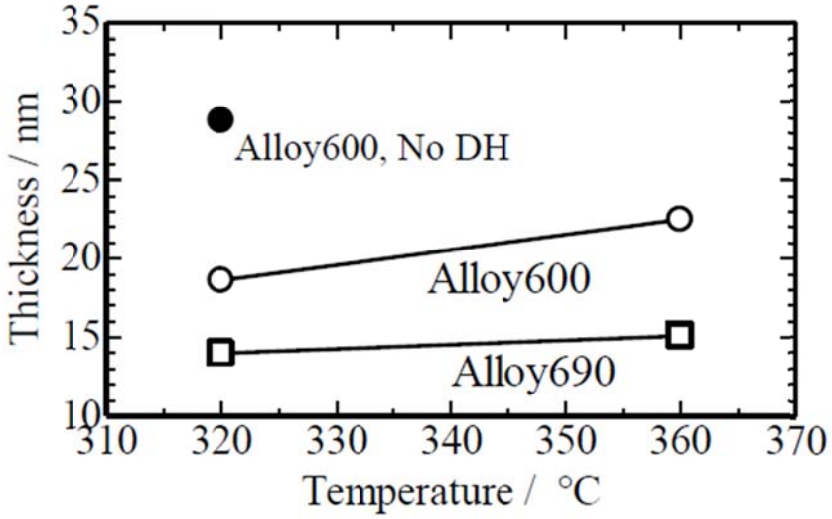

Fig. 5-4 Thickness of oxide films formed on Alloy 600 and Alloy 690 exposed to a simulated PWR primary water at 360 ºC and 320 ºC for 24 h, estimated by intensity attenuation of the Ni metallic spectrum yielded in the substrate alloy.

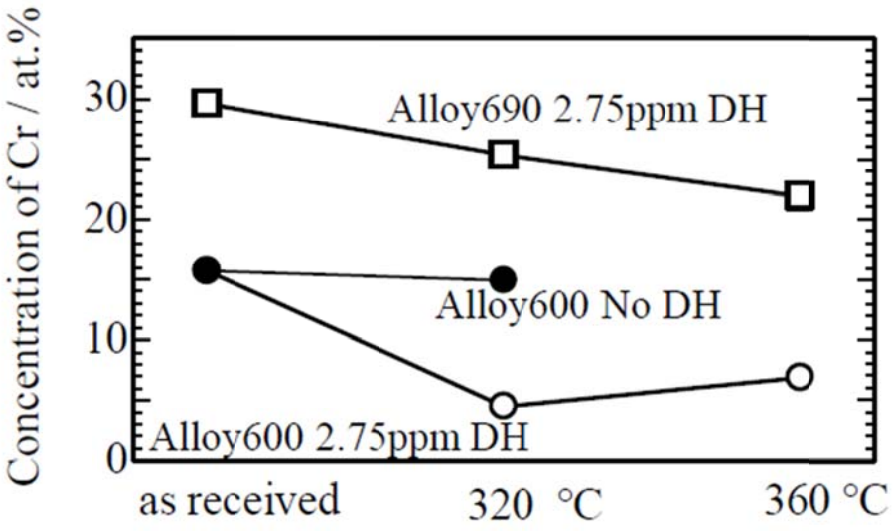

Fig. 5-5 Cr concentration in the substrate alloy underneath oxide films. Specimens are as received and exposed to a simulated PWR primary water at 360 ºC and 320 ºC.

5.4 Discussion

Oxide layers formed in high temperature and high pressure aqueous solutions as in PWR environments have been extensively examined[7)-21)]. Nakagawa etal.[12)] and Terachi etal.[13)] studied oxide films formed on Alloy 600 for 1000 h in simulated PWR primary water environment by using X-ray diffraction (XRD) and transmission electron microscopy (TEM). Results revealed that granular $NiFe_2O_4$ and needle-like Fe-Ni spinel oxides were deposited on Cr rich barrier type oxide layers that were formed on specimens exposed to the solution with DH at 320 °C. On the other hand, Ni-rich thick oxides were formed on the Cr rich continuous oxide layer on Alloy 600 that was immersed in the solution without DH. It is also noted that a Ni-rich metallic layer was grown underneath the oxide layers of the specimen immersed in solution with DH. Ohtsuka et al.[20)] investigated oxide films formed on Alloy 600 and Alloy 690 that were exposed to similar environments for up to 500 h and reported that granular Ni-rich spinel oxides were formed and distributed on the smooth oxide layer mainly composed of Cr. The thickness of the oxide layer was also reported to be approximately 20 nm after 24 h immersion, and then increased with time to approximately 40 nm after 500 h. On the other hand, Marcus et al.[14)] examined the very early stages of passive film formation on Alloy 600 in PWR primary water environment at 325 °C, that is, in this study specimens were immersed in a high temperature aqueous solution for short periods of a few tens of seconds upto 500 s. Then the immersed specimens were characterized by XPS and scanning tunneling microscopy (STM). In such short periods, the thickness of passive film is less than a few nanometers. Therefore, photoelectrons over the entire thickness of the passive film could be detected by a conventional XPS apparatus and analyzed. An ultra-thin layer

with the thickness of approximately 1 nm was formed during 0.4 - 4 min and the layer was mainly composed of an inner Cr oxide layer and a covering hydroxide layer of Cr with a small amount of Ni. During further immersion, the inner oxide layer grew with time to reach the thickness of around 2 nm after 8 min. The thickness and composition of the passive layer were quantitatively determined based on the three-layered structure model of $Ni(OH)_2/Cr(OH)_3/Cr_2O_3$.

As described above, it has been reported that oxide films grown in the PWR primary water environment consist of a barrier type inner Cr-rich oxide layer covered with a continuous hydroxide layer and heterogeneous granular or needle-like oxides over them. The present study also revealed from the SEM observation that the smooth oxidized layer was covered with needle-like corrosion products, meaning that the oxide layers observed in the present study might also have a complex heterogeneous structure as illustrated in Fig. 5-6(a). In previous studies performed using XPS, passive films with the thickness of less than few nanometers were formed at room temperature and therefore could be analyzed quantitatively without any sputtering based on the duplex layered model (inner oxide layer and outer covering hydroxide layer)[27)-31)]. Although the oxide layers formed in the present study were thick (few tens of nanometers in thickness), photoelectrons yielded over the entire thick oxide layer and also from substrate alloy were detected due to the high photon energy of the incident X-rays. However, as described above, as the oxide layer may be heterogeneous, the simple duplex structure model can not be applied. Although in the present study an angle resolved HAX-PES measurement was performed, the outermost surface component of the passive film could not be identified. Therefore, the structure of the oxide layers is assumed to be; Contaminant layer/Outer oxide/Hydroxide/Inner

oxide/Substrate alloy, (from top surface to bottom), provided that the needle-like oxides, distributing over the hydroxide layer, are assumed as a continuous outermost layer (Fig. 5-6(b)). According to this model, the thickness and composition of each layer are calculated based on the following procedure.

The intensity of photoelectrons of an element z in the outer oxide layer, I_z^{oo}, hydroxide layer, I_z^{hyd}, and inner oxide layer, I_z^{io}, can be expressed as eqs. (5.3), (5.4), and (5.5), respectively;

$$I_z^{oo}=\Psi X C_z^{oo}\sigma_z\lambda_z^{ox}\{1-\exp(-m/\lambda_z^{ox})\}\exp(-t^{con}/\lambda_z^{con}) \quad (5.3)$$

$$I_z^{hyd}=\Psi X C_z^{hyd}\sigma_z\lambda_z^{ox}\{1-\exp(-l/\lambda_z^{ox})\}\exp(-m/\lambda_z^{ox})\exp(-t^{con}/\lambda_z^{con}) \quad (5.4)$$

$$I_z^{io}=\Psi X C_z^{io}\sigma_z\lambda_z^{ox}\{1-\exp(-d/\lambda_z^{ox})\}\exp(-l/\lambda_z^{ox})\exp(-m/\lambda_z^{ox})\exp(-t^{con}/\lambda_z^{con}) \quad (5.5)$$

where m, l and, d are thickness of outer oxide layer, hydroxide layer, and inner oxide layer, respectively; λ_z^{ox} is the inelastic mean free path in the oxide or hydroxide layer for photoelectrons yielded from element z. If the outer oxide layer consists of elements A, B, and C, and z in eq.(5.4) is substituted by A, B, or C, then followings are derived.

$$I_A^{oo}=\Psi X C_A^{oo}\sigma_A\lambda_A^{ox}\{1-\exp(-m/\lambda_A^{ox})\}\exp(-t^{con}/\lambda_A^{con}) \quad (5.6)$$

$$I_B^{oo}=\Psi X C_B^{oo}\sigma_B\lambda_B^{ox}\{1-\exp(-m/\lambda_B^{ox})\}\exp(-t^{con}/\lambda_B^{con}) \quad (5.7)$$

$$I_C^{oo}=\Psi X C_C^{oo}\sigma_C\lambda_C^{ox}\{1-\exp(-m/\lambda_C^{ox})\}\exp(-t^{con}/\lambda_C^{con}) \quad (5.8)$$

Provided that C_z^{oo} is the molar concentration of z per unit volume (mol/cm^3, z: A, B, C), in the outer oxide layer, the eq. (5.9) is obtained.

$$M_A C_A^{oo} + M_B C_B^{oo} + M_C C_C^{oo} = \rho^{OO} \quad , \tag{5.9}$$

where M_Z is atomic weight of element z (g/mol) and ρ^{OO} is density of outer oxide layer (g/cm^3). By using eqs. (5.6)-(5.8), Eq. (5.9) can be modified to eq. (5.10).

$$\begin{aligned} & M_A I_A^{oo} / [\{\Psi X \sigma_A \lambda_A^{ox} (1-\exp(-m/\lambda_A^{ox}))\exp(-t^{con}/\lambda_A^{con})\}] \\ & + M_B I_B^{oo} / [\{\Psi X \sigma_B \lambda_B^{ox} (1-\exp(-m/\lambda_B^{ox}))\exp(-t^{con}/\lambda_B^{con})\}] \\ & + M_B I_A^{oo} / [\{\Psi X \sigma_C \lambda_C^{ox} (1-\exp(-m/\lambda_C^{ox}))\exp(-t^{con}/\lambda_C^{con})\}] = \rho^{OO} \end{aligned} \tag{5.10}$$

If ρ^{OO} is provided, the thickness of the outer oxide layer, m, is obtained from eq. (5.10) as only m is unknown parameter in eq, (5.10). Consequently C_A, C_B and C_C are also computed from eqs. (5.6)-(5.8). Similar procedure can be applied for the hydroxide layer and the inner oxide layer by using eqs. (5.4) and (5.5), respectively. Although in the present study the photo ionization cross-section of oxygen, σ_O, was not available, alternatively, it is assumed that the outer oxide, hydroxide, and inner oxide are composed of $NiO+Fe_2O_3$, $Ni(OH)+Fe(OH)_2$, and $Cr_2O_3+FeOOH$, respectively. Therefore, the molar concentrations of oxygen in each layer are automatically determined and eq. (5.10) should be also modified to the following equation, provided that elements A, B, and C form oxides of A_2O_3, BOOH, and CO, respectively;

$$M_A C_A^{oo} + M_B C_B^{oo} + M_C C_C^{oo} + M_O(1.5 C_A^{oo} + 2 C_B^{oo} + C_C^{oo}) = \rho^{OO} \, , \tag{5.10}'$$

where M_O is the molar weight of oxygen.

The calculated thickness and cation fraction are summarized in Table 5-4. As mentioned above, the oxygen concentration in each layer is not calculated. It became apparent that the hydroxide layer consisted mainly of Ni hydroxide, except for Alloy 690 immersed in the solution at 360 °C. The amount of Cr hydroxide on Alloy 690 was higher than that on Alloy 600, which corresponds to the Cr content of each substrate alloy.

Needle-like oxides (might be Ni-Fe spinel oxide) that were distributed on the top surface were heterogeneous as shown in Fig. 5-3, and were also incorporated in the model for quantitative calculation as a continuous outer oxide layer as shown in Fig. 5-6 (b). Therefore, the calculated thickness of the outer oxide layer corresponds to the amount of deposited oxides over the top surface. It should be noted that both Ni oxides were formed more at 360 °C than at 320 °C.

As shown in Table 5-4, the inner oxide layer consists mainly of Cr oxide. The Cr content in the inner oxide on Alloy 600 and Alloy 690 exposed to solutions with 2.75 ppm DH are similar each other. The highly Cr enriched inner oxide layer may act as barrier layer against corrosion. However, the Cr content in the inner oxide formed on Alloy 600 after the exposure to the solution without DH at 320 °C is slightly smaller compared to that in the solutions with 2.75 ppm DH. The thicknesses of the inner oxide layer (varied from 0.95 nm to 6.1 nm) are found to be underestimated as these values are relatively comparable to that formed in aqueous solution at room temperature except for Alloy 690 that were exposed to the solution at 360 °C. Summation of thicknesses of the layers for each specimen is smaller than the thickness of the estimated total oxide layer shown in Fig. 5-4. The reason of this inconsistency is currently unknown. Marcus et al. reported that considerable amount of B_2O_3 is

incorporated in the oxide films formed in simulated PWR primary water containing borate[14]. Although boron was not analyzed in the present study, boric oxide can be possibly incorporated in the oxide layer. If such other components were incorporated in the oxide layer also in the present work, higher thickness would be obtained for inner oxide layer.

As described in the literatures[12), 13), 36)], the redox potential in a simulated PWR primary water is located around NiO/Ni equilibrium. Therefore, NiO can be more stable for more elevated temperatures and also for lower DH. Therefore, oxide layers formed at 320 °C is less stable than those formed at 360 °C. As described in the present study, oxide layers majority of which is Ni(OH) are grown at 360 °C and 320 °C. In particular, almost no Ni oxide is incorporated in the oxide layers formed at 320 °C. Furthermore, thicker mainly Cr oxide layer is obtained at 360 °C compared to that at 320 °C. In the condition at which NiO is unstable, Cr and Fe are also likely to dissolve. Therefore, Cr and Fe are depleted from the substrate alloy underneath the oxide layer as shown in Fig. 5-5. As a result, oxide layers composed of mainly Ni(OH) are formed. It might be possible that at the PWR operating temperature (approximately 320 °C), the passivity of Ni based alloys is unstable, especially for low Cr bearing materials such as Alloy 600. This might be a clue to understand the high susceptibility of Ally 600 to IGSCC in the environments examined.

Table 5-4 Calculated thickness and cation fraction of each layer in the oxide films formed on specimens immersed in the simulated PWR primary water for 24 h.

Specimen	Solution temperature	Thickness (nm)				Cation concentration in each layer (molar fraction in %)						
						Outer		Hydroxide			Inner oxide	
		Outer oxide	Hydroxide	Inner oxide	Summation	Ni^{2+}	Fe^{3+}	Ni^{2+}	Cr^{3+}	Fe^{3+}	Cr^{3+}	Fe^{2+}
Alloy 600 2.75ppm DH	360 °C	0.19	14.4	2.3	16.9	29.2	70.8	67.0	28.6	4.4	79.7	20.3
	320 °C	0.12	8.6	1.2	9.9	0.0	100.0	73.0	21.9	5.1	81.2	18.8
Alloy 690 2.75ppm DH	360 °C	0.26	9.6	6.1	16.0	24.0	76.0	18.5	78.6	3.0	81.3	18.7
	320 °C	0.1	6.5	1.2	7.8	0.0	100.0	42.4	49.9	7.7	89.9	10.1
Alloy600 NoDH	320 °C	0.25	10.8	0.95	12.0	50.3	49.7	83.3	11.8	4.8	69.8	30.2

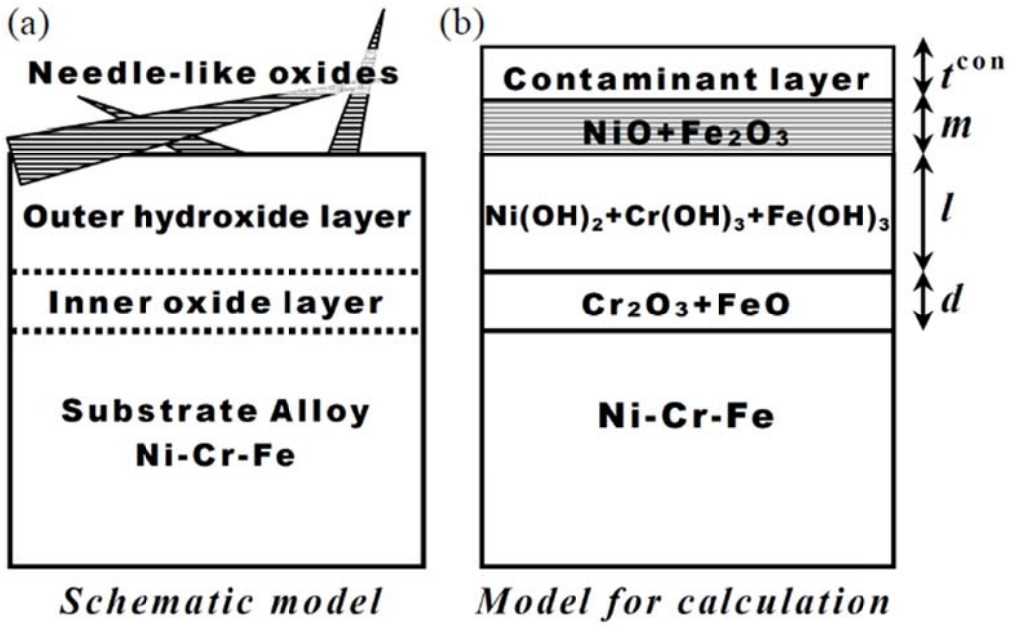

Fig. 5-6 (a) Schematic drawing of the oxide films formed on Alloy 600 and Alloy 690 in simulated PWR primary water. (b) Simplified layered model for numerical calculation of XPS results.

5.5 Conclusion

Using HAX-PES, photoelectrons were detected from the oxide layer of up to 25 nm thickness. They could also be observed simultaneously in the substrate alloy underneath the oxide layer without any sputtering techniques. The substrate alloy adjacent to the oxide layers was deficient in Cr, and on the other hand was enriched with Ni. Especially, the Cr content in the substrate alloy of the specimen exposed to the solution at 320 ºC was approximately 1 mass%. Oxide layers formed in PWR primary water environment consisted of an inner oxide layer of mainly Ni and a covering outer hydroxide layer of Ni and Cr. Furthermore needle-like oxides covered the top surface. A considerable amount of the needle-like oxides, which might be the spinel of Fe and Ni, were formed in the solution without dissolved hydrogen. Almost no Ni was included in the oxide, and most of Ni in the oxide layer was incorporated as hydroxide. On the other hand, although Cr was included in both hydroxide and oxide, more Cr was incorporated in the oxide layer formed at 360 °C compared to the case at 320 °C. By comparing oxides formed at 320 ºC and 360 ºC, it was found that the less protective films were formed at 320 ºC.

References

1. H. J. Schenk, Material Performance (1976) 25.
2. C. H. Shen and P. G. Shewmon, Metallurgical Trans. (1990) 1261.
3. P. L. Andreson, J. Hickling, A. Ahluwalia and J. Wilson, Corrosion **64** (2008) 707.
4. H. Nagano, K Yamanak, T. Minami, M. Inoue, T. Yonezawa, K. Onimura, N. Sasaguri and T. Kusakabe, Proc. 2nd Int. Symp. (1985).
5. P. L. Andresen, M. M. Morra, J. Hickling, A. Ahluwalia and J Wilson, Proc. 13th Int. Symp. (2007).
6. K. Arioka, T. Yamada, T. Miyamoto and T. Terachi, Corrosion **67** (2011) 1.
7. N. S. McIntyre, D. G. Zetaruk and D. Owen, J. Electrochem. Soc. **126** (1979) 750.
8. T. Shibata and S. Fujimoto, Trans. Japan Inst. Metals **28** (1987) 424.
9. Z. Szklarska-Smialowska, W. K. Lai and Z. Xia, Corrosion **46** (1990) 853.
10. T. M. Angeliu and G. S. Was, J. Electrochem. Soc. **14** (1993) 1877.
11. F. Carrette, M. C. Lafont, G. Chatainier, L. Guinard and B. Pieraggi, Surf. Interface Anal. **34** (2002) 135.
12. T. Nakagawa, N. Totsuka, T. Terachi and N. Nakajima, J. Nuclear Sci. Tech. **40** (2003) 39.
13. T. Terachi, N. Totsuka, T. Yamada, T. Nakagawa, H. Deguchi, M. Horiuchi and M. Oshitani, J. Nuclear Sci. Tech. **40** (2003) 509.
14. A. Machet, A. Galtayries, S. Zanna, L. Klein, V. Maurice, P. Jolivet, M. Foucault, P. Combrade, P. Scott and P. Marcus, Electrochim. Acta **49** (2004) 3957.
15. J. M. Le Canut, S. Maximovitch and F. Dalard, J. Nucl. Mater. **334** (2004) 13.
16. Y. Takeda, T. Shoji, M. Bojinov, P. Kinnunen and T. Saario, Appl. Surf. Sci. **252** (2006) 8580.
17. M. Bojinov, A. Galtayries, P. Kinnunen, A. Machet and P. Marcus, Electrochim. Acta **52** (2007) 7475.
18. A. Marchetti, S. Perrin, Y. Wouters, F. Martin and M. Pijolat, Electrochim. Acta **55** (2010) 5384.
19. I. Betova, M. Bojinov, V. Karastoyanov, P. Kinnunen and T. Saario, Corros. Sci. **58** (2012) 20.
20. T. Ohtsuka, Y. Hamaguchi, M. Sakairi, K. Fushimi, Y. Sakakibara and G. Nakayama, Proc. JSCE Materials and Environments 2013 (2013) 79.

21. W.-S. Kim, H. Tsuchiya, M. Sato, J. Y. Son, M. Machida, K. T. Jung and S. Fujimoto, submitted to Zairyo-to-Kankyo.
22. M. Nagayama and M. Cohen, J. Electrochem. Soc. **109** (1962) 781.
23. N. Sato and G. Okamoto, J. Electrochem. Soc. **110** (1963) 605.
24. N. Sato and M. Cohen, J. Electrochem. Soc. **111** (1964) 512.
25. M. Seo, R. Saito and N. Sato, J. Electrochem. Soc. **127** (1980) 1909.
26. K. Asami and K. Hashimoto, Corros Sci. **17** (1977) 713.
27. I. Olefjord and L. Wegrelius, Corros Sci. **31** (1990) 89.
28. E. De Vito and P. Marcus, Surf. Interface Anal. **19** (1992) 403.
29. P. Marcus and J.M. Grimal, Corros Sci. **33** (1992) 805.
30. R. H. Jung, H. Tsuchiya and S. Fujimoto, Corros. Sci. **58** (2012) 62.
31. W.-S. Kim, H. Tsuchiya and S. Fujimoto (submitted to Materials Transaction).
32. A. Rossi and Elsener, Materials Sci Forum **185-188** (1995) 337.
33. M. C. Biesinger, B. P. Payne, L. W. M. Lau, A. Gerson and R. S. C. Smart, Surf. Interface Anal. **41** (2009) 324.
34. S. Tougaard, (1998) http://www.quases.com.
35. S. Tanuma, C. J. Powell and D. R. Penn, Surf. Interface Anal. **21** (1994) 165.
36. B. Totsuka and Z. Szklarska-Smialowska, Corrosion **43** (1987) 734.

Chapter 6 General Conclusions

In the present study, the author has investigated the photoelectrochemical response of passive films formed on Ni-based alloys. As a result, the following conclusions have been derived.

Chapter 1

The author has introduced the overview of characterization of passive films, especially focusing on characterization of semiconductive properties, followed by the purpose of the present thesis.

Chapter 2

The chapter 2 reports semiconductive properties of passive films formed on pure Ni and Ni-Cr alloys in a pH 8.4 borate buffer solution and a sulfuric acid solution using the photoelectrochemical response. Photoelectrochemical action spectra obtained from observed photocurrent spectra are separated into two components exhibiting band gap energies of 2.3 eV and 3.5 eV that are attributed to outer hydroxide and inner oxide layers of the passive films, respectively. By considering the potential dependence of the photoelectrochemical response and photocurrent transients, the passive films on pure Ni and Ni-Cr alloys in the solutions are proposed to consist of p-type oxide layer and n-type hydroxide layer. The pH of the solutions does not affect the electronic band structures of passive films on pure Ni and Ni-Cr alloys, but significantly influences the amplitude of photocurrent and the flat band potential.

Chapter 3

In the chapter 3, semiconductive properties of passive films on Alloy 600 and

Alloy 690 in a 0.1M H_2SO_4 solution and a pH 8.4 borate buffer solution are investigated using the photoelectrochemical response. From the analysis of photoelectrochemical response obtained, it is proposed that passive films formed on the alloys in the solutions consist of an inner p-type oxide layer with the band gap energy of approximately 3.5 eV and a covering n-type hydroxide layer with the band gap energy of 2.3 eV, analogy to passive films formed on pure Ni and Ni-Cr alloys in the both solutions. By comparing to the photoelectrochemical responses obtained for Ni-Cr alloys, it becomes clear that Fe included in Alloy 690 affects photoelectrochemical responses when incorporated into the passive films, that is, in the sulfuric acid solution the photoelectrochemical responses are not affected because only small amount of Fe is incorporated into passive films due to the selective dissolution of Fe whereas in the borate buffer solution passive films on Alloy 690 contain a certain amount of Fe, and as a result larger photoelectrochemical responses are observed for passive films on Alloy 690 than for those on Ni-30Cr alloy. From the results obtained for high-purity Alloy 690, it was clear that impurities included in commercial Alloy 690 led to no changes in semiconductive properties of passive films even if impurities were incorporated in passive films.

Chapter 4

In the chapter 4, passive films formed on Alloy 600 and Alloy 690 in high temperature and high pressure water environments are investigated on focus on the influence of the dissolved hydrogen and cold working. XPS revealed that passive films formed on Alloy 600 and Alloy 690 consist of an outer hydroxide layer and an inner oxide layer. The dissolved hydrogen changes the chemical composition of passive films formed on the alloys, resulting in variation in photocurrent response depending on the

dissolved hydrogen level. Photocurrent obtained for the passive films formed under low concentration of the dissolved hydrogen is large compared to that for the films formed under high concentration of the dissolved hydrogen. Cold working also affects the photocurrent response only on Alloy 600. This can be related to more local strain in the alloy, especially at grain boundaries, introduced by cold working.

Chapter 5

Oxide films of Alloy600 and Alloy690 formed during exposure to a solution simulated as the primary side water of a pressurized water reactor were characterized using hard X-ray photoelectron spectroscopy. Specimens were immersed in a solution containing 500 ppm B + 2 ppm Li with or without dissolved hydrogen at 320 ºC or 360 ºC for 24 h. Photoelectrons generated in the oxide films of up to 25 nm in thickness and also in the substrate alloy underneath the oxide films could be observed simultaneously without any destructive techniques like sputtering. The oxide films were mainly composed of Ni hydroxide and an oxide of Cr and Fe, accompanying needle-like oxides distributed on the surface. Further, alloyed Cr was depleted from the substrate alloy directly underneath the oxide layer. Although Cr was incorporated both in the hydroxide and oxide, more Cr is included in the oxide film formed at 360 ºC. It is considered that the oxide film formed at 320 ºC is less protective. Therefore, at 320 ºC, more Cr and Fe were dissolved in the solution and Ni may have remained in the substrate alloy and also as a hydroxide in the oxide film.

Additionally, the author hopes that the photoelectrochemical response of passive films obtained in this study will be contributed to reveal the electronic structure and for semiconductive properties of passive film formed Ni-based alloys in various

environments, in particular at high temperature and high pressure water as those structures and properties are strongly related to corrosion resistance of the alloys.

Publications

Publications related to this thesis:

1. **WheeSung Kim**, Hiroaki Tsuchiya, Shinji Fujimoto**,**
   Electrochemical characterization of passive films on Ni-based Alloys in acidic and neuterials solutions,
   Materials Transaction, 56 [4] (2015), 593-599.

2. Shinji Fujimoto, **WheeSung Kim**, Masugu Sato, JinYooung Son, Masatake Machida, Hiroaki Tsuchiya, KiTeak Jung**,**
   Characterization of oxide films on Alloy 600 and Alloy 690 formed in simulated PWR primary side environments using Hard X-ray Photoelectron Spectroscopy,
   Journal of Solid State Electrochemistry, (2015) in press.
   DOI 10.1007/s10008-015-2817-8.

3. **WheeSung Kim**, Hiroaki Tsuchiya, Masugu Sato, JinYoung Son, Masatake Machida, KiTaek Jung, Shinji Fujimoto**,**
   Electrochemical properties of oxide films formed on cold worked Alloy 600 and Alloy 690 in simulated PWR primary side environments,
   Zairyo-to-Kankyo, Vol. 64 (2015), in press.

Other Publications:

1. **W. S. Kim**, W. S. Hong, S. H. Park, K. B. Kim,
   Activation Energy and Interface reaction of Sn-40Pb/Cu & Sn-3.0Ag-0.5Cu/Cu,
   Kor. J. Mater. Res., Vol.17, No.8, p.402 ~ 407 (2007)

2. W. S. Hong, **W. S. Kim**, N. C. Park, K. B. Kim,
   Activation Energy for Intermetallic Compound Formation of Sn-40Pb/Cu and Sn-3.0Ag-0.5Cu/Cu Solder Joints,
   Journal of KWJS., Vol.25, No.2, P.49 ~ 55 (2007)

3. W. S. Hong, **W. S. Kim**, B. S. Song, K. B. Kim,
Thermal Shock Cycles Optimization of Sn-3.0Ag-0.5Cu/OSP Solder Joint with Bonding Strength Variation for Electronic Components,
Kor. J. Mater. Res., Vol.17, No.3, p.152 ~ 159 (2007)

4. W. S. Hong, **W. S. Kim**, S. H. Park, K. B. Kim,
Polarization Behaviors of SnCu Pb-Free Solder Depending on the P, Ni, Addition,
Kor. J. Mater. Res., Vol.15, No.8, p.528 ~ 535 (2005)

Acknowledgements

The author would like to express his grateful gratitude to ***Professor Shinji Fujimoto*** of The Department of Materials Science and Engineering, Osaka University, for his kind guidance, helpful suggestions, constructive discussion and invaluable encouragements throughout this work and then offering constant assistance during the doctor's course in Osaka University.

The author would like to thank ***Professor Toshihiro Tanaka*** and ***Professor Hiroshi Utsunomiya*** of The Department of Materials Science and Engineering, Osaka University, for reviewing this thesis and their valuable comments.

The author is very grateful to ***Dr. Hiroaki Tsuchiya*** of The Department of Materials Science and Engineering, Osaka University, for his helpful suggestion, discussion and guidance throughout this work.

The author would like to thank ***Mr. J. Nakata*** of Osaka University for the technical assistance. The author also would like to thank past and present students in the Professor Fujimoto Group for their friendships and helps.

This work was supported by "Priority Assistance for the Formation of Worldwide Renowned Centers of Research-The Global COE Program (Project: Center of Excellence for Advanced Structural and Functional Materials Design)" from the Ministry of Education, Culture, Sports, Science and Technology (MEXT), Japan.

Finally, the author would like to express the deep appreciation to the author's parents, and sisters, ***Dong-Suk Kim***, ***Woo-Yun Lee***, ***Ji-Young Kim*** and ***Ji-Hee Kim*** for their hearty encouragements, understanding and support.

Whee-Sung Kim

January, 2015